Hydro-Mechanical Properties of Compacted Sand-bentonite Mixtures Enhanced with Cement

Anoosheh Iravanian

Submitted to the
Institute of Graduate Studies and Research
in partial fulfillment of the requirements for the degree of

Doctor of Philosophy
in
Civil Engineering

Eastern Mediterranean University
September 2015
Gazimağusa, North Cyprus

Approval of the Institute of Graduate Studies and Research

Prof. Dr. Serhan Çiftçioğlu
Acting Director

I certify that this thesis satisfies the requirements as a thesis for the degree of Doctor of Philosophy in Civil Engineering.

Prof. Dr. Özgür Eren
Chair, Department of Civil Engineering

We certify that we have read this thesis and that in our opinion it is fully adequate in scope and quality as a thesis for the degree of Doctor of Philosophy in Civil Engineering.

Assoc. Prof. Dr. Huriye Bilsel
Supervisor

Examining Committee

1. Prof. Dr. S. Feyza Çinicioğlu

2. Assoc. Prof. Dr. Huriye Bilsel

3. Assoc. Prof. Dr. İlknur Bozbey

4. Assoc. Prof. Dr. Zalihe Sezai

5. Asst. Prof. Dr. Mehmet Metin Kunt

ABSTRACT

Engineered barriers used in waste containment systems are usually a composite compacted material, such as sand-bentonite. The containment elements such as the landfill liners should be designed to prevent leachate and ground water permeation through them. A bentonite content of 5-15% has been recorded to have improved the performance of the composite material, providing a low hydraulic conductivity, whereas sand component contributed to the mechanical stability of the system. According to engineering specifications a hydraulic conductivity less than 10^{-9} m/s is required to maintain structural integrity of the containment system. Therefore, a thorough understanding of engineering behavior of the selected materials must be experimentally ascertained. This study consists of an experimental work on the hydro-mechanical behavior of sand-bentonite and sand-bentonite-cement mixtures to be proposed as barrier materials for the disposal of municipal waste in a semi-arid climate. The barriers are unsaturated on placement and remain so throughout long periods of dryness, however may become saturated during short periods of flooding, which is the expected climatic regime in a semi-arid climate. Liners may remain saturated for prolonged periods when they are subjected to permeation of leachates and/or ingress of ground water. Therefore, both saturated and unsaturated behavior is essential to study for ensuring integrity of the waste disposal facility and the sustainability of the system as well as protection of the geo-environment. In the first stage of the experimental program, based on swell potential and compressibility characteristics, two mixtures were selected which consisted of 15% Na-bentonite (SB), and 15% Na-bentonite and 5% cement (SBC) added to uniform sand respectively. SB was selected as a control material to assess the degree of

enhancement of cement additive. In the second stage of the experimental study volume change, including swell-shrinkage, compressibility with effects of curing (28 days), salinity (1 mol. NaCl), and temperature (60°C) are investigated on the 28-day cured specimens of the selected mixtures. In order to study the unsaturated behavior, the key element of unsaturated soils, the soil-water characteristic curve (SWCC) was obtained for each mixture, which were used to predict the unsaturated volume change parameters, as well as unsaturated hydraulic conductivity function. The macro-structural behavior was also explained at micro-structural level by scanning-electron microscopy study. The SEM images have revealed the thixotropic changes in the SB as well as curing effect of cement included (SBC) specimens revealing the tobermorite formation due to hydration process of cement. In the last stage of the testing program, strength tests, including unconfined compression and tensile testing were carried out. Tensile strength is considered to be as important as the compressive strength, mainly when the liners are thin and/or subjected to desiccation shrinkage in a semi-arid climate. Tensile testing methods are not within usual testing program of a geotechnical survey. Therefore, a significant emphasis is given herein to different tensile testing techniques (split tensile, flexural strength and double punch) investigating on their practical applicability to compacted buffer material. Correlations were made between all the strength tests including the compressive strength, and recommendations were derived for prediction approaches of compressive and tensile strength in the most feasible way. Finally it was concluded that when 15% bentonite included SB was selected as barrier material, the hydraulic conductivity exceeded the maximum allowed limit when subjected to a high concentration of salt permeation and when temperatures in the system rose to 60°C. However, when 5% cement was included in addition to 15% bentonite, all the

engineering properties have improved notably and the hydraulic conductivity remained below the maximum limit provided effective confining pressures were higher than 400 kPa.

Keywords: Landfill, sand-bentonite, cement, volume change, strength

ÖZ

Katı atık depolama sistemlerinin sıkıştırılmış şilteleri genelde kompozit bir malzeme olan kum-bentonit kullanılarak tasarlanır. Özellikle alt katmanın katı atık sızıntısının çevreye ve yer altı suyunun da depolama sistemine girmesini önleyecek şekilde tasarlanması gerekmektedir. %5-15 arası kullanılan bentonitin kompozit malzemenin performansını artırdığı ve hidrolik iletkenliği düşük katmanlar oluşmasına yaradığı, kumun ise sistemin mekanik stabilitesini sağladığı gözlemlenmiştir. Mühendislik şartnamelerinde, geçirimsiz katmanların hidrolik iletkenliğinin 10^{-9} m/s'yi geçmemesi gerektiği belirtilir. Dolayısıyla seçilen malzemenin mühendislik davranışı deneysel olarak detaylı bir şekilde incelenmeli ve beklenilen özellikleri sağlayacağından emin olunmalıdır. Bu çalışma, yarı kurak bir iklim için katı atık depolama sisteminin katmanları olarak uygun olabilecek kum-bentonit ve kum-bentonit-çimento karışımları üzerinde yapılan hidro-mekanik davranışın irdelendiği deneysel çalışmayı içerir. Katmanlar, yerinde sıkıştırıldıkları anda suya doygun halde değillerdir ve bu durum yarı kurak iklimlerde görülen uzun süren kuru mevsimlerde böyle devam eder. Ancak kısa süreli de olsa sellerin olabileceği yağmurlu mevsimlerde tamamen suya doygun hale de gelebilirler. Ayrıca buna, yeraltı suyu veya katı atık sızıntıları da neden olabilir. Dolayısıyla, katı atık depolama şiltelerinin sağlıklı tasarımı için suya doygun veya doygun olmayan durumlarda da irdelenmeli ve iklimsel ve çevresel faktörlerin etkilerinin sistemin sürekliliği üzerindeki olumsuzlukları araştırılmalıdır. Bu çalışmanın ilk etabında, farklı kombinasyonlardaki kum-bentonit ve kum-bentonit-çimento karışımlarının şişme potansiyeli, kompresibilite ve hidrolik iletkenlik değerlerine göre %15 bentonit katkılı karışımla %15 bentonit ve %5 çimento katkılı iki karışım seçilmiştir. İkinci

aşamada ise kürlenmiş (28 gün) numuneler üzerinde şişme-büzülme ve şişme kompresibilite deneyleri, yüksek konsantrasyonlu NaCl tuzu solüsyonunda ve ayrıca 60°C ısı etkisinde çalışılmıştır. Suya doygun olmayan davranışın çalışılması için gerekli olan zemin-su muhtevası eğrileri (su tutma eğrileri) elde edilerek, suya doygun olmayan zeminlerin hacimsel değişim ve hidrolik iletkenlik davranışı tahminleri için gerekli parametreler elde edilmiştir. Çimento katkının özellikle kürden sonra geçirimsiz katmanın hacimsel değişimlerini olumlu etkilediği makro seviyede incelenirken, buna neden olan mikro değişim de "taramalı elektron mikroskopisi (SEM)" tekniğiyle de irdelenmiş ve çimentonun mekanik davranışını iyileştiren tobermorit oluşumu gözlemlenmiştir. Araştırmanın son aşamasında, basınç ve gerilme mukavemeti deneyleri farklı kür zamanlarında çalışılmıştır. Gerilme mukavemeti özellikle basınç altındaki ince katmanlar ve iklimsel nedenlerle kurumadan dolayı büzülme eğilimi olan katmanlarda, gerilme mukavemeti en az basınç mukavemeti kadar önemlidir. Gerilme mukavemeti genelde geoteknik araştırmalarda rutin metodlar arasında değildir. Dolayısıyla, bu çalışmada farklı gerilme mukavemeti ölçüm teknikleri araştırılıp, sıkıştırılmış geçirimsiz katmanlara uygulanabilirliği incelenmiştir. Farklı yöntemlerle bulunan mukavemet sonuçları arasında ilişkiler kurularak pratik yöntemlerle önceden tahmin etme ilişkilendirmeleri çalışılmıştır. Sonuç olarak, %15 bentonit katkılı kum-bentonit karışım kullanılacak olursa, tuz ve ısı etkisi altında hidrolik iletkenliğin maksimum değeri geçtiği; buna karşılık, %5 çimento katkılı karışım kullanıldığında, sadece ısının, düşük efektif basınçlar altında hidrolik iletkenliği artırdığı gözlemlenmiştir.

Anahtar kelimeler: Katı atık depolama sahası, kum-bentonit, çimento, hacimsel değişimler, mukavemet.

ACKNOWLEDGMENT

This thesis could not have been written without great moral advices and suggestions of Assoc. Prof. Dr. Huriye Bilsel who was not only a supervisor but also a role model for me. She encouraged me throughout my academic and social life, and supported me with her deep knowledge, time, patience and care. I was so lucky to have her as my supervisor.

I would like to express my deepest appreciations to my lovely family. My parents Soraya Omidi and Ardeshir Iravanian who encouraged me to have graduate studies and were very supportive throughout these years. They indebted me with their endless patience and love.

My sincere respect and love goes to my dear friend Assist. Prof. Dr. Suna Bolat who was beside me through nervous break downs, sleepless nights, hard times and many fun times. I could not thank her enough for her practical advices and contribution during final processes of this thesis.

I am so grateful to my colleagues and friends, especially the laboratory engineer Mr.Ogün Kılıç who helped me throughout laboratory works, setting up new experiments and backing up with his practical ideas.

TABLE OF CONTENTS

LIST OF TABLES

LIST OF FIGURES

LIST OF ABBREVIATIONS AND SYMBOLS

Ψ	Suction
A	Angle of cone
γ_w	Unit weight of water
δ_w	The relative velocity vector
δ_3	Cell pressure
$\Delta H/H_0$	The relative change in axial strain
Δu	Change in pore water pressure
$\Delta V/V_0$	Relative change in volumetric strain
σ_t	Tensile strength
Φ	Internal friction angle
Q	Volumetric water content,
y_m	Matric suction
y_t	Total suction
A	Area of burette
A	Area of the sample
A	Radius of the disc
a and b	Constants obtained from straight line fits giving the highest R^2 value
AEV	Air-entry value
a_{gr}	Fitting parameter corresponding to initial break of equation (i.e., representing the large particle size)
a_{sh}	The minimum void ratio the dried specimens attained

a_t	Coefficient of compressibility with respect to a change in matric suction
B	Bentonite
B	Width of sample
B	Radius of specimen
B	Ratio between İncrease in pore water pressure and increase in cell pressure
b_m	Coefficient of water content change with respect to a change in matric suction
b_{sh}	Minimum water content values at which volume change commenced
b_t	Coefficient of water content change with respect to a change in net normal stress.
C	Cement
C	Cohesion
CAH	Calcium aluminate hydrates
CASH	Calcium aluminum silicate hydrates
CBR	California Bearing Relation
C_c	Coefficient of curvature
C_c	Compression index
C_c1	Compression index before the threshold stress
C_c2	Compression index after the threshold stress
C_m	The slope of void ratio with respect to suction, and

C_r	Recompression index
CSH	Calcium silicate hydrates
c_{sh}	Curvature of the shrinkage curve and is referred to as shrinkage limit
C_t	Slope of void ratio curve with respect to pressure
C_m	Volumetric deformation index for the soil structure
C_u	Uniformity coefficient
C_v	Coefficient of consolidation,
D	Particle diameter
D	Diameter of sample
D_{10}	Effective diameter
D_{50}	Mean diameter
DDL	Diffused double layer
d_m	Minimum particle diameter (mm)
D_m	Soil water characteristic surface with respect to suction,
D_t	Slope of water content in respect to pressure,
e_0	The first void ratio of considered section.
e_1	Last void ratios of considered section
e(w)	Void ration at any water content
F	Applied force
FEBEX	Full scaled engineered barriers experiment
g(x)	Reshaping factor

GCL	Geosynthetic clay liner
H	Difference of height of water in lower burette and upper burette in (cm)
H	Height of specimen
H_{dr}	Height of drainage equal to half of height of sample
K	Hydraulic conductivity
k_s	Saturated hydraulic conductivity
L	L is length of sample
L	Length
MDD	Maximum dry dens
m_{gr}	Fitting parameter corresponding to curvature of equation
m_v	Coefficient of compressibility,
n_{gr}	Fitting parameter corresponding to maximum slope of the equation
P	Applied load
p_0	First effective consolidation pressure in selected section
p_1	Last effective consolidation pressure in selected section
PB	Bias pressure
P.I.	Plasticity index
P_p	Percent passing at any particular grain-size
p_s	Swell pressure
PTF	Pedotransfer function
q_u	Unconfined compressive strength

S	Sand
$S_{(t)}$	Ultimate swell
SB	Sand-bentonite
SBC	Sand-bentoniteücement
SEM	Scanning electron microscopy
SWCC	Soil water characteristic curve
T	Difference between t_1 and t_2 in seconds
t_{90}	The time that 90% of consolidation is completed
T_v	Coefficient of time
$V_{l(ti)}$	Volume reading of lower burette at ti in (cm^3).
$V_{u(ti)}$	Volume reading of upper burette at ti in (cm^3)
W	The gravimetric water content,
WRC	The water retention curve

Chapter 1

INTRODUCTION

The solution to minimize the pollution caused by sanitary waste is to design a landfill as a control system. Waste disposal systems should be designed and constructed with safety as the main concern. Hence, containment components like liners and covers should be designed to prevent the migration of leachate and restrict any ground water permeation to the landfill (Montanez, 2002). The first stage is to isolate the waste at surface and bottom to minimize seepage of rainfall to the waste from the top and stop leachate of contaminated water to the ground water from the bottom part of the system. The soil and water table adjacent to waste disposal unit can be protected by a cover and liner system containing compacted clay and geomembranes or composite engineered barriers, such as sand-bentonite.

1.1 Waste Disposal and Landfill

Engineering properties of the compacted layer like low permeability and stability during construction and operation, plays the main role in choosing the suitable material in landfill liner. A soil liner prevents the leakage of polluted water to the surrounding environment while the surface environment is separated from the waste by a cover layer or cap which limits incidences such as erosion and being dug by animals. It limits the permeation of rainfall water while lets the landfill gas to percolate out of the waste. Therefore the aim of designing landfills is to build “encapsulated” waste-dumps with efficient barriers to the leachate (Blight and Fourrie, 2005; Bielinski et al., 2001).

These types of landfills are named as “dry containment” and by definition the waste would stay largely intact, consequently the cover/liner system would need a long design life. In spite of this, there has been a recent tendency to switch the waste storage methods from dry storage, to quicker decomposition of waste by applying landfills as “flushing bioreactors”. Accelerated stabilization moderates the necessity of long-term containments and usually functions by recirculation of leachate to maintain the water content of the solid waste at favorable levels for biodegradation (Kazimoglu et al., 2003).

If the waste disposal sites are not accurately chosen and not entirely isolated, the human health and surrounding environment can be exposed to serious hazards. Apart from odor problems, the leakage of polluted fluids from the waste to the ground and subsequently ground water table can cause considerable risks to flora and fauna and also people’s health (Bielinski et al., 2001).

The absorptive capacity of municipal solid waste (MSW) is typically distinguished using the term of field water capacity, and it refers to “amount of moisture that a porous medium can retain, against gravity, before discharge”. The difference between the primary moisture content of waste and its field moisture capacity is referred as “absorptive capacity”. As the moisture content in waste gets higher than its field moisture capacity, or when the amount of infiltration exceeds its absorptive capacity, the leachate is discharged. Though, the absorptive capacity of waste is usually related to physical properties of the waste such as age, porosity, density and composition (Zornberg et al., 1999).

Hydraulic barriers use a low permeability material to prevent downward migration of water into the waste. Soils with low values of permeability, such as compacted clay layers, are commonly used in construction of landfill linear and cap. The stability during construction and operation of the landfill is expected from these types of soils. Natural sands and other cohesionless materials are also applied, by adding admixtures to modify their properties. Typical components of hydraulic barrier systems are: surface layer, protection layer, internal drainage layer, hydraulic barrier layer, gas transmission layer, and foundation layer (Kumar and Stewart, 2003).

Blight and Fourrie (2005) offered a kind of hydraulic barrier namely infiltrate-stabilize-evapotranspire (ISE) cap. This cap allows the rain infiltration to enter the waste during wet weathers and later during the dry weather excess infiltration is removed from waste and cap by evaporation. Considering that stabilization and decomposition of the waste is dependent on presence of water to endorse bacteriological activities, the ISE cap intend to accelerate the decomposition process by limited water infiltration to the waste and then removing the excess water in dry seasons. However during possible droughts when there is insufficient rainfall to permeate the waste, an ISE cap functions as an evapotranspirative cap.

Different barrier types may be joint in a single cover system depending on the project requirements. Currently, the most widely used type of cover systems are hydraulic barrier covers. Gas collection and control is necessary at most of landfills. Soil thickness may vary based on project specific conditions (Rowe, 2001).

1.2 Sand-Bentonite Barriers

Use of compacted expansive clays, bentonite and sand-bentonite mixtures as hydraulic barrier materials for dumping systems and particularly nuclear waste disposal systems has turned to be an attractive subject in the recent studies. Compacted mixtures of sand bentonite are regularly used as an alternative for compacted clay in landfill barriers because of their lower tendency for volumetric change in climatic variations (Kraus et al, 1997).

1.2.1 Bentonite

Bentonite is basically composed of a group of minerals called "montmorillonite". The physical characteristics, regulated by the amount of montmorillonite, include the large specific surface area, large cation exchange capacity (CEC), low hydraulic conductivity and high swell potential. The reason that dissolved cations in the pore water get attracted to the surface of bentonite, and therefore swell, is the negative net electrical charge existing on surface of bentonite particles. Diffused double layer (DDL) is referred to the layer of water and adsorbed ions that surround a bentonite particle. The overlapping of DDL restricts the flow of water and other electrolytes through the soil and results in a low permeability (Chalermyanont and Arrykul, 2005). Saturated Na-bentonite can absorb water up to five times of its own mass which leads to forming a gel-like material that is about 15 times bigger in volume (Ameta and Wayal, 2008).

1.2.2 Swell Characteristics

Primary clay mineral present in soils is one of the main factors influencing the volume change behavior of soils in arid and semi-arid areas. It has been noticed that diffuse double layer repulsion, the stress state and bonding are also playing major roles in volume change behavior of expansive unsaturated soils. There are basically

two mechanisms controlling the liquid limit and volume change behavior in fine grained soils suggested by Sridharan (2003). In the first mechanism compressibility of clay is initially controlled by the shearing strength at the near contact points and volume changes take place by shear displacement or sliding between particles (in kaolinitic soils) and in the second mechanism compressibility is basically controlled by primary diffuse double layer repulsive forces (in montmorillonitic soils i.e. bentonite). It has been noticed that behavior of both saturated and unsaturated clays are governed by the mentioned mechanisms, which depend on whether the clay is kaolinitic or montmorillonitic (Sridharan, 2003).

Expansive materials such as bentonite undergo a volume change and swell when exposed to water. In constant volume condition, swelling pressure is developed as water is absorbed by the bentonite. Assuming that water is the only wetting fluid in isothermal condition, in a particular material with known dry density, the extent of swell pressure depends only on the amount of water absorbed by soil, as it governs the separation distance between two clay platelets, which in case of restricted swelling it leads to swelling pressure increase. A comparison between liquid limits obtained with water and a non-polar fluid, CCL_4, (Carbon tetrachloride) shows that non-swelling kaolinitic soils gives higher liquid limit in CCL_4 rather than in water while in swelling soils, the higher liquid limit is observed with water. This phenomenon lays on this fact that ionic behavior of clay particles with water (DDL) is the chief explanation for high volume changes in expansive clayey soils (Sridharan, 2003).

Kumar and Yong (2002) concluded that the swelling index increases with enhancement of bentonite, which is a consequence of high swelling characteristics of bentonite. They also observed that the addition of bentonite has smaller influence on compression index in comparison with its influence on swelling index.

1.2.3 Characteristics of Sand-bentonite Mixtures

Considering grain size distribution, hydraulic conductivity, chemical activity and strength, sand and bentonite are completely different soil types. Nevertheless, when mixed together at right proportions can form an excellent material to be used as engineering barrier against fluids seepage, by having low hydraulic conductivity and yet acceptable shear strength (Farajollahi and Wareham, 1998).

A mixture of sand and bentonite is suitable to be used as a hydraulic barrier such as cover or liner of a landfill, due to the fact that sand provides strength and stability and accounts as the "skeleton" of the mixture while the very fine particles of bentonite reduce the permeability of the mixture by filling the voids remained between the sand particles. The bentonite is mixed into the site soil either by pugmill (a machine in which materials are simultaneously ground and mixed with a liquid) or spreading it on the loose soil surface (Kumar and Yong, 2002).

In various experimental works it was confirmed that addition of bentonite to sand results in reduction of maximum dry density of mixture and increases the optimum water content (Chalermyanont and Arrykul, 2005; Ameta and Wayal, 2008; Kumar and Yong, 2002). This fact is related to unique characteristics of bentonite. Elucidating that while fine content is mixed with sand more moisture is needed in compaction to attain maximum density. Furthermore, water act like lubricant that

permit soil particles move easier toward each other, therefore the volume of air voids minimizes and higher dry density would be achieved. On the other hand excessive water content (beyond the optimum water content) would cause high swell of bentonite and occupying the mold instead of sand. Hence a considerable decrease in dry unit weight occurs. Therefore, it can be stated that optimum moisture content (OMC) raises along with increase of bentonite content in mixture while the relative maximum dry unit weight reduces. Kumar and Yong (2002) clarify this observation by attributing the reduction in maximum dry unit weight by increase in bentonite content to high swelling characteristics of bentonite that could form a gel-like material around the soil particles. The effective size of soil particles increases when this gel forms around the soil particles, which results in increase in void volume, and consequently decrease in dry unit weight.

Liquid limit (LL) and plastic limit (PL) of a particular soil are basically controlled by the amount of clay existing in it. Thus increase in LL and PL of the sand-bentonite mixtures is expected as clay content is increased along with addition of bentonite. Deciding the proportion of bentonite to be added to soil depends a lot on grain size of solids however, for the soils with broad range of grain size, the amount of bentonite used is typically less than 6% on a dry weight basis. Nevertheless for the uniform-sized sands it can vary between 10 to 15% (Kumar and Yong, 2002).

Ameta and Wayal (2008) in their study on sand-bentonite materials claimed that coefficient of consolidation under different pressures decreases in lower bentonite contents while it has a little change in greater bentonite contents.

1.2.4 Hydraulic Conductivity of Sand-bentonite Mixtures

The hydraulic conductivity of bentonite depends on many factors including void ratio and fabric. In a saturated bentonite-sand mixture the void ratio of bentonite depends on the amount of bentonite in the mixture and the free spaces remained between the sand particles (Farajollahi and Wareham, 1998).

Chapius (1990) employed flexible-wall and rigid-wall permeameter tests to estimate the hydraulic conductivity of compacted sand-bentonite liners. It is known that an ideal sand-bentonite mixture for permeability measurements can be obtained by modeling saturated bentonite and sand as a homogeneous, two-component mixture assuming that (a) there is no free water remained in sand because all of it has been absorbed by bentonite, (b) there is a continuous matrix of saturated bentonite and sand particles acting relatively impervious and (c) the presence of sand does not affect the bentonite fabric (Chapuis, 1990; Farajollahi and Wareham, 1998).

Grain size distribution of the base material (sand), the geological origin and the incident resulting in formation of material, whether natural or artificial, are the other factors affecting the permeability of a sand-bentonite mixture. Hydraulic conductivity of sand and bentonite mixtures were studied in different studies and found to vary from 1×10^{-6} m/s to 1×10^{-11} m/s for sand with different amounts of Na-bentonite. It was also confirmed that with the same dry density, the permeability reduced with increase of bentonite content (Kumar and Yong, 2002; Chalermyanont and Arrykul, 2005; Ameta and Wayal, 2008) and furthermore it is proved that the sand mixed with Na-bentonite had less hydraulic conductivity at a certain dry density compared to sand mixed with Ca-bentonite.

Kumar and Yong (2002) comprehended that reduction in hydraulic conductivity (k) of sand-bentonite mixtures was because of high specific surface of betonite particles, that allow them to hold a part of water on double layer and not let the water molecules flow as freely as the remaining water in the voids. They also concluded that the high swell potential of the bentonite and fineness of bentonite particles are the main reasons in reduction of hydraulic conductivity.

On the other hand, decrease in hydraulic conductivity of sand-bentonite mixtures could be due to bentonite forming a gel or paste, by adsorbing water, around the sand particles that fills most of the pores and restricts the water connectivity between the voids, which leads to slower water flow and hence reduction in permeability. Alternatively, the very fine bentonite particles lower the hydraulic conductivity by reducing the clod size and elimination of inter-clod pores that could cause smaller minifabric pores (Kumar and Yong, 2002).

1.2.5 Shear Strength of Sand-bentonite Mixtures

The structure and fabric in compacted soils is dependent on the compaction conditions, like compaction effort, water content and dry density (Tripathy et al., 2003). Kumar and Yong (2002) state that adding bentonite to a soil mixture results in a reduction in interparticle repulsion and hence an increase in flocculation of the soil structure. Lambe (1969) affirmed that higher repulsion leads to lowering shear strength, therefore the sample would have a greater shear strength since bentonite is added and repulsion is reduced. Knowing that for an average particle spacing and at any given void ratio the dispersed particles are weaker. Therefore higher flocculation

rate means a more random particle orientation, and thus a greater shear strength by increase of bentonite content (Kumar and Yong, 2002).

Chalermyanont and Arrykul (2005) found that bentonite added to the mixture decreases the shear strength when soaked in water, because of its high swell potential. The cohesion of the samples would increase parallel to the increase of bentonite content. Even by addition of small amounts of bentonite, such as 5%, properties of sand would change from sand-like material with high friction angle and low cohesion to clay-like material with low internal friction angle and high cohesion. However, it is also mentioned that in high contents of bentonite, in case of high hydration, the swell would be so high that there would be no significant change in hydraulic conductivity and the mixture becomes gradually cohesionless and hence attain weak shear strength.

1.3 Enhancement of Cement in Sand-bentonite Mixtures

Stabilizing soil with cement addition is an economic common practice in many engineering applications for improving the engineering properties of soil. Majority of soils can be stabilized by adding 7% to 16% cement by volume. The granular soils need lower amounts of stabilizer while plastic soils like silt and clay need higher amounts, though for some soils, proportions higher than 16% may be needed to fulfill the requirements of design criteria (Laguros, 1962).

Cement may be used in small quantities as an additive to increase strength of compacted sand-bentonite, reduce hydraulic conductivity and possibility of crack formation (Maher and Ho, 1993; Kvennas et al., 2009; Consoli et al., 2010; Verastegui Flores et al., 2010; Consoli et al., 2013).

.

Effect of curing in cement hydration process within the soil leads to formation of elongated tobermorite-like gels, calcium silicate hydrates (CSH), around the soil particle edges and with further curing the CSH fibers increase and result in a homogenous structure that combine the particles of clay and cement together. The change in structure and fabric of soil developed by this process reflects in mechanical properties of soil in terms of increasing strength and durability. The hydration process proceeds over a long period yet at a continuously decreasing rate (Mitchell and El Jack, 1966).

According to Grubbs (1965) the degree of stabilization achieved by cement addition in soils depends on type of soil, amount of cement added, amount of free water in soil during compaction and density achieved after compaction. The calcium ions released during the initial cement hydration reactions and the cation exchange leads to reduction in plasticity of the cement stabilized soil. Bonding between the adjacent soil grains and cementation is the other effect of cement addition to cohesive soils.

1.4 Aims and Scope

This study presents an approach to select a composite material to be used as landfill cover/liner. An extensive experimental work was performed for determining volume change, hydro-mechanical properties, strength properties and durability of statically compacted sand bentonite mixtures in comparison to samples containing 5% cement. The influence of cement addition on compaction properties, swell behavior, compressibility, shrinkage, soil water characteristic curve, durability and compressive, tensile and flexural strength of sand-bentonite mixtures were studied through various test methods.

This study is an experimental work aimed to verify the usage of cement together with sand and bentonite as landfill cover and liner materials.

1.5 Outline of the Thesis

In Chapter 2 initially a review of sand bentonite and cement properties are given. In order to find the right mixture of sand and bentonite, and to observe the effect of cement on it some experiments were carried out. The samples are 10% and 15% bentonite-sand mixtures and 5% and 10% bentonite-sand with 5% cement addition. The results from the compaction and swell-compressibility tests and hydraulic conductivity determinations were used to choose the suitable material proportions for the rest of the research.

In Chapter 3, volume change properties and durability of 85% sand-15% bentonite are studied in comparison to 80% sand-10% bentonite-5% cement through a set of experiments. Durability tests included volume change studies under aging effect, cyclic swell-shrink, effect of saline water (1 mol. NaCl) permeation and elevated temperature (60°C). This chapter also includes the unsaturated behavior of the compacted mixtures.

Chapter 4 has focused on importance of strength properties of sand-bentonite and sand-bentonite-cement samples were studied via different experiments. Tensile strength of samples was tested indirectly using three methods (flexural strength, split tensile, double punch) and the results were correlated with each other as well as unconfined compressive strength for different curing periods. For flexural strength determination, a beam shaped mold was designed and a modified test method was carried out to measure and compare the flexural strength of samples. An empirical

method was used to predict undrained cohesion and internal angle of friction of samples relating to tensile and unconfined compressive strength. For split tensile and double punch tests modifications to triaxial testing system were made.

In Chapter 5, the achievements of this study are discussed and overall conclusions are given together with the recommendations for further research.

Chapter 2

DETERMINATION OF THE SUITABLE SAND-BENTONITE-CEMENT PROPORTIONS

2.1 Introduction

Rapid development of industry in the recent decades has led to production of huge amounts of waste every day by factories and building industry. Quantity of leftovers and urban garbage has also increased drastically, of which most of it is burnt or simply stored in waste dumps, while some are recycled and fed back to the industry (Bielinski et al., 2001; Kazimoglu et al., 2003). Thus, environmental problems increased imposing a major health hazard. Various methods of minimizing hazardous accumulation of waste are proposed, which include storage in impermeable compacted buffer materials. The use of such layers which consist of clays and sand-bentonite mixtures or synthetic materials that possess low permeability prevents the contaminant transport to environment.

2.2 Literature Review

Compacted clay barriers, which constitute covers and liners, are the most significant parts of landfills. Wherever available, soil found on-site and local soils are generally used to build these barriers, if they are suitable to be compacted to standard specifications, providing the desired hydraulic conductivity. In semi-arid regions prone to cyclic wetting-drying due to prolonged periods of dryness followed by short but occasional flooding rains, barriers are continuously subjected to repetitive cycles of wetting and drying. In such areas clay amended soils are used instead, such as

compacted sand-bentonite mixtures, due to their low hydraulic conductivity. Material selection for barriers is usually based on local availability, and different soil types both natural and processed clays can be used as barrier materials.

2.2.1 Bentonite

Bentonite as a clay material with high amounts of montmorillonite appears to be a good option due to its high water absorption capacity and very low hydraulic conductivity, which are categorized as sodium or calcium bentonite based on the external cation adsorbed during mineral formation. Sodium bentonite is more widely used than calcium as it has a much higher swell capacity and very low hydraulic conductivity. Montmorillonite is an alteration product of volcanic ash, a highly colloidal mineral composed of one gibbsite sheet squeezed in between two silica sheets. In between each layer of montmorillonite there are few amounts of exchangeable cations and large quantity of water molecules. The negative charge of outer layer of this mineral attracts water molecules and it makes the basal spacing of it to range from 9.6 Å to complete separation in full hydration (Mitchell1 1993; Das 2006). When water comes in contact with montmorillonite it penetrates into spaces between its layers. The amount of water held in between the clay sheets can vary from one to four molecules depending on type of cation and vapor pressure, this property results in huge amounts of volume change in some clay types (van Olphen, 1963). The fluid enters to the inter layer of sodium montmorillonite and forms a thick viscous diffuse double layer around the clay sheets, causing the clay particles to swell. This swelling can continue till complete separation of the clay sheets (Kenney et al., 1992).

2.2.2 Sand-bentonite Mixtures

Desiccation of waste containment material leads to crack formation, and hence creation of preferential flow paths for hydraulic leakage. Sand-bentonite mixture can meet the hydraulic conductivity criteria without suffering from shrinkage cracking provided bentonite content is not too high which may cause shrinkage cracking upon desiccation and thus leakage of contaminants. Bentonite is used as a sealing material in disposal systems because of its high swelling capacity, water retention properties, and low hydraulic conductivity. When wet, the clay fills the sand voids producing a very low hydraulic conductivity for the mixture (Mollins et al., 1996). Using sufficient amounts of bentonite will produce a combination that can absorb water and swell in saturated condition and simultaneously be fairly resistant to desiccation cracks in dry seasons (Stewart et al., 2003). The sand component of the mixture decreases the shrinkage on drying and below a certain bentonite content the sand particles are in contact, providing mechanical stability and preventing shrinkage. The granular particles of sand maintain the strength and stability of composite while the small particles of bentonite seal the voids between them and reduce the hydraulic conductivity. Initially when compacted as a liner material, it will be in unsaturated condition, possessing a high suction capacity, absorbing water from the surrounding geological medium. The hydraulic conductivity and the swelling capacity are very much dependent on the confining conditions, temperature, composition and quantity of water available.

Engineering specifications for landfill liners permit a hydraulic conductivity lower than 1×10^{-9} m/s and requires the stability of the system in the operation process. To achieve these goals suitable materials must be selected which is usually based on

local availability, and until present many different soil types, both natural or processed have been used. The type of clay preferred for this purpose is bentonite, due to its high swelling capacity, hence less amount can be used. The least amount of bentonite providing the aforementioned requirements is preferred to minimize the cost. According to the hydraulic conductivity tests using distilled water, if bentonite content is more than 5% by dry weight, the requirements are satisfied. However, conditions such as landfill leachate permeation and elevated temperatures in the landfill may increase the hydraulic conductivity (Mollins et al., 1996). Low hydraulic conductivity requires continuity of the bentonite matrix within the mixture, and this in turn requires both adequate bentonite content and adequate bentonite distribution (i.e. mixing). In well-compacted mixtures containing up to 20% bentonite in dry mass, sand forms the load-supporting framework and gives the mixtures dimensional stability or in other words, crack resistance at macro level (Kenney, 1992).

The swelling properties of compacted FEBEX (full-scale engineered barriers experiment) bentonite and the influence of initial water content and dry density were studied by Lloret and Villar (2007). According to this study swelling deformation of heavily compacted bentonite is majorly affected by the vertical pressure applied on the sample during its saturation. It is also mentioned that increase of dry density results in an exponential increase in swell pressure and swelling strain. However, the effect of initial water content on swelling properties of bentonite was found to be lower than the effect of initial dry density. Muntohar and Hashim (2003) concluded that swelling pressure, swelling and compressibility increase of kaolinite and bentonite mixed with sand has a direct relation with bentonite content. Furthermore, the swelling and compressibility behavior of samples is affected by size and

percentage of non-swelling fraction of soil. They also divided the swelling process into three stages, initial swelling, which the swell is happening within the inter-voids, primary swelling and secondary swelling. Sällfors and Öberg-Högsta (2002) studied the hydraulic conductivity of sand-bentonite mixtures, focusing on variation of the hydraulic conductivity as a function of bentonite content, compaction and degree of saturation. They proposed a parameter which reflects the amount of bentonite per pore volume and can be calculated based on the amount of bentonite and the dry density of the soil mixture. Thus, the hydraulic conductivity could be predicted as a function of different degrees of compaction. Chalermyanont and Arrykul (2005) indicated that addition of 5% bentonite or more can decrease the hydraulic conductivity of sand bentonite about four orders of magnitude. Komine and Ogata (1999) performed an experimental work on sand bentonite mixtures to be used for disposal facilities of radioactive wastes from nuclear power stations. They have stated that swelling characteristics of sand-bentonite mixtures is dependent on the dry density and bentonite content of mixtures. Using scanning electron microscopy analysis they observed that the voids of mixtures were filled up by the volume increase of hydrated bentonite.

2.2.3 Cement Enhancement

Cement can be used as a secondary additive in order to increase the strength of the compacted sand-bentonite, reduce the hydraulic conductivity and possibility of crack formation. Using small amounts of cement in stabilizing the soil, both as slurry or mixed with soil is studied by many researchers (Stavridakis and Hatzigogos, 1999; Bellezza and Fratalocchi, 2006; Tchakalova and Todorov, 2008). A major factor in considering a soil-cement liner for sanitary or hazardous waste landfill sites is its compatibility with stored wastes. Adaska (1985) in testing on a full scaled hydraulic

barrier indicated that after one year of exposure to leachate from municipal solid wastes such as toxic pesticide formulations, oil refinery sludge, toxic pharmaceutical wastes and rubber and plastic wastes, the soil-cement got hardened considerably and cored like Portland cement concrete, in addition, it became less permeable during the exposure period. Bellezza and Fratalocchi (2006) presented the results of an experimental study on effectiveness of 5% cement in compacted soil-cement mixtures considering 28 days curing time. The Proctor standard effort was used to prepare their samples and they reported that for soils having fine fraction > 20% and plasticity index of >7 hydraulic conductivity was always less than 2×10^{-7} cm/s, which is a reasonable hydraulic conductivity for the waste containments. They finally concluded that adding 5% cement can be adequate to guarantee a low hydraulic conductivity provided that the in situ mixing, compaction procedure and curing conditions are kept close to the laboratory test conditions.

This chapter investigates the possibility of using locally available beach sand amended by commercially available bentonite and choosing the most suitable mixture, through studying compaction, swell and compressibility characteristics of different proportions of sand and bentonite with and without cement enhancement. Particular attention was given to the saturated hydraulic conductivity of the selected mixtures to be below the maximum allowed value of 1×10^{-9} m/s. A more comprehensive experimental investigation on the aging effect, durability, unsaturated behavior and strength characteristics are included in Chapters 3 and 4.

2.3 Materials and Methods

2.3.1 Materials

As a base material poorly graded sand from Silver Beach near Famagusta, North Cyprus was selected, with uniformity coefficient C_u= 1.53, coefficient of curvature C_c= 0.99, effective diameter D_{10}= 0.14 and mean diameter D_{50}= 0.20. The sample was taken in autumn after repetitive rains and therefore the amount of soluble salts was very low, and it was concluded that there was no need to wash off the salts before utilizing in this study. The primary cementing material used was bentonite (non-treated) obtained from Karakaya Bentonite Inc., Turkey. The selected material is a clay mineral and is in accordance with standard specifications for drilling fluids, API 13 A. It is completely natural with a sodium-based content and contains at least 90 % montmorillonite. It is in conformity with TS EN 13500 (Nontreated Bentonite Specifications). It easily disperses and does not become lumpy when added to water. Bentonites include mostly montmorillonites with minor amounts of non-clay minerals, such as quartz, dolomite and feldspars. Commercial bentonite is mainly montmorillonite with some impurities, such as quartz. Landfill liners are constructed with Na-montmorillonite. Montmorillonite contains alumino-silicate minerals with a structure of 2:1 unit layer (lamellae) which are 10 Å thick. Montmorillonite unit particles contain 1-16 lamellae. The unit particles aggregate to form clusters in 10^7-10^9 in numbers. Therefore unit layers (lamellae form unit particles, and the unit particles form particle clusters. Therefore, as far as pore sizes are concerned there are interlayer pores, interparticle pores (micropores) and intercluster pores (macropores). The XRD images of cement, bentonite and sand used in study are shown in Figure 2.1.

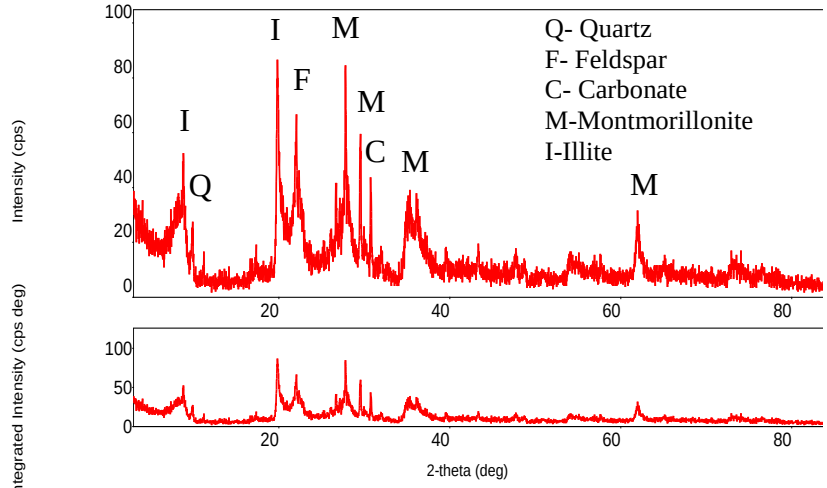

(a)

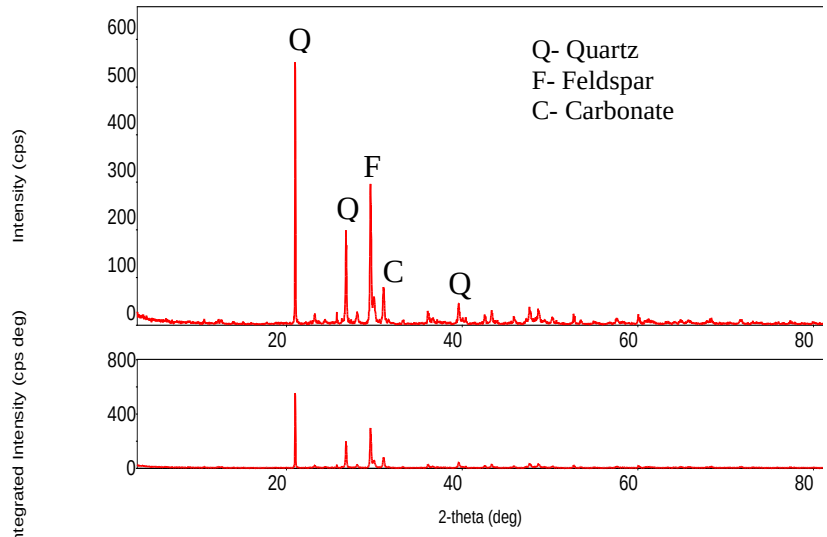

(b)

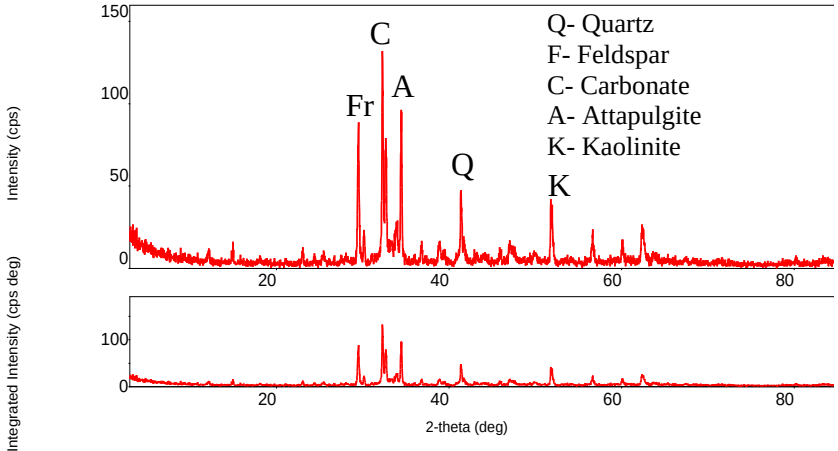

(c)

Figure 2.1. XRD images of (a) bentonite, (b) cement and (c) sand.

Material used in this study possesses a high swelling capacity, with liquid limit of 486% and plastic limit of 433%. The chemical composition in Table 2.1 reveals that it is a pozzolanic material with total percentage of SiO_2, Al_2O_3 and Fe_2O_3 being more than 70%.

Table 2.1. Chemical composition

Oxides	**Amount (%)**
SiO_2	61.28
Al_2O_3	17.79
Fe_2O_3	3.01
CaO	4.54
Na_2O	2.70
MgO	2.10
K_2O	1.24

2.3.2 Sample Preparation

The mixtures of 15% bentonite-85% sand, 10% bentonite-90% sand, 5% bentonite-5% cement-90% sand and 15% bentonite-5% cement-80% sand by dry weight were prepared by pre-drying sand and bentonite in oven at 40°C. Sand was then passed through a 2.00 mm sieve to limit the impurities like sea weeds and shell fragments. Measurement of specific gravity of bentonite through normal test standards for soils was not applicable because of its very high adhesive characteristics and swell potential. Therefore, the standard test method for measurement of density of hydraulic cement was applied using kerosine (ASTM, C 188-09). After measuring specific gravity of sand and cement the specific gravity of the mixtures were calculated by Equation 2.1 suggested by Montanez (2002), the measured and calculated specific gravities are shown in Table 2.2.

$$G_s = \frac{100}{\left(\%\frac{sand}{G_{sand}}\right) + \left(\%\frac{bentonite}{G_{bentonite}}\right) + \left(\%\frac{cement}{G_{cement}}\right)} \tag{2.1}$$

Table 2.2. Properties of used materials and mixtures.

	Sand	Bentonite	Cement	10%B-90%S	15%B-85%S	15%B-5%C-80%S	5%C-5%B-90%S
Gs	2.684	2.508	3.137	2.665	2.656	2.676	2.694

C:Cement, B: Bentonite, S: Sand.

The optimum water content and maximum dry density were calculated through standard Proctor compaction test ASTM D698. In order to attain homogenous moisture content within each sample, the batches were mixed thoroughly in mechanical mixer, sealed in double nylon bags and kept 24 hours previous to each compaction. For the cement included samples, half of the water and cement were preserved and added to the mixture just before the compaction.

2.3.3 One-dimensional Swell Test

Soils susceptible to swelling can be identified by classification tests. These identification procedures were developed by correlations of classification test results with results of one-dimensional swell tests performed in oedometers (ASTM-D2435) on compacted soil specimens. To investigate the swelling characteristics of sand bentonite and sand bentonite cement mixtures in this study, one dimensional swell test was carried out using oedometers. In Figure 2.2 the schematic of oedometer cell used for swell and consolidation tests is shown. Mixtures were prepared 24 hours prior to the test at their optimum water content, and were statically compacted in rings of 50 mm inner diameter and 19 mm height. In order to obtain identical samples at targeted maximum dry density, the wet mass needed to reach the volume of sample (50 x 14mm) was calculated and placed inside the consolidation rings. In order to place all the sample inside the ring, bulk mixture was softly tapped with the help of a metal rod. The sample inside the ring then was statically compacted with a 50 mm diameter metal hammer attached to a CBR machine with 28 kN load ring at a rate of 1 mm per minute. 5 mm extra space between top of sample and edge of ring

was left for probable swelling. At the end of preparation samples were weighed to make sure the target mass +/- 1 gr was reached. The samples were then covered in cellophane and left in desiccator for curing.

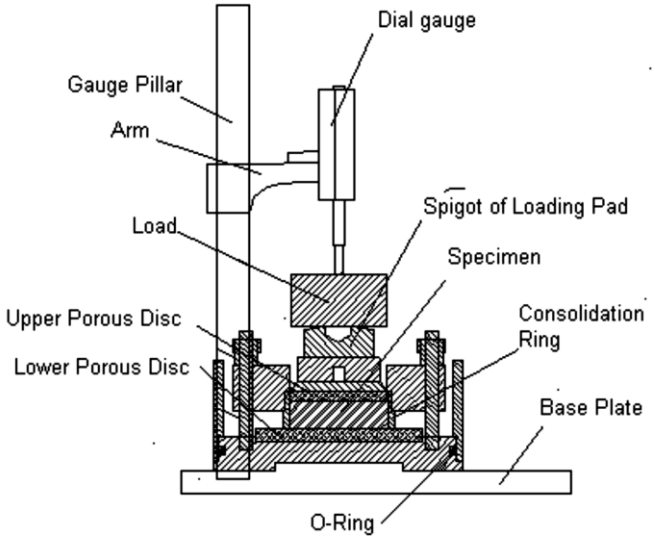

Figure 2.2. Schematic of one-dimensional swell equipment (Bilsel, 2002).

For swelling test the samples were inundated under a low surcharge of 7 kPa and swell was measured through time. Specimens were allowed to swell until the increase in free swell with time became marginal. The effect of sand on compressibility properties of natural bentonite was investigated by one-dimensional consolidation test applying consolidation pressures up to a maximum of 3530 kPa.

2.4 Experimental Results and Discussions

This section includes the results of preliminary testing on different mixtures of selected materials, accomplished to choose the most suitable proportion of a sand-bentonite barrier material with and without cement enhancement. Further and more detailed experimental analyses and results on the hydro-mechanical behavior of the selected mixtures are included in the subsequent chapters.

2.4.1 Compaction Test

In all of the samples, addition of more bentonite to the mixture increases the optimum water content and maximum dry density. Higher optimum water contents are due to the higher water holding capacity of bentonite in comparison to sand. On the other hand, fine particles of bentonite work as a lubricant between the sand grains and by making a decent matrix, lead to a better compaction and hence higher dry densities. Compaction curves of both 10% and 15% bentonite added mixtures are quite flat showing that the small water content variations would not affect the dry density noticeably. However, addition of cement to the mixture will increase the maximum dry density significantly due to the higher specific gravity of cement, cementing action and reduction of water absorption. Cement containing samples demonstrate high sensitivity to water content variations and small increments of moisture cause visible reductions in dry density. The Proctor compaction curves are shown in Figure 2.3. Since sand is not capable of adsorbing water replacement of 5% sand with cement in 15%B-5%C mixture did not have a noticeable effect on optimum water content compared to 15% B mixture with no cement, although dry densities increased with addition of cement. Reduction of bentonite in 5%B-5%C mixture causes decrease in optimum water content, although it has an appreciable increase in maximum dry density. The compaction characteristics are given in Table 2.3.

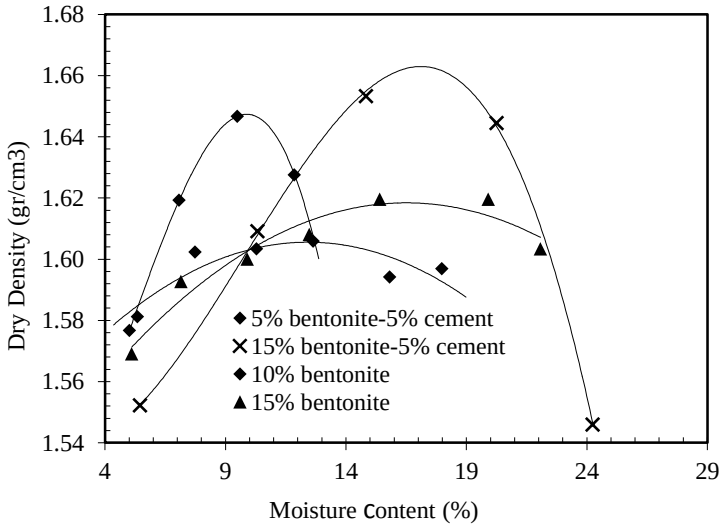

Figure 2.3. Compaction curves.

Table 2.3. Compaction characteristics of samples used.

Compaction parameters	10%B-90%S	15%B-85%S	15%B-5%C-80%S	5%C-5%B-90%S
Maximum dry density (g/cm^3)	1.606	1.624	1.663	1.65
Optimum water content (%)	12.50	17.00	17.00	9.50

2.4.2 One-dimensional Swell Behavior

One dimensional swell test was carried out on two statically compacted samples from each mixture compacted to maximum dry density and optimum water content. The average preliminary swell curves are plotted in Figure 2.4. While 15% bentonite containing samples swelled up to 32%, reducing the bentonite by 5% amount caused the samples to swell 20% less. However, addition of cement to the mixtures lead to strong bonding between the soil particles and prevent swelling; therefore the maximum swell of cement containing 5% bentonite and 15% bentonite mixtures were not any higher than 0.02%.

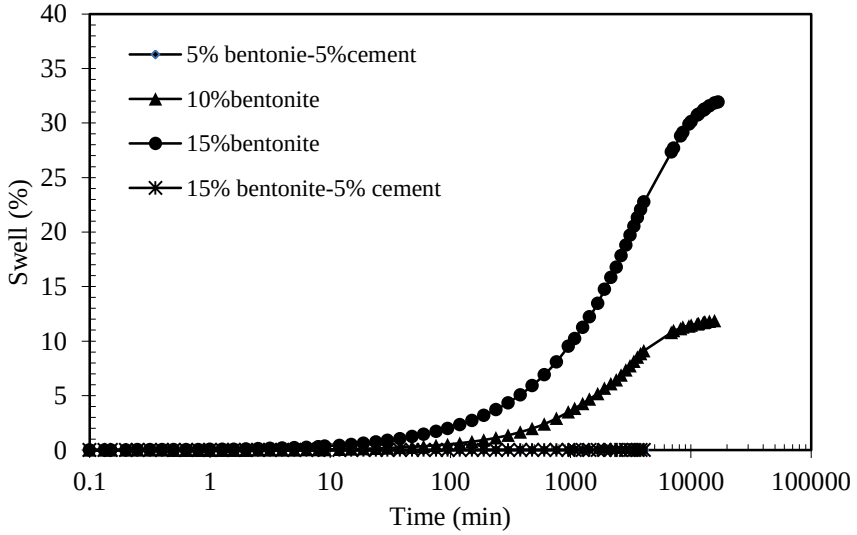

Figure 2.4. One dimensional free swell curves.

2.4.3 Consolidation Test Results

Oedometer test was performed on swelled samples and the average results are plotted in Figure 2.5. The test results present a considerable reduction in the compression and rebound indices when cement is added to sand-bentonite. Therefore sand-bentonite mixture which possesses high compressibility and swell index when mixed with cement experienced a noticeable reduction in volume change, which is a desirable mechanical behavior as far as waste barriers in semi-arid climates are concerned. A wide extent of volume changes would lead to detrimental effects on the performance of the barriers, changing the fabric and hence the most important parameter which is the hydraulic conductivity, either in saturated or unsaturated states. Further study of these results can lead to the confirmation of swelling pressures being considerably reduced due to marked reduction in plastic properties of soil samples, hence the decrease in swell potential.

Preconsolidation pressure of compacted soils can be considered as a degree of bonding created by stresses of compaction. Lower the preconsolidation stresses,

lower will be the expected one-dimensional swell. A distinct improvement can be observed on the compressibility and swelling properties in cement added specimens which are presented by a comparatively flat curve in Figure 2.5.

Consolidation curve of 15% bentonite content samples were very steep showing a high void ratio variations between 7 and 1569 kPa pressures. Reduction in the amount of bentonite makes a significant difference by lowering the void ratio and compressibility at the initial point. Comparing with 15% bentonite mixture, lower void ratio of 10% bentonite content mixtures in the starting point explain a better compaction and denser sample. The volume change of cement containing samples were very low in both swell and consolidation parts. Smooth curves with small changes of void ratio under different loads are observable characters of stable dense samples containing cement.

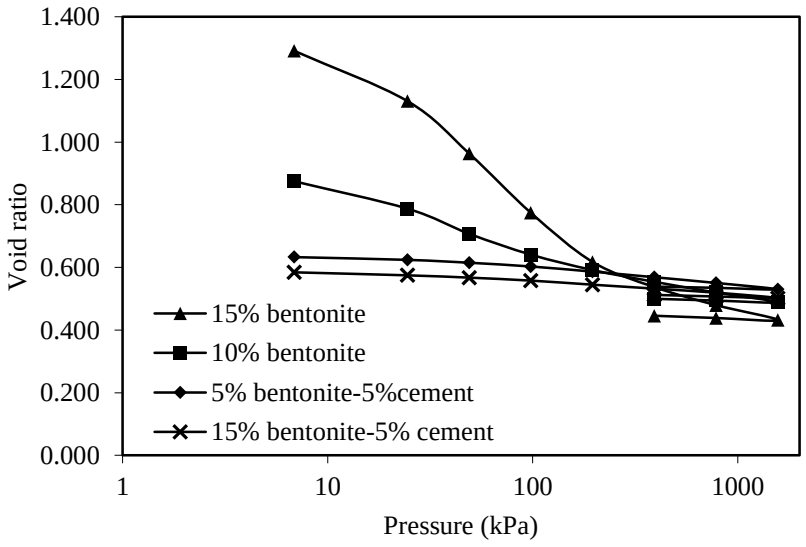

Figure 2.5. Consolidation test results.

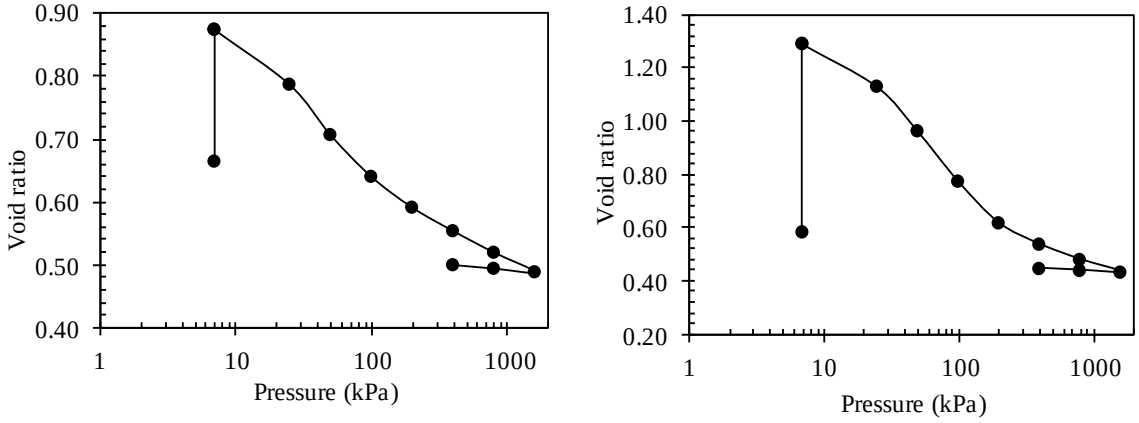

(a) (b)

Figure 2.6. Consolidation curves of (a) 15% bentonite and, (b) 10% bentonite samples.

The samples without cement had a high tendency for swell as shown in Figure 2.6. The compressibility is also high but the curves surprisingly display two different slopes. It is suggested that sand-bentonite mixtures containing different amounts of bentonite can exhibit two characteristic conditions: at lower than a threshold stress (approximately 200 kPa) the behavior of the mixture is similar to the clay alone, the bentonite particles tend to separate sand particles and support the whole of the applied pressure. A threshold pressure level is finally reached after which there is little variation in the void ratio with increasing effective pressure which can be inferred that the incremental stress from the threshold value forward is carried mainly by the sand. As the bentonite particles are mostly consolidated, the sand matrix supports most of the stress (Stewart et al., 2003). The bilinear characteristic of sand-bentonite is clearly visible in graphs of void ratio versus pressure. As it is shown in Figure 2.6 the slope changes at about the same values of initial void ratio, meaning that the bentonite part of soil absorb the water and swells leading to higher void ratios. Subsequently, the same part of sample gets compressed when it is exposed to stress and gradually leave out the water till it reaches the initial void ratio, the point at which sand particles appear to be the main part of mixture. From this

point onward the sand particles are the dominant structure of soil tolerating the stress and since sand cannot be compressed as much as bentonite, the slope of curve and coefficient of compressibility decrease. Compression index before and after the threshold stress is shown as C_{c1} and C_{c2} in Table 2.4. Based on the swelling-compressibility behavior it can be concluded that the mechanical behavior of bentonite consists of a microstructural level due to swelling of active minerals, and macrostructural level at which major structural changes occur. This observation is in good agreement with the findings of Gens and Alonso (1992), who stated that bentonite supports load by the contact between the clusters and by diffuse double layer in the pores in between clusters, and that below 200 kPa vertical stress, bentonite void ratio decreases almost linearly, whereas above 200 kPa the void ratio still changes with pressure but at a much slower rate.

Comparison of cement added mixtures shows that the amount of bentonite added to the mixture was not enough to break the cementitious bonds between soil particles and both of 15% and 5% bentonite mixtures with cement show low compressibility and no swell pressure.

Table 2.4. Consolidation parameters.

Mixtures	C_{c1}	C_{c2}	C_r	c_v (m^2/min)	(7-200 kPa)	(200-1570 kPa)	Swell Pressure (kPa)
					m_v (m^2/N)	m_v (m^2/N)	
15B-85S	0.468	0.141	0.0183	3.93E-6	1.63E-03	7.96E-04	250 kPa
10B-90S	0.212	0.103	0.0199	4.97 E-6	6.99E-05	4.08E-05	80 kPa
5B-5C-90S	0.057	_____	0.0179	5.64 E-6	1.58E-04	2.40E-05	
15B-5C-80S	0.053	_____	0.0186	2.59 E-6	8.36E-05	1.65E-05	

B:bentonite, C:cement, S: sand

Since the amount of settlement in a specimen subjected to surcharge load has direct relationship with the drainage of water through the sample, therefore the saturated

hydraulic conductivity of samples can be empirically calculated from Equation 2.2, given the coefficient of consolidation, $c_{v,}$ and coefficient of compressibility, m_v. These parameters were also evaluated in four different stress ranges from compression curves:

$$k_s = \gamma_w . m_v . c_v \tag{2.2}$$

where, k_s is saturated hydraulic conductivity and γ_w is unit weight of water. c_v was calculated from Equation 2.3.

$$c_v = \frac{T_v \times H_{dr}^2}{t_{90}} \tag{2.3}$$

where H_{dr} is height of drainage equal to half of height of sample, T_v is the time factor, and t_{90} is the time that 90% of consolidation is completed obtained from deformation versus root time plot. Coefficient of volume compressibility in any pressure range can be calculated from Equation 2.4.

$$m_v = \frac{a_v}{1 + e_0} \tag{2.4}$$

where a_v is the coefficient of compressibility calculated from Equation 2.5, and e_0 is the initial void ratio of the selected pressure range.

$$a_v = \frac{e_0 - e_1}{p_1 - p_0} \tag{2.5}$$

where e_0 and e_1 are the first and last void ratios of considered range and p_1 and p_0 are the last and first effective consolidation pressures of the pressure range.

All samples displayed low hydraulic conductivity as expected due to presence of bentonite. The very fine particles of bentonite reduce the permeability of the mixture by filling the voids between the sand particles. As Kumar and Yong (2002) indicate low hydraulic conductivity of sand-bentonite mixtures is because of high specific surface of bentonite particles that allow them to hold a portion of water on their double layer and prevent water molecules from flowing among voids. They conclude that high swell potential and fineness of bentonite are the main reasons in reduction of hydraulic conductivity.

Addition of cement considerably reduces the hydraulic conductivity by forming cementation bonds between the particles and reducing the connected pores which can lead the water flow. The hydraulic conductivity of samples under higher ranges of pressure is less than the hydraulic conductivity of the same sample exposed to lower pressures. When the effective consolidation pressure increases, particles tend to rearrange, bentonite working as a lubricant gel in between sand particles, enabling denser packing of particles without breakage.

Table 2.5. Saturated hydraulic conductivity, k_s (m/s).

Effective stress range	Soil mixtures			
(kPa)	15B-85S	10B-90S	5B-5C-90S	15B-5C-80S
7-200	0.92×10^{-9}	0.62×10^{-9}	0.47×10^{-9}	0.353×10^{-10}
200-1570	0.36×10^{-10}	0.31×10^{-10}	0.25×10^{-10}	0.700×10^{-11}

B:bentonite, S:sand, C:cement

For achieving a low permeability it is essential that the bentonite matrix has continuity in the mixture, in other words a homogenous mixture is required to ensure that the hydraulic conductivity measured is representative of the mixture. A heterogenous mixture leads to occurence of more permeable channels within the microstructure, hence increased hydraulic conductvity. Hence, low hydraulic

conductivity requires continuity of the bentonite matrix within the mixture, and this in turn requires both adequate bentonite content and adequate bentonite distribution (i.e. mixing).

Based on the saturated hydraulic conductivity values in Table 2.5, it can be concluded that mixture denoted by 15B-5C-80S has given the most suitable hydraulic conductivity, less than 10^{-9} m/s over both effective stress ranges selected, which is the maximum allowed value given in the Landfill Manuals of the Environmental Protection Agency (EPA, 2000).

2.5 Conclusi64ons

From the experiments carried out and analyses of the results it can be concluded that:

1. In all of the samples, addition of more bentonite to the mixture increases the optimum water content and maximum dry density. Fine particles of bentonite work as a lubricant between the sand grains and by making a decent matrix, lead to a better compaction and hence higher dry densities.
2. Addition of cement to the mixture increases the maximum dry density drastically. Cement containing samples demonstrate high sensitivity to water content variations and small increments of moisture cause visible reductions in dry density.
3. 15% bentonite content samples swelled up to 32% while 10% bentonite content samples have strains of 12% under 7 kPa surcharge.
4. Addition of cement to the mixtures leads to strong bonding between the soil particles and prevent swelling.

5. The volume change of cement containing samples were very low in both swelling and consolidation processes. Small changes of void ratio under different loads is a noticeable character of stable dense cement containing samples.
6. The bilinear characteristic of sand-bentonite is clearly visible in graphs of void ratio versus pressure. The slope of both 10% and 15% SB curves change at about the same value of initial void ratio of 0.60 and effective consolidation pressure of 200 kPa.
7. In sand-bentonite composites, bentonite absorbs the water and swells to higher void ratio. Subsequently, the same part of sample gets compressed when it is exposed to stress and gradually leaves out the water till it reaches the initial void ratio, the point at which sand skeleton appears to take the load. From this point onward the sand particles are carrying the applied load and therefore, slope of curve decreases.
8. All samples displayed low hydraulic conductivity due to presence of bentonite. The very fine particles of bentonite reduce the permeability of the mixture by filling the voids between the sand particles.
9. Addition of cement reduces the hydraulic conductivity significantly by creating bonds between the particles and reducing the connected pores which can lead the water flow.
10. The hydraulic conductivity of samples under higher ranges of pressure is less than the hydraulic conductivity of the same sample exposed to lower pressures.

Finally based on the first stage of the experimental program 80%S-15%B-5%C (SBC) mixture is selected as a possible alternative for a landfill barrier to be recommended in a semi-arid climate, since the compacted specimens of this mixture has yielded the lowest hydraulic conductivity. As a control sample 85%S-15%B (SB) is also selected to further study and investigate the hydro-mechanical and micro behavior with and without cement inclusion in the proceeding chapters.

Chapter 3

VOLUME CHANGE AND HYDRAULIC PROPERTIES OF CEMENT ENHANCED SAND BENTONITE

3.1 Introduction

The hydro mechanical properties of compacted expansive soils and their application in waste containments is still a research topic of interest, mainly using a secondary additive for enhancement of sand-bentonite mixture, such as cement and other pozzolanic additives, observing their effect on physical and engineering properties. This chapter consists of a comprehensive experimental study on the volume change and hydraulic properties of the selected proportions of sand-bentonite mixtures to be used as buffer layers of waste repository, with and without cement enhancement. The volume change properties, hydraulic conductivity and hydraulic properties of compacted sand-bentonite mixtures enhanced with 5% cement (SBC) was tested and compared with results of untreated sand bentonite (SB) samples. Since compacted sand-bentonite with or without cement addition is proposed as the key component of a repository system, its characteristics will govern the behavior of the whole system. Therefore, the effect of cement addition, aging/curing, repeated wetting-drying processes due to climatic changes and/or the drainage of leachates (dominantly NaCl), elevated temperatures due to bio-chemical reactions within the repository must all be understood thoroughly for establishing a sustainable system. This chapter also includes a concise literature on the engineering parameters not explained in Chapter 2, such as shrinkage phenomenon, effect of cement addition to soils,

curing/thixotropic effects, salt permeation and temperature effects on engineering behavior of soils, cyclic swelling-shrinking, and unsaturated soil behavior.

3.2 Shrinkage Behavior

Desiccation in soil results primarily from a thermodynamic imbalance between the soil pore water and its surrounding environment, which motivates evaporation and a transfer of moisture within the soil. Generally, the fluid movement develops through both gaseous and liquid phases. Considering the equilibrium thermodynamics laws, the phase change between vapor and liquid occurs directly at the interface between the phases, therefore, the specific vapors and liquid Gibbs potentials remain equal (Mainguy et al., 2001). This process leads to liquid pressure decrease and suction increase in desiccating region according to Kelvin's law, and simultaneously, it generates a gradient of suction within the soil. External pressures, heat and shrinkage deformations also cause additional pore fluid pressure generation and fluid movements (Peron et al., 2009).

The evaporation and drying mechanism would occur as liquid molecules evaporate easier from the meniscus surface on the warmer area than they do from the surface located in the cooler area. Thus, capillary forces will uplift the pore liquid toward the warmer zone since there will be a difference of surface tensions between menisci (Kowalski, 2003).

Basically the procedure of shrinkage at its micro-scale in a soil is a reduction in pore water pressure and increase in suction which is caused by evaporation at interphase menisci of fluid and air. When the soil is saturated, the interphase of menisci is located at the external edges of soil sample. At the micro-scale this interphase is a

mean of suction application on boundary of soil, which results in increase of effective stress compression on soil matrix and leads into shrinkage. In non-expansive fine soils it can be assumed that mechanisms related to adsorbed water are not dominant for a large range of water content (Peron et al., 2009).

3.3 Cement Stabilization

Chemical stabilization is a widely used soil improvement method. Portland cement is a commonly used cementing material. There are two major chemical reactions governing the behavior of bentonite and cement: the primary hydration reaction when water is added and the secondary pozzolanic reaction between bentonite and cement, when lime is released by cement. The hydration process creates the primary cementitious products, causing the initial strength gain. The secondary reaction, however occurs between the silica and alumina present in bentonite and calcium ions present in cement, forming cementitious products of calcium aluminate hydrates (CAH), calcium silicate hydrates (CSH), and calcium aluminum silicate hydrates (CASH). These cementitious materials as well as calcium hydroxide stabilize both granular and fine-grained soils.

Hydration of the cement inside the sample start with addition of water, it starts with dissolution of cement particles, forming a solution that contains compounds. Eventually concentration of these compounds in water reaches to a point that they precipitate out as solid hydration products on the surface of anhydrous cement. Over time formation of hydration products leads to stiffening, solidification and strength gain. Hydration of the calcium silicates in cement results in production of CSH and CH as given in Equation 3.1 and Equation 3.2. Calcium silicate hydrate CSH is a

poorly crystalline/amorphous component providing the basic strength gain in Portland cement. This strength is mostly due to covalent and ionic bonding within the complex structure and van der Waals bonding in fewer extents. The setting and hardening properties of cement within the sample is related to physical properties of the calcium silicate. Although the gel like hydrates appear amorphous, the electron microscopy study shows their crystalline character. It is interesting to mention that one of the hydrates known as CSH(I), has a layer structure similar to clay mineral structure like in montmorillonite and halloysite (Neville, 1981).

$$2C_3S + 7H \rightarrow C_3S_2H_8 + 3CH \quad (3.1)$$

$$2C_2S + 7H \rightarrow C_3S_2H_8 + CH \quad (3.2)$$

Early product of CSH forms during early hydration and away from surface of cement particles, filling the voids. Late product of CSH forms during later hydration, and it takes shape of the cement grains. The inner/late product tends to be more resistant to physical change during drying of sample. The other product of hydration of the calcium silicates is calcium hydroxide CH or $Ca(OH)_2$. This product does not contribute much to strength gain but keeps the pore water alkaline.

Moreover hydration of the calcium aluminates in Portland cement results in production of ettringite, which is a needle-like mineral. These needle interlocks keep a lot of water and contribute to stiffening of mixture and result in gaining some early strength (Neville, 1981).

3.4 Thixotropy

Strength of remolded soil is lower than that of undisturbed soil, due to breaking of the natural bonds between the particles. If, after disturbance, the soil is kept at

constant density and water content, it regains its strength partially or completely. This phenomenon is known as “thixotropy”, strength regain or age-hardening, described by Mitchell (1993) as isothermal, reversible, time dependent process which occurs under constant composition and volume and involves the hardening of soils at rest, and softening when disturbed (Blazejczak et al., 1995).

Compaction is a rapid process, therefore it cannot maintain water equilibrium at different microstructure levels, inter-aggregate and intra-aggregate pores, inside the sample. Water redistribution occurs in a compacted specimen due to suction equilibration (decrease) at constant water content after compaction, which is a very slow process due to low permeability and strong clay-water bonds (Delage et al., 2006). Aging of compacted sand-bentonite also causes structural changes. According to Rao and Tripathy (2003) particle rearrangement occurs with time causing formation of bonds during the aging process which reduces the swell potential due to increase in shear strength of compacted expansive soils. Therefore, both water redistribution and bonding within the bentonite cause increase in shear strength and decrease in swelling (Ye et al., 2013).

3.5 Durability of the Compacted Landfill Barriers

3.5.1 Cyclic Swell-shrink

Akcanca and Aytekin (2012) worked on influence of wetting–drying cycles on swelling pressures of sand–bentonite mixtures used in the construction of sanitary landfills and the effect of lime treatment. After five cycles of wetting and drying they concluded that the swelling pressure decreases when lime is added to the mixtures, moreover, experiments showed that the beneficial effect of lime stabilization to

control the swelling pressures gets partly lost by the wetting–drying cycles. Study on shrinkage pattern in cyclic swell–shrink behavior of compacted expansive soil specimens done by Tripathy and Subba Rao (2009) revealed that shrinkage of compacted saturated soil specimens to a predetermined height in each shrinkage cycle provides similar conditions as that of the controlled suction swell–shrink cycles. The water content of soil specimens and hence soil suction was found to remain nearly constant for each pattern of shrinkage.

3.5.2 Effect of Temperature

One of the main characteristics of sanitary landfills is the heat generation within the waste, which is due to exothermic aerobic and anaerobic reactions. The aerobic reactions start right after dumping the waste in upper layer of the landfill. These reactions produce a lot of heat and the amount of heat is very much relative to the oxygen consumption. Measurements of generated heat in landfills confirm a peak immediately after the deposit of waste, followed by a reduction and stabilization period. About 80% of heat generation during landfilling process is developed by aerobic waste decomposition. By addition of new layers, the waste can reach less oxygen and a lag-phase of 6 to 12 months with no reactions occurs. After the lag-phase anaerobic methanogenesis reactions start to proceed which is result of enthalpy of the organic matter degradation. These heat generation and transportation of it within the sanitary waste results in a temperature field that range from 30°-60°C. However, the temperature on the surface of landfill stays close to the temperature of environment (Sethi and Molfetta, 2007).

According to literature review liners made of compacted clays are only efficient as long as the heat and moisture fluctuations are not high, otherwise the cracks would be formed and cause hydraulic conductivity to increase (Galvao et al., 2008).

Data taken from landfills indicate that the temperature in liners can reach to 30°C-40°C in normal landfill operations. Though with circulation of leachate the temperature in liner increases faster and may exceed 40°C. Temperatures up to 60°C may occur at the bottom of landfill where the amount of leachate is higher (Rowe, 2005).

Various studies have been carried out on raised temperature effect on behavior of waste system. Villar and Lloret (2004) reported the results on influence of temperatures between 20°C and 80°C on hydro-mechanical behavior of compacted bentonite. Yesiller et al. (2008) determined the cover temperature variations for four different municipal solid waste landfills and stated that the average temperature generally increased by 2°C per meter depth. The measured temperatures within the landfills in different seasons were varying between 13°C-30°C while the average ambient temperature was in the range of -1.5°C-25°C. Arifin and Schanz (2007) used a modified isochoric cell to determine swelling pressure of compacted bentonite and sand-bentonite mixtures at 80°C and reported that increase in temperature reduces the swelling pressure. They also concluded that the reduction in swell pressure is caused by a decrease in hydration force of bentonite within the samples. Therefore, the presence of sand inside the mixtures would be beneficial as it reduces the temperature effects.

3.5.3 Effect of Salinity

In the case of presence of saline solution, less fluid is required to neutralize the negatively charged sheets of sodium montmorillonite. If the valences of the cations inside the solution or ion concentration are large the parting distance between the sheets will stay small. The structure of bentonite in presence of saline fluid is consisting of swollen intact montmorillonite particles, being surrounded by thin viscous diffuse ionic layers (Kenney et al., 1992). Chemical composition of the saturating fluid affects the swelling capacity of bentonite, an increase in salinity of saturation fluid results in decrease of swell potential, however, the role of salinity becomes less noticeable at higher densities (Siddiqua et al., 2011).

The salinity of pore fluid has a significant effect on a range of parameters in soil. Increasing the concentration of NaCl in solution leads to decrease of rate of evaporation and shrinkage and generally increases the stiffness in soils (Najm et al., 2012).

Drame et al. (2007) explains that introducing cement and calcium silicate hydrate CSH to salt solutions results in expansion of samples. To clarify the behavior of cement using explanations of expansion provided by both the osmotic and the electrical double layer (EDL) theories used for explanation of swelling of smectite clays in contact with osmotic media.

3.6 Concepts of Unsaturated Soils

Soil suction is one of the most important parameters governing the response of unsaturated soils. It is commonly referred to as the free energy state of soil water.

The soil suction as quantified in terms of the relative humidity is commonly called "total suction". Matric suction is comprised of the surface attractive forces for water and cations and the surface tension effects of water in soil. The total and matric suctions are shown to be primarily functions of water content and therefore essentially independent of dry density (Krahn and Fredlund, 1972).

3.6.1 SWCC

The compacted sand-bentonite barriers are frequently unsaturated in semi-arid areas. Therefore, soil suction is a key factor in influencing the hydraulic properties, volume change and strength. Hydraulic properties consist of soil-water characteristic curve (SWCC), and hydraulic conductivity function. SWCC is a measure of water storage capacity of soil for a given soil suction. It describes the relationship between the volumetric water content, θ, or the gravimetric water content, w, and the matric suction, ψ_m (u_a-u_w) or the total suction (that is matric plus osmotic suction), ψ_t. It has a similar role as the consolidation curve in saturated soil mechanics, and controls the behavior of hydraulic conductivity, shear strength and volume change at different suctions during wetting and drying processes. Therefore, SWCC can be considered as one of the most fundamental hydraulic characteristics of unsaturated soils. The water content of a soil decreases as suction increases following a drying path (desorption). On the other hand, the water content increases when the suction decreases following a wetting path (adsorption). For engineering practice, however, a single valued function, usually the desorption curve, is used in characterizing the hydraulic properties of unsaturated soils. The drying curve has a breaking point corresponding to the matric suction when the soil starts to desaturate, called the air-

entry value (AEV), and is identified as the suction at which air enters the largest pores of the soil (Fredlund and Rahardjo, 1993; Rahardjo and Leong, 1997).

Soil-water characteristic curve (SWCC) in unsaturated soil mechanics, or the water retention curve (WRC) in soil science represents the relationship between the water retained in the pores, either in terms of gravimetric or volumetric water content, and soil suction. Suction component is the matric suction at low suctions (<1500 kPa) and total suction for high suctions (>1500 kPa). This curve is very vital in deriving the unsaturated soil property functions, which include hydraulic conductivity, shear strength and volume change. In addition to these, SWCC contains significant information regarding the amount of water retained as well as pore size distribution and the stress state in soil-water (Sillers et al., 2001).

Sun et al. (2010) studied the hydro-mechanical behavior of heavily compacted sand bentonite mixtures by measuring the suction both with pressure plate method and filter paper method. The soil-water characteristic curves obtained from both methods display consistent results. Moreover, it was concluded that change in suction paths affects the mechanical behavior of sample. The yield strength of a sample that is first wetted and then dried to a known suction is lower than a sample which is directly wetted to that suction.

In Figure 3.1 three phases of desaturation process is depicted on a typical SWCC (Sillers et al., 2001).

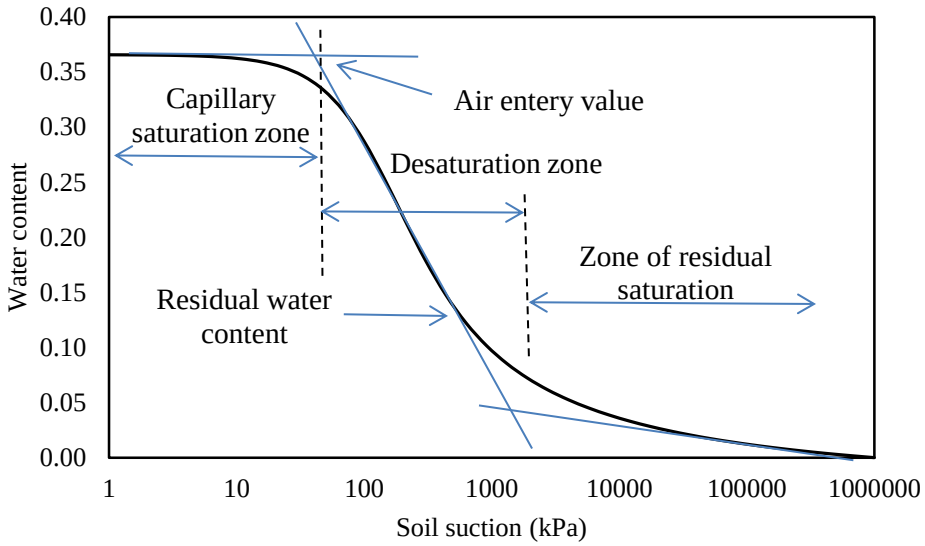

Figure 3.1.Soil-water characteristic curve displaying the desaturation phases.

1. Capillary saturation zone: in this zone, even though the pore-water is in tension, capillary forces can keep the soil almost saturated until the air-entry value (AEV), which is the bubbling pressure at which air starts penetrating the largest pores.

2. Desaturation (funicular) zone: in this zone air displaces the water in the pores progressively until the residual water content is reached. At this value, the water in the pores becomes immobile within the soil matrix, and further increase of suction does not cause any significant change in water content.

3. Zone of residual saturation: water is tightly held to the soil and there is little hydraulic flow through the pores, which occurs mainly as vapor flow. In this zone the term “soil suction” refers to the energy required to remove water from a unit mass of soil. This zone terminates at oven dry condition, when

zero water content is obtained and the corresponding suction is accepted as 1,000,000 kPa. Water is completely withdrawn in this condition.

Soil-water characteristic curve data can be derived from laboratory tests, to which a mathematical function can be fitted. There are many mathematical functions in the literature proposed for this purpose. In identifying conceptual models for the SWCC estimation process, some of the classifications prove to be useful, (a) a soil property function which is a relationship between a physical soil property and either soil suction or the stress state of the soil, (b) a pedotransfer function (PTF) which is a function that has its arguments on basic soil data such as the grain-size distribution or porosity and yields a soil property function. It is like an estimation method that describes the soil-water characteristic relationship based on other soil characteristic, (c) a SWCC which is either a monotonic, single-valued function that yields water content for a given scale of soil-water potential expressed as soil suction or two functions of the monotonic type to describe the drying and wetting branches (Tietje and Tapkenhinrichs, 1993; Fredlund et al., 2002a).

Determining the relationship of water content and suction of the soil samples by direct methods can be expensive and time consuming. Since soil-water characteristic curve is affected by other physical properties, such as texture and structure, it is possible to develop empirical relationships to estimate soil-water characteristic curve. Many attempts have been made to determine the SWCC indirectly from easily measured properties attainable from routine soil survey data. Bouma (1989) introduced the term “pedo transfer function” (PTF), which he described as translating data that we have into what we need, that is predictive functions of certain soil

properties from other easily, characteristically, or economically measured properties (Minasny et al., 1999). Figure 3.2 depicts typical soil-water characteristic curves of different soil types.

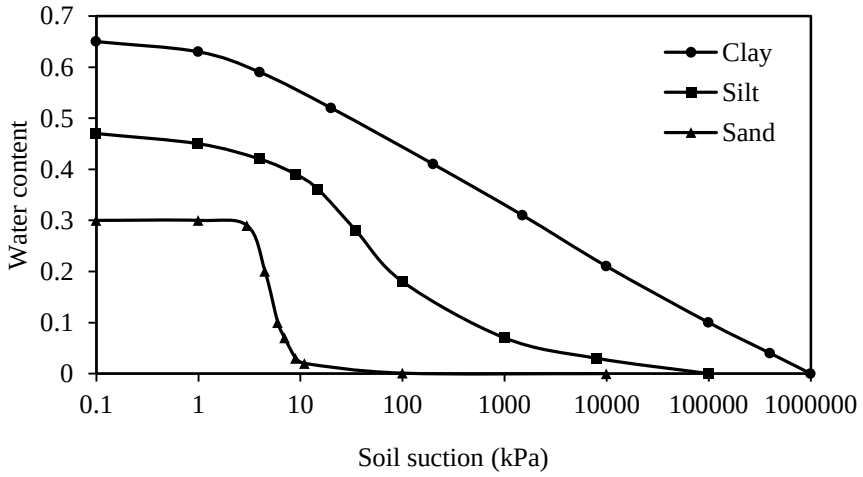

Figure 3.2.Typical soil-water characteristic curves for clay, silt and sand.

3.6.2 Constitutive Surfaces

Constitutive relations for an unsaturated soil can be obtained by forming relationships between the deformation variables and stress variables of soil, which yield the volumetric deformation coefficients (Fredlund and Rahardjo, 1993). The change in void ratio is used as the deformation variable for saturated soils, while for unsaturated soils void ratio and gravimetric water content are used as the deformation variables. Therefore, there will be two constitutive relations, the water phase which describes the variation in volume of water, and the soil structure phase which describes the change in void ratio under different stress conditions. The relationship between void ratio and soil suction shows the limit boundary condition of the void ratio constitutive surface (Fredlund et al., 2002b). The water content and soil structure constitutive equations can be expressed as in Equation 3.3 and 3.4.

$$dw = b_t d(\sigma_{mean} - u_a) + b_m d\,(u_a - u_w) \quad (3.3)$$

$$de = a_t d(\sigma_{mean} - u_a) + a_m d\,(u_a - u_w) \quad (3.4)$$

where,

b_t is coefficient of water content change with respect to a change in net normal stress $d(\sigma_{mean} - u_a)$.

b_m is coefficient of water content change with respect to a change in matric suction, $d\,(u_a\text{-}u_w)$.

a_t is coefficient of compressibility with respect to a change in net normal stress, $d(\sigma_{mean} - u_a)$.

a_m is coefficient of compressibility with respect to a change in matric suction, $d(u_a - u_w)$.

The constitutive equations for an unsaturated soil can be shown graphically in the form of three-dimensional constitutive surfaces, with deformation variables plotted against stress state variables. The above coefficients are the slopes of the constitutive surface at a point. If the stress states are plotted on a logarithmic scale, the plots are linear over a large range of stresses and the slopes of the curves on the extreme planes are called volumetric deformation indices: C_t, C_m for the soil structure and D_t, D_m for the water phase.

3.7 Methods

3.7.1 Hydraulic Conductivity Measurement by Flexible Permeameter

Hydraulic conductivity of soil and other porous materials can be measured by Tri-flex permeability system. The test setup includes a master control panel, permeability test cell and water de-airing tank system (Figure 3.3). An auxiliary control panel can

be connected to the master control panel and provide capacity of testing three specimens at the same time.

The samples prepared for direct measurement of hydraulic conductivity were compacted statically with the help of CBR machine, at their maximum dry density and optimum water content with diameter and height of 7 cm and 14 cm respectively. After placing the sample in test cell, it was filled with water and burette channels and tubes were de-aired. Then a small amount of pressure was given in order to remove the remained air from cell lines and porous stones. In this experiment the saturation was achieved by increasing the pore pressure, using the application of the same upper and lower pressures. The inflow of testing chamber was connected to the Tri-Flex equipment to maintain a constant pressure. The outflow was also connected to upper burette therefore the outer and inner flow volume would be determined by reading the inner meniscus of water in the burettes.

For checking the saturation degree, B value was calculated by increasing the cell pressure a few increments and reading the level of water meniscus in lower burette responsible for back pressure. B value can then be calculated through dividing increase in pore water pressure (Δu) by increase in cell pressure ($\Delta\sigma_3$). B value above 95% is generally accepted as an indication of sufficient saturation in specimen. However, for less pervious rocky material, in this case cement included samples, a lower B value remaining constant after successive increments of cell pressure is acceptable (ASTM D5084–10). The completion of saturation depends on permeability of sample and magnitude of applied back pressure. Nevertheless, application of excessive back pressures may result in reorientation of grains,

migration of fine particles and deformation of sample (ELE Manual, 1998). Achieving full saturation is a long process in sand bentonite and cement enhanced samples because of low hydraulic conductivity of mixtures. For very stiff soils and weak rocks it is difficult to achieve B equal to 1. In such a case it would be adequate if the B values for several increments of cell pressure stays constant. Typically in triaxial tests back pressure saturation is carried out at 300-1000 kPa, but may be 200 kPa for soft soils. It should be noted that dissolving the air in water takes time (Fell et al., 2005). Figure 3.3 shows the Tri-flex apparatus which was used for measuring the hydraulic conductivity of compacted samples.

Figure 3.3.Tri-flex master control panel and de-airing tank system.

In this study saturation process took about 4 weeks for SB and 6 weeks for SBC samples with a back pressure of 300 kPa and 400 kPa respectively. Leaving the samples for saturation for extended time periods may increase the risk of fungi formation which influences the physical properties of soil. On the other hand excessive back pressure, which reduces the saturation time, may result in washing

out the fine colloidal particles of bentonite and reorientation of particles in samples. Therefore, the amount of back pressure should be chosen carefully which is usually achieved by trial and error.

After completion of saturation the permeability test procedure was performed by producing an upward flow through the specimen. Measuring the upper and lower burette water levels over the time the saturated hydraulic conductivity of sample can be calculated according to falling head method theory, using Equation 3.5. The test continues until the measured values are stable which usually takes 1-2 days.

$$k = \frac{al}{2At} ln \left[\frac{P_B + h(t_1)}{P_B + h(t_2)}\right] \tag{3.5}$$

where $h(t_1) = \frac{V_u(t_1) - V_l(t_1)}{a}\ cm$

$h(t_2) = \frac{V_u(t_2) - V_l(t_2)}{a}\ cm$

a is the cross-sectional area of burette, l is the length of sample, A is the cross-sectional area of the sample, t is difference between t_1 and t_2 in seconds, P_B is Bias pressure, the difference between the lower burette channel applied pressure and upper burette channel applied pressure, h is difference of height of water in lower burette and upper burette in cm, $V_u(t_i)$ is volume reading of upper burette at t_i in cm^3 and $V_l(t_i)$ is volume reading of lower burette at t_i in cm^3.

3.7.2 Filter Paper Suction Measurement

Filter paper technique is one of the oldest suction evaluation methods that is reliable and economical, applicable over a wide range of suctions from 10 to 1000000 kPa. In order to measure the matric suction of soils, contact filter paper method test was carried out on compacted SB and SBC samples. Specimens of SB and SBC were

compacted statically to their maximum measured dry density at optimum water content and saturated under 7 kPa surcharge till the primary swelling process was completed. Then samples were taken out of the water, weighed and left in the oven to desiccate at 40˚C. The specimens were packed in air tight containers one at a time at different stages of drying, in close contact with three filter papers (Whatman No. 42). A close contact is crucial for the measurement of matric suction. Consequently bubble wraps were placed around and on the specimens before closing the lids of the containers to ensure a firm contact. The top filter paper (sacrificial paper) was used as a protection for the other two papers. The moisture content of sacrificial paper is not taken into consideration for indirect measurement of suction. The containers were then tightly sealed and were placed in styrofoam boxes filled with glass wool and preserved for 10 days of suction equilibration period (Bilsel, 2002). Some steps of filter paper method procedure are shown in Figure 3.4. The test data were best-fit using Fredlund and Xing (1994) and van Genuchten (1980) equations. The air-entry value, residual water content, residual matric suction and fitting parameters of the SWCCs were found using the SoilVision computer software (SoilVision Systems Ltd., 2001).

Figure 3.4.Filter paper test procedure.

3.7.3 Cyclic Swell-shrink Test

Wetting–drying cycles are accomplished by allowing specimens to swell and then dry to at least as compacted water content, repeating this process on the same specimens for several consecutive cycles (Villar and Lloret, 2004). In some studies swell-shrink cycles are performed on swelling soils and drying temperature is kept at room temperature or maximum at 40˚C (Rao et al, 2001; Guney et al., 2007). In this study cyclic swell-shrink test was performed on statically compacted specimens of 50 mm diameter and 15 mm height. Samples were prepared at their maximum dry density and optimum water content and cured in desiccator for 28 days. They were then left for one-dimensional swell under 7 kPa pressure in distilled water using oedometer cells. Swell of samples were monitored and after reaching the point where there was no further swelling the samples were taken out of water. This procedure took 20-30 days for SB and 10-15 days for SBC samples. The samples were then left in 40˚C oven and height, diameter and mass were measured through desiccation period until the readings were steady. The samples were then left for swelling and the same procedure was repeated up to five swell-shrink cycles. The advantage of this test is the ability to perform the test on the same sample in several cycles.

3.7.4 One-Dimensional Swell-Consolidation at Elevated Temperature

One dimensional swell and consolidation test was operated at 60°C temperature by circulating the hot water through oedometer cell. For keeping the hot water circulating around sample a consolidation cell was manufactured out of kestamid material having outlet on top and inlet at the bottom of cell wall for water circulation. Kestamid, also known as cast polyamide or cast nylon, is an engineering plastic used frequently in industrial uses for its superior mechanical, physical and chemical

properties. It is lighter, harder and more durable than materials like aluminum, steel and fiber. The water pipe of inlet water was connected to the water pump in constant temperature bath and outlet of water pipe was directed to the other end of the bath to close the cycle. The temperature of water could be monitored from thermostat of bath and kept constant at 60˚C. Figure 3.5 shows the temperature controlled consolidometer used, as well as the schematic of test setup.

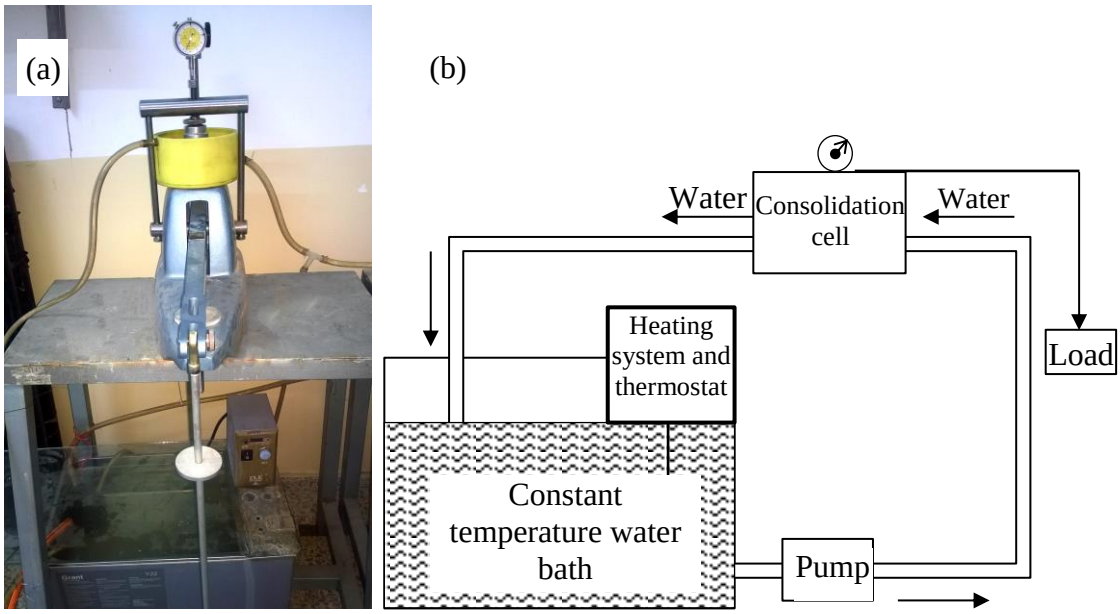

Figure 3.5. (a) Temperature controlled consolidometer, (b) schematic layout of consolidation test in elevated temperature.

3.8 Experimental Results and Discussions

The major characteristics required for efficient performance of barrier materials are hydraulic conductivity, structural integrity and durability. To achieve this, a low hydraulic conductivity must be maintained throughout the service life of barriers. Therefore, the combinations of materials selected in this study were tested in volume change, including swell-shrinkage and compressibility under non-cured and cured conditions, as well as in durability tests such as volume change under elevated

temperature and changing pore water chemistry, and climatic factors, such as water retention and cyclic wetting-drying behavior. Resistance to shrinkage, and hence cracking was also investigated. Volume change and hydraulic conductivity were studied under saturated and unsaturated states. The latter being correlated to suction and water retention capacity during desiccation phase. The change in hydraulic conductivity with curing, changing pore water chemistry, elevated temperature, in saturated and unsaturated conditions were tested and/or predicted.

3.8.1 Effect of Curing on Swell and Compressibility

Figure 3.6 presents the range of free swell in SB samples as percent strain with respect to elapsed time in minutes ($\Delta H/H_0$ versus time for different mixtures of sand-bentonite). The results of swelling test on one day cured samples represent an average of 30% swell in presence of 15% bentonite. At low effective stresses bentonite swells sufficient enough to separate the sand particles. There are two factors which influence the final void ratio of the bentonite after swelling: the ionic concentration of the pore solution, and the bentonite fabric after compaction. Bentonite-sand mixtures possess high strength and low compressibility with very low hydraulic conductivity, achieved by mixing sufficient sand for stability and bentonite to seal the voids. Another beneficial aspect of this mixture is its resistance to shrinkage during desiccation.

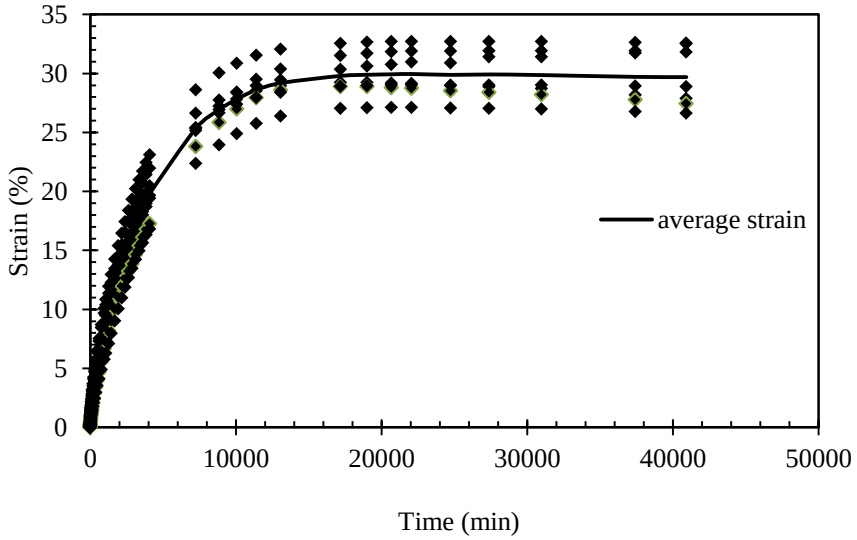

Figure 3.6. The range of swell percentage of SB with respect to time.

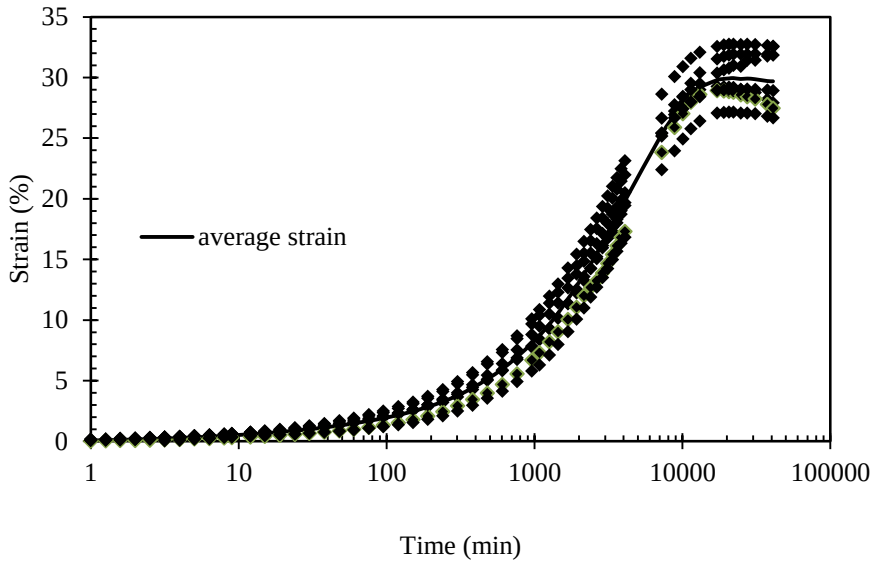

Figure 3.7. The range of swell percentage with respect to logarithm of time.

Figure 3.7 depicts the swell percentage of one day cured SB plotted with respect to logarithm of time. On this graph the time taken for completion of swell deformation can be observed which is significantly high. The logarithmic plot can provide detailed information on different stages of swelling process, which is explained in Figure 3.8. As it can be observed in this figure the curve can be divided into three

stages. Applying this information to the curve in Figure 3.7, the initial swelling stage is completed at about 7% of total swell percentage. This phase generally takes less than 10% of the total swelling and is basically because of swelling of the bentonite particles within the voids of the non-swelling sand fraction. Dakshanamurthy (1978) remarked two phases of swelling. The first phase hydration of clay particles and molecules of water are adsorbed on surface of montmorillonite which is known as interlayer or inter-crystalline swelling. The second phase of swelling takes place due to double-layer repulsion. Considerable amount of volume change happens in this phase.

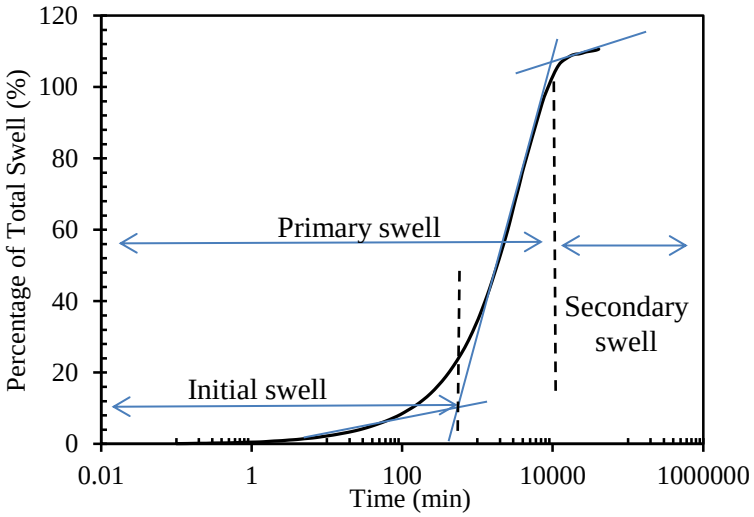

Figure 3.8. Time-percent swell of total swell curve.

Primary swelling phase progresses when the voids cannot accommodate any further clay swelling. It occurs faster than initial phase and after its completion swell continues at a slower rate. The time needed for completion of primary swelling generally increases with increase of bentonite content (Muntohar, 2003). It can be observed from Figure 3.7 that the initial swelling phase completes in about 600 minutes and end of primary swelling occurs in about 11400 minutes. Figure 3.9

presents the effect of curing time on SB in one- dimensional swell. 28 days curing period decreased the swelling of SB by 3%.

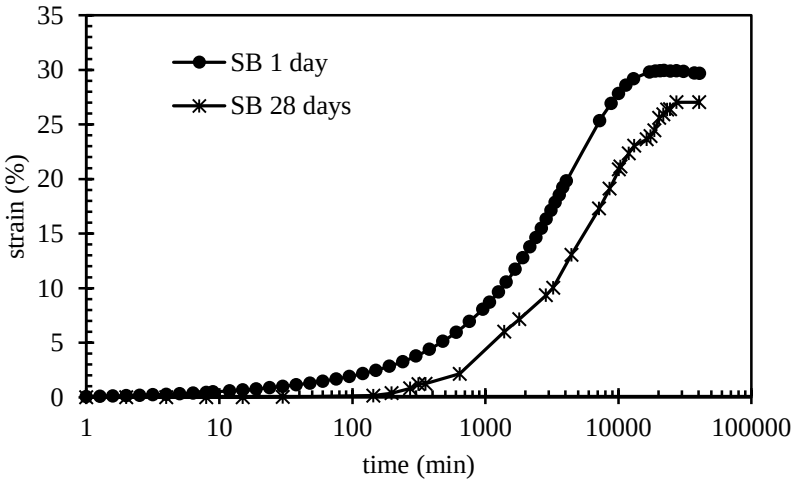

Figure 3.9. Swell of 1-day and 28-day cured SB samples.

The swell test was applied on cement enhanced samples as well, but the bonding between the grains prevents absorption of water molecules and therefore the swell percent of sand bentonite cement mixtures were observed to be almost zero. The bonding between grains occurs as a result of cement hydration. As it was expected the effect of cement on suppressing the swell endures and swell percentage of both 1-day and 28-day cured SBC samples is about zero, as can be depicted in Figure 3.10. The stabilization occurs because of the cementation bonds forming between the calcium silicate and aluminate, the cement hydration products with the soil particles. With addition of cement, cement powder gets in contact with moist soil and forms a paste like material that coats the lumps. The cementing material binds the particles together increasing stiffness of the soil and therefore it leads to reducing the swelling parameters.

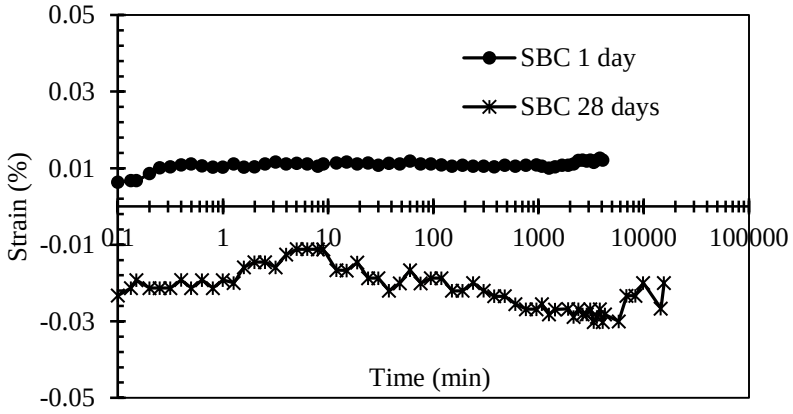

Figure 3.10. SBC swell curves.

Figure 3.11 presents the consolidation curves of non-aged and aged sand-bentonite mixtures. The thixotropic effect caused by the presence of bentonite can be observed distinctly with the flattening of the curve within a period of 28 days. The compacted sand-bentonite specimens in the first day of reconstitution still are not in equilibrium in their micro structure, which in time develops due to redistribution of pore pressures and ionic movement which causes particle rearrangement (Diaz-Rodriguez, 1999).

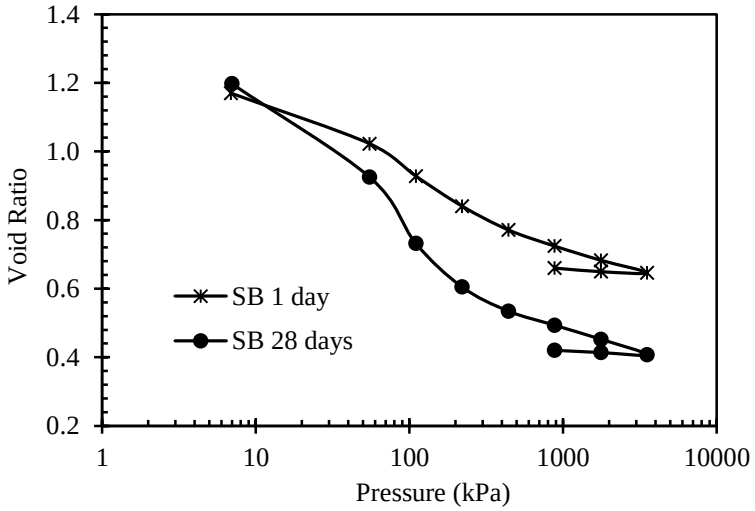

Figure 3.11. SB samples tested 1 day after compaction and 28 days after compaction.

As compaction is a rapid process water in inter-aggregate and intra-aggregate pores cannot be maintained in equilibrium. After the process of compaction water

redistribution occurs in the specimen due to suction equilibration at constant water content after compaction, which is a very slow process due to low permeability and strong clay-water bonds (Delage et al., 2006). This equilibration period also causes structural changes, due to particle rearrangement with time causing formation of bonds during aging. This process reduces the swell potential as well as compressibility due to increase in shear strength of compacted expansive soils (Rao and Tripathy, 2003; Ye et al., 2013).

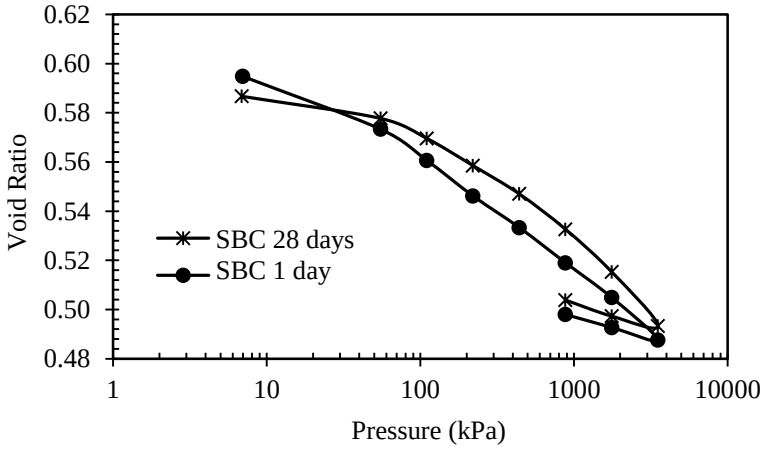

Figure 3.12. SBC samples tested 1 day and 28 days after compaction.

Figure 3.12 represents the consolidation curve of SBC samples with 1 and 28-day curing time. In Figure 3.13 comparison between compression curves of 28-day cured SB and SBC is shown. Compressibility properties and swell pressure of SB and SBC samples are presented in Table 3.1 and 3.2 respectively.

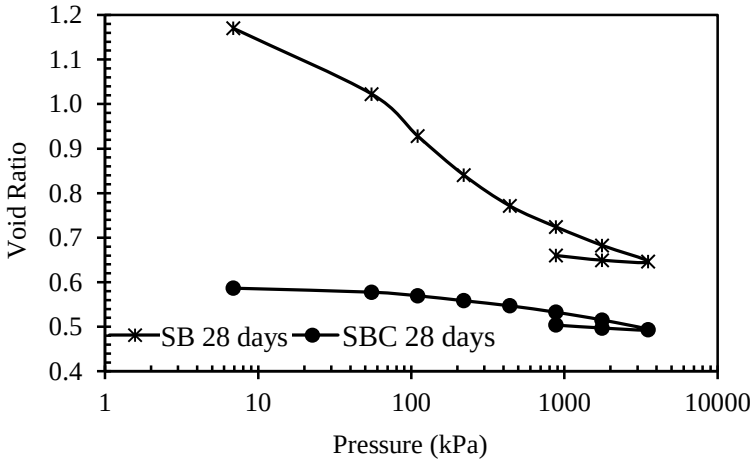

Figure 3.13. The void ratio versus effective stress behavior of 28-day cured SB and SBC samples in distilled water.

Based on the results presented in Table 3.1, the bilinearity of the consolidation curve remains in the behavior of the cured specimens as well, with significant reduction in the initial compression index, while no appreciable change is noticed in the second stage of the consolidation curve, after the threshold stress of 220 kPa. The compression index of SBC, however reduced to 0.045 from 0.053 as a result of curing which can be correlated to continuation of hydration process of cement within the sample.

Table 3.1. Compressibility properties and swell pressure of SB with curing time.

		1-day cured	28-day cured
SB	C_{c1}	0.468	0.284
	C_{c2}	0.141	0.151
	C_r	0.0183	0.0232
	p_s'	250	220

Table 3.2. Compressibility properties and swell pressure of SBC with curing time.

		1-day cured	28-day cured
SBC	C_c	0.053	0.045
	C_r	0.0186	0.017
	p_s'	----------	----------

3.8.2 Effect of Pore Water Chemistry on Swell and Compressibility of Cured Specimens

This section presents data on the swell-compressibility and hydraulic conductivity of Na-bentonite and sand-bentonite mixtures subjected to 1 mol. NaCl solution. This solution is selected since it is representative of salt solutions in leachates as well as possible salt water intrusion in coastal areas. Na^+ and Cl^- are the common elements causing underground and surface water contamination in urban areas. Sources of Na^+ and Cl^- originate from agricultural chemicals, from septic systems, animal waste, landfills and road deicing agents. Another source is salt water intrusion occurring in coastal areas. Table 3.3 presents the average amounts of elements present in the eastern part of the Mediterranean Sea. As can be observed, the major constituents are Cl^- and Na^+.

Table 3.3. Chemical contents of the sea water (Bashitialshaaer et al., 2009).

Elements in sea water	Amount mg/L
Chloride (Cl^-)	21.200
Sodium (Na^+)	11.800
Sulfate (SO_4^{2-})	2.950
Magnesium (Mg^{2+})	1.403
Calcium (Ca^{2+})	423
Potassium (K^+)	463
Bicarbonate(HCO_3^-)	-
Strontium (Sr^{2+})	-
Bromide (Br^-)	155
Borate (BO_3^{3-})	72
Fluoride (F^-)	-
Silicate (SiO_3^{2-})	-
Iodide (I^-)	2
Others	-
Total dissolved solids (TDS)	38.600

Table 3.4 presents the maximum amounts of elements constituting inorganic composition of leachates from landfills receiving primarily domestic wastes (DoE,

1995). It shows that landfill leachate is dominated by sodium and chloride ions but with considerable amounts of other components.

Table 3.4. Composition of leachates from landfills receiving primarily domestic wastes (after DoE, 1995).

Elements	Maximum (mg/L)
Ammoniacal N	1700
Calcium	1440
Magnesium	470
Sodium	688
Potassium	492
Chloride	3410
Sulphate	730
Alkalinity (as CaCO3)	8840
Phosphate	15.8

It has been experimentally shown that swelling percentage and hydraulic conductivity are strongly dependent on the pore fluid. The swelling behavior of a sand- bentonite mixture is a function of pore fluid, applied effective stress and clay content. Under low stresses, the clay swells in dilute solutions to an extent to separate the sand particles, reaching to a finer void ratio similar to what can be achieved by bentonite alone. Under high stresses, or in stronger solutions, bentonite does not have the capacity to swell sufficient enough to force the sand particles apart, and thus the swelling is confined within the sand pore volume. According to Gens and Alonso (1992) mechanical behavior of bentonite consists of a microstructural level due to swelling of active minerals, and macrostructural level at which major structural changes occur. According to Studds (1996) bentonite swelling decreases based on the increasing valence, when 0.01-0.1 molar salt solutions are used. In 1 molar salt solution, however, it is sufficient enough to suppress the diffuse double layer irrespective of the magnitude of the valence.

The one dimensional swell tests were carried out on both SB and SBC samples and the result are shown in Figure 3.14. The swell percentage of cement enhanced samples are very low as expected and identical to when it is tested in distilled water but for SB samples one mole addition of salt to the water caused initial swell to reduce from 29% to 0.5%. It can be concluded that while presence of salt in pore water pressure increases the swell percentage in cement enhanced sample, it can suppress the swelling of sand-bentonite samples dramatically. This is in good agreement with the findings in literature depicting the decrease in swelling capacity of bentonite with the increase in salinity of permeating fluid.

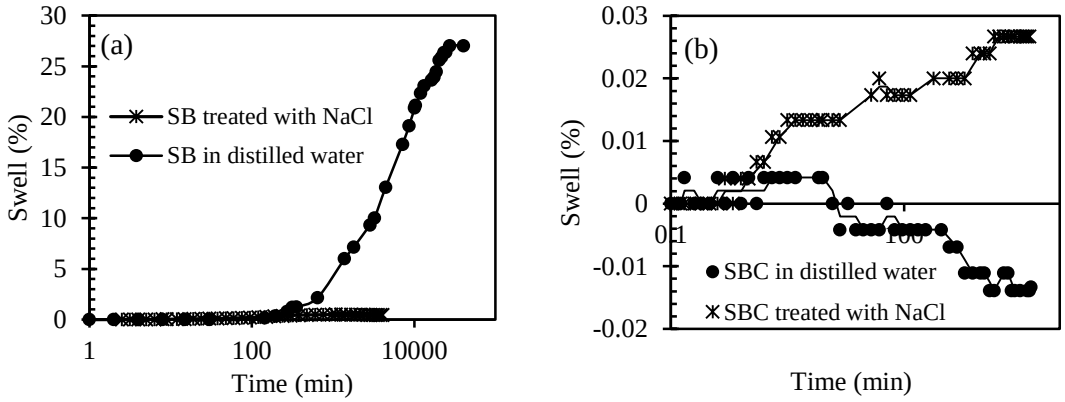

(a) (b)

Figure 3.14. Swell curves of (a) SB and (b) SBC permeated with NaCl compared with distilled water permeated ones.

Drame et al. (2007) in a study on volume change of Portland cement in saline solution explains that in cement pastes, concentration dependent expansion take place when exposed to the NaCl solutions. The ordinary Portland cement (OPC) paste contains alkali substituted CASH, CH and relatively small amounts of other compounds. Both CASH and CH contribute to expansion of the cement pastes immersed in salt solutions. There are three main competing effects contributing to volume change:

1. Shrinkage due to extended leaching of CH from CSH.

2. Structural collapse resulting from osmotic forces, as an instance, mass transfer of water from the CSH to the surrounding salt solution.

3. Expansion due to intercalation effects including cationic hydration forces and the dissolution of both structural and bulk CH.

Figure 3.15 shows the comparison between swell curves of NaCl permeated cured SB and SBC samples.

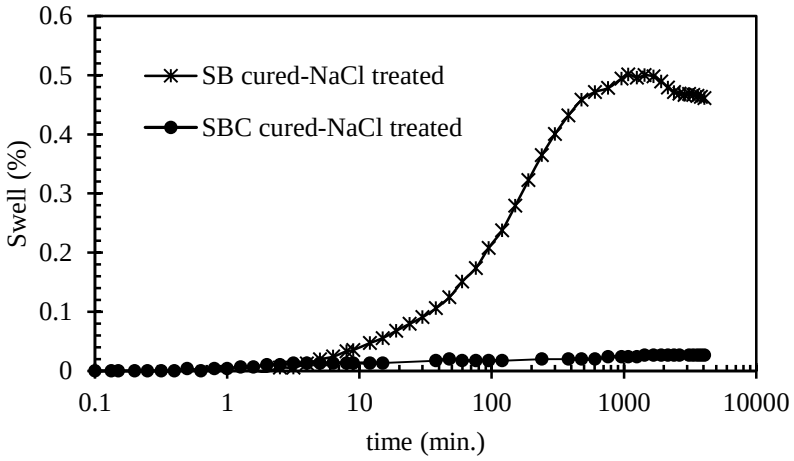

Figure 3.15. Swell curves of SB and SBC in one mole NaCl solution.

Figure 3.16 depicts the void ratio versus effective pressure curves of SB samples obtained in distilled water and NaCl solution. As it can be seen the threshold of sand and bentonite mixtures is almost eliminated by the effect of salt and the compressibility of sample is reduced significantly. As swell potential of sand bentonite samples are affected by salt, the starting void ratio of compression curve is dramatically decreased in comparison with the samples tested in distilled water.

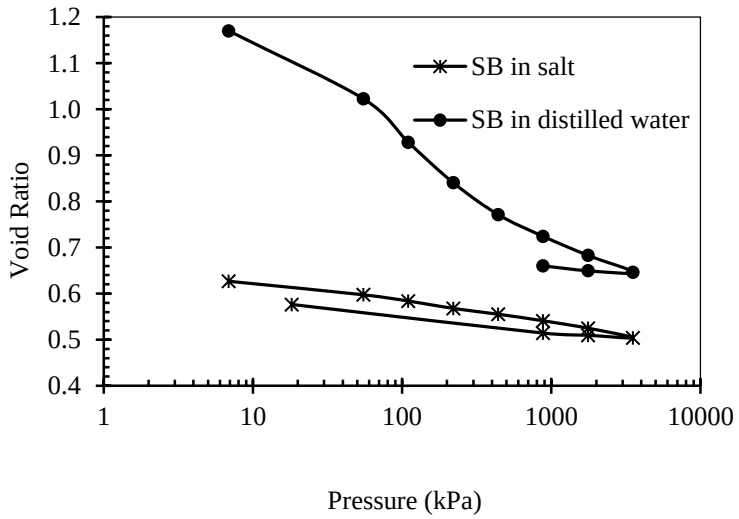

Figure 3.16. Consolidation curves of 28-day cured SB samples with and without NaCl permeation.

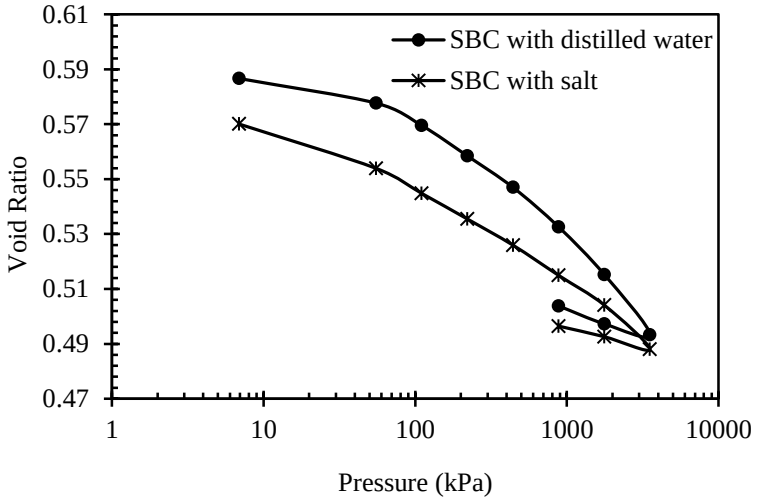

Figure 3.17. The consolidation curves of 28-day cured SBC samples with and without NaCl permeation.

In Figure 3.17 the consolidation curves of SBC samples obtained in distilled water and NaCl solution are presented. The effect of NaCl on cement treated samples is noted as a minor reduction in compression index. Figure 3.18 shows the comparison of consolidation curves of SB and SBC obtained in NaCl solution. Application of NaCl solution suppresses the compressibility characteristics of SB significantly, and the curve obtained looks very similar to cement enhanced samples.

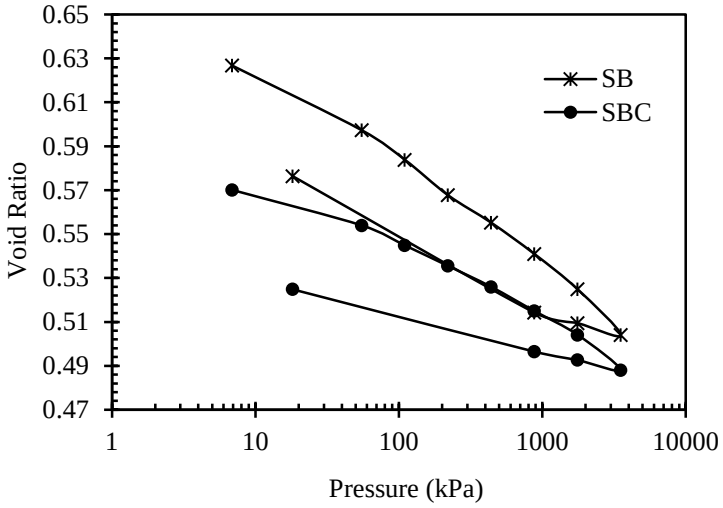

Figure 3.18. Consolidation curves in 1 mol. NaCl solutions for 28- day cured SB and SBC.

3.8.3 Effect of Temperature on Swell and Compressibility of Cured Specimens

As it can be seen in Figure 3.19 increasing the temperature resulted in increase of one dimensional swell percentage of cement enhanced samples to 1.3%. On the other hand it reduced the swell percentage of SB samples from 27% at room temperature to about 20% at 60°C. The swell curves of SB and SBC samples at 60°C are shown together in Figure 3.20 for comparison.

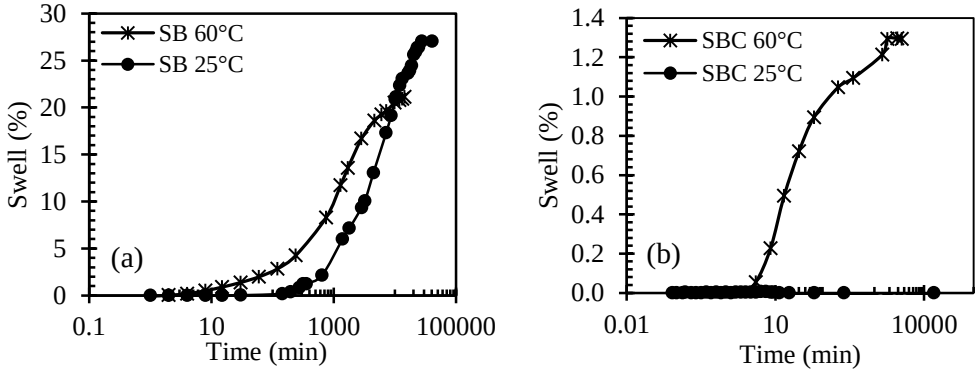

Figure 3.19. Swell curves of (a) SB and (b) SBC at 60°C compared with room temperature.

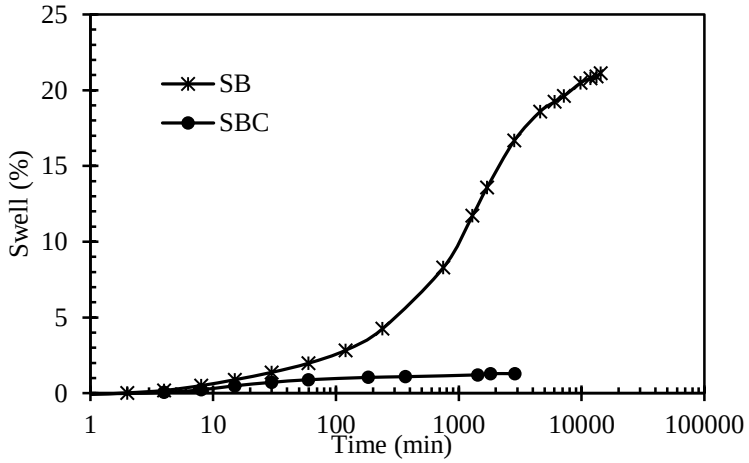

Figure 3.20. Swell curves of SB and SBC at 60°C.

In Figure 3.21 the compressibility curves of SB samples tested at 25°C and 60°C are shown. At high temperature SB samples are still highly compressible and elastic, additionally the threshold effect endures which results in a bilinear compression curve. Elevation of temperature slightly increased the compression index of SB in the first portion of compression line, along which bentonite particles are mostly responsible for the behavior of compressibility of sample, however in the second portion compression index reduces in comparison to compression index of the sample tested at room temperature.

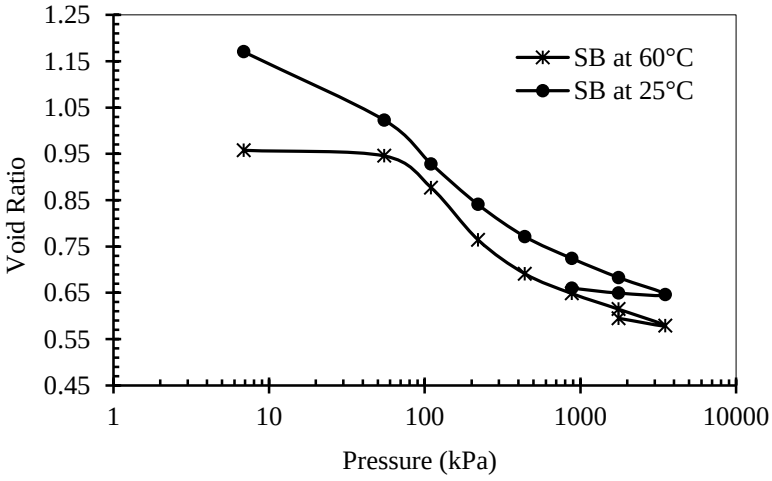

Figure 3.21. Consolidation curves of 28-day cured SB samples at 25ºC and 60ºC.

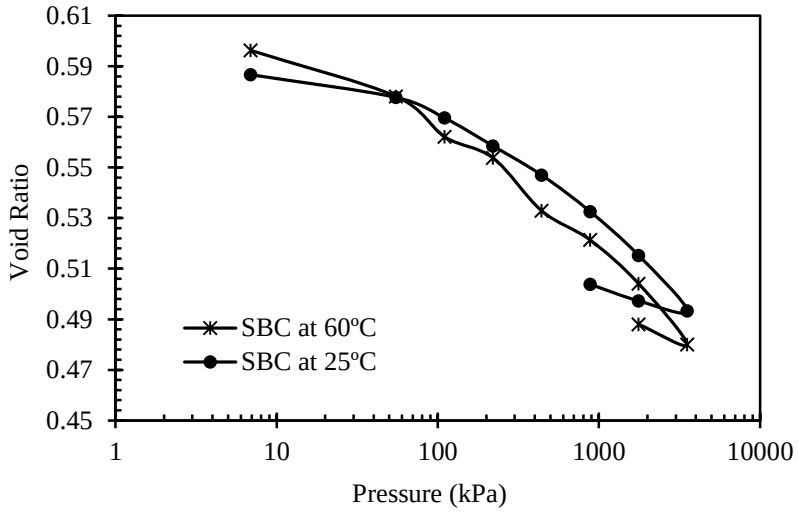

Figure 3.22. Consolidation curves of 28-day cured SBC samples at 25ºC and 60ºC.

The effect of temperature on SBC sample is shown in Figure 3.22 with a slight increase in compressibility of sample at 60ºC. Figure 3.23 illustrates the comparison of the compressibility behavior of SB and SBC at 60°C.

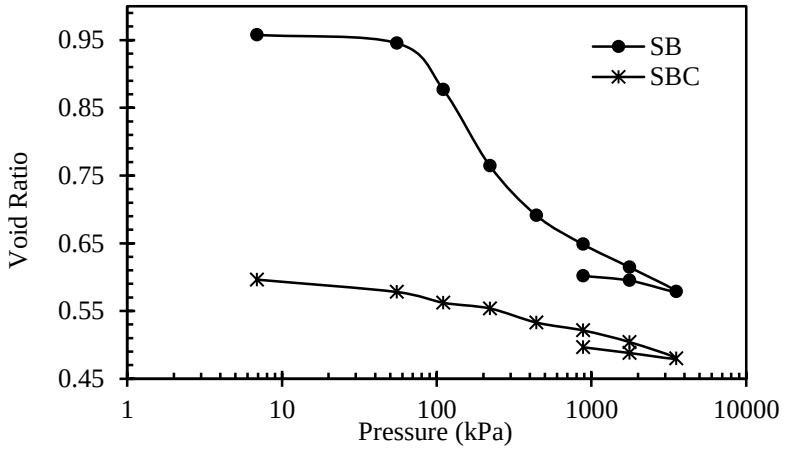

Figure 3.23. Consolidation curves at 60°C.

Compressibility properties and swell pressure of SB and SBC samples are tabulated in Tables 3.5 and 3.6 respectively. According to Tsuchida et al. (1991), heating provides the same effect as aging on clay samples. They mentioned that this aging is caused by cementation which is accelerated by heating. Clay particles are closely

rearranged because heating reduces the thickness of the adsorbed water layer on the surface of soil particles. As a result, the specimen develops a new structure, exhibiting higher stiffness against successive loading (Tsutsumia and Tanakab, 2012). However, Lingnau et al. (1996) indicated that heating sand-bentonite as buffer material up to 100°C has effect on compressibility, stiffness, strength and pore water pressure generation, but none of the changes are extreme (more than 10%).

Table 3.5. Compressibility properties and swell pressure of SB.

		1-day cured	28-day cured	1mol. NaCl	at 60°C
SB	C_{c1}	0.468	0.284	0.047	0.308
	C_{c2}	0.141	0.151	----------	0.124
	C_r	0.0183	0.0232	0.017	0.038
	p_s'	250	220	14	240

Table 3.6. Compressibility properties and swell pressure of SBC.

		1-day cured	28-day cured	1mol. NaCl	at 60°C
SBC	C_c	0.053	0.045	0.035	0.055
	C_r	0.0186	0.017	0.014	0.027
	p_s'	----------	----------	----------	20

3.8.4 Prediction of Ultimate Swelling

The swell which converges to a value very close to an asymptote drawn close to the swell curve at secondary swell stage is usually taken as the ultimate value. The shape of swell (%) versus time graph resembles the shape of a rectangular hyperbola. Kondner (1963) was the first to suggest that the non-linear stress-strain curves of soils could be represented by a rectangular hyperbolic equation, which could be linearized by plotting the results in a modified form. Swell-time relationship represents a rectangular hyperbola, then the time/swell versus time relationship would be a straight line. Hence using this concept the ultimate swell could be predicted. From the reciprocal of the slope of the straight line obtained from

time/swell versus time plot (Muntohar, 2003; Nagaraj et al., 2010; Dafalla and Al-Shamrani, 2011)

The ultimate swell can be predicted using the hyperbolic model given in Equation 3.6.

$$S\,(t) = \frac{dh(t)}{h_0} = \frac{t}{(a + bt)} \tag{3.6}$$

Komine and Oggata (1994) proposed to obtain the maximum swell by finding the limiting value at infinite time as given in Equation 3.7.

$$S_{max} = \lim_{t\to\infty} \left(\frac{1}{\frac{a}{t}+b}\right) = \frac{1}{b} \tag{3.7}$$

Where t is the time from the start of water inundation, S(t) is the vertical swell at time t, and a and b are constants obtained from straight line fits giving the highest R^2 value. Theoretically, it takes infinite time to reach the ultimate swell value, which cannot be practically measured in the laboratory. Therefore, prediction from the initial stages of swell is advantageous instead of continuing till equilibrium, which can take place in months or even over a year. The hyperbolic curves of SB specimens are as shown in Figure 3.24. Figure 3.25 depicts the time/swell (%) versus time plots, which are fitted with straight lines with fitting parameters a representing the ordinate and b the slope of the lines. The experimentally determined swell percentages, as well as times of completion of each swell type, as well as straight line fitting parameters and the predicted maximum swell percentages are presented in Table 3.7. The SBC specimens are non-swelling, therefore not included in this part.

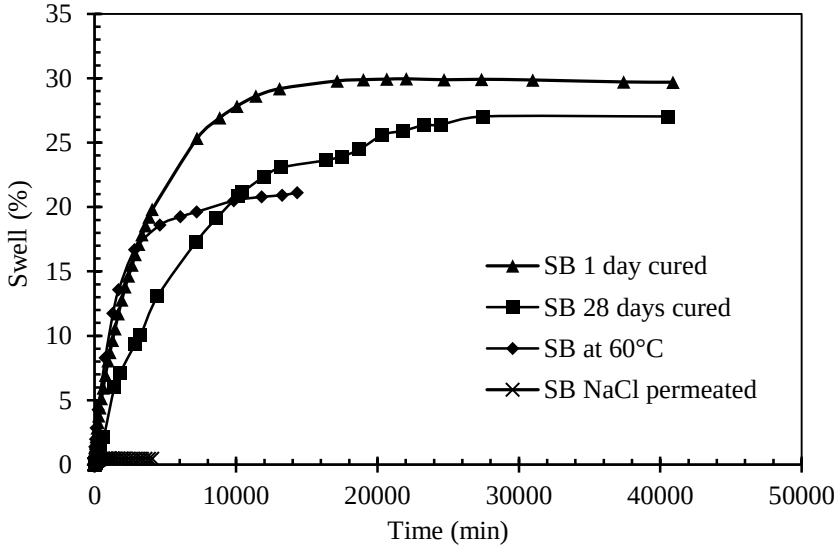

Figure 3.24. Hyperbolic curves of SB specimens.

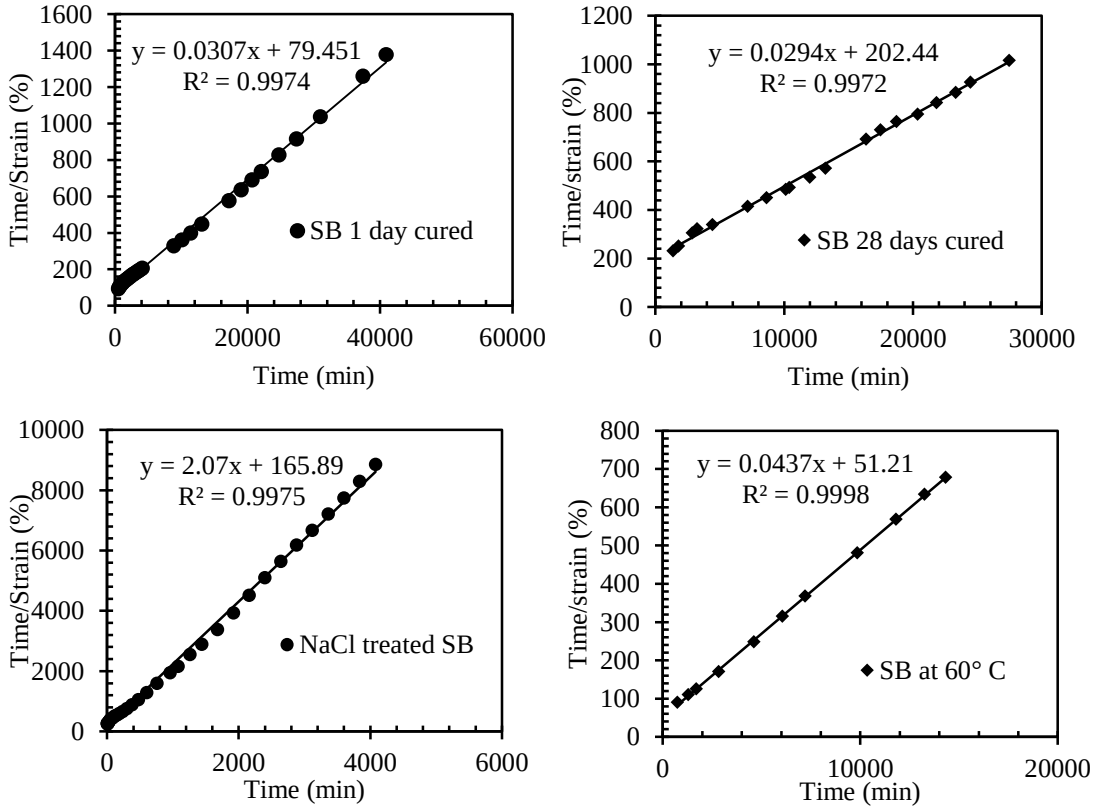

Figure 3.25. Time/swell versus time relationships of SB samples.

Table 3.7. Swell properties and predicted swell values.

Swell properties	1 day cured	28-day cured	NaCl treated	60° C treated
Initial swell (%)	3	2.50	0.06	3
Time for initial swell (min)	500	1400	45	300
Primary swell %)	28	26	0.46	20
Time for primary swell (min)	11600	20362	400	4700
Maximum swell measured (%)	30	27	0.46	21.12
Hyperbolic constant, a	75.1	202.4	165.9	51.2
Hyperbolic constant, b	0.0309	0.0294	2.07	0.044
Ultimate swell predicted (%)	32.4	34	0.48	22.9

Examining the measured and predicted ultimate swell percentages, it can be observed that the predicted values are higher than the measured values. This increment is approximately 7% for the 1-day cured, NaCl permeated and 60°C treated specimens. The increment in 28-day cured specimens, however is approximately 26%, which indicates that the secondary swell of the cured SB specimens proceeded gradually and would have reached a higher value in a longer time, had the test was not ceased earlier. Therefore, the one-dimensional swell tests actually require much longer time, which is not a feasible technique, hence predictions can give a faster and quite reasonable values.

3.8.5 Saturated Hydraulic Conductivity

Two methods were used to determine the hydraulic conductivity of the sand-bentonite mixtures. These were the Tri-flex flexible permeameter test and an indirect method based on consolidation data, using the square root of time method. The technical difficulties were involved in the flexible permeameter, including the back pressure application for saturating the soil samples and the prolonged periods of saturation period causing fungi to form and deteriorate the samples. It was observed that the amount of bentonite was high causing significant swelling, hence preventing consistent reading of the flow data. This observation is in good agreement with

previous research recommending to use time-dependent volume change data from consolidation test to determine the hydraulic conductivity of sand-bentonite mixtures when the bentonite content is more than 5%. The experimental methods employed in determination of saturated hydraulic conductivity of compacted sand-bentonite are time intensive. Therefore, analytical or indirect methods are preferred. The indirect method utilized in this work is the determination of hydraulic conductivity from consolidation data. Taylor's square-root of time method is preferred due to easiness and quicker application.

Hydraulic conductivity is not a fundamental property of soil and depends on various factors such as, particle size and pore-size distribution, particle shape and texture, mineralogical composition, void ratio, degree of saturation, soil fabric, nature and type of fluid and temperature (Head, 1982). In Table 3.8 and 3.9 the hydraulic conductivity values of 1-day cured SB and SBC along with different ranges of effective confining pressures, calculated from consolidation test data are shown respectively. Table 3.10 and 3.11 present the consolidation test results and the predicted hydraulic conductivity values for 28-day cured SB and SBC samples respectively. The addition of cement reduced the saturated hydraulic conductivity in all pressure ranges. Nontananandh et al. (2005) in an investigation on microstructure of a cement-stabilized soil concluded that addition of cement decreased the coefficient of permeability in cured samples. Growing reaction cementitious products such as calcium silicate hydrate (CSH) and tobermorite in clay fabrics form bindings and results in reduction of pore spaces and therefore reduces hydraulic conductivity. It can be observed that in SB and SBC, saturated hydraulic conductivity significantly

reduces by a factor of 10^{-3} and 10^{-4} respectively when the effective confining pressure range inreases to 220-400 kPa.

Table 3.8. SB 1 day cured.

Pressure range		Void ratio		m_v (m^2/N)	c_v (m^2/min)	k (m/s)
6.9	220	1.156	0.600	0.00417019	0.0022	9.0001E-08
220	441	0.600	0.530	0.00048764	0.00051	2.45932E-11
441	882	0.530	0.487	0.00014248	0.00043	5.9967E-12
882	3530	0.487	0.398	4.7316E-05	0.00028	1.29175E-12

Table 3.9. SBC 1 day cured.

Pressure range		Void ratio		m_v (m^2/N)	c_v (m^2/min)	k (m/s)
6.9	220	0.5948	0.5461	0.00035278	0.00018	1.03823E-08
220	441	0.5461	0.5333	8.9047E-05	0.00028	4.07656E-12
441	882	0.5333	0.5190	4.9337E-05	0.00036	2.91833E-12
882	3530	0.5190	0.4875	1.7668E-05	0.00023	6.77E-13

Table 3.10. SB 28 days cured

Pressure range		Void ratio		m_v (m^2/N)	c_v (m^2/min)	k (m/s)
6.9	220	1.170	0.840	0.00284678	0.0001908	8.88076E-08
220	441	0.840	0.771	0.00055472	0.0002385	2.1631E -11
441	882	0.771	0.724	0.00018402	0.00011925	3.58796E-12
882	3530	0.724	0.646	4.8466E-05	0.0002385	1.88993E-12

Table 3.11. SBC 28 days cured

Pressure range		Void ratio		m_v (m^2/N)	c_v (m^2/min)	k (m/s)
6.9	220	0.5867	0.5585	0.00020623	7.45313E-05	2.51307E-09
220	441	0.5585	0.5470	8.0418E-05	7.45313E-05	9.79967E-13
441	882	0.5470	0.5326	5.0088E-05	6.60208E-05	5.40665E-13
882	3530	0.5326	0.4933	2.2146E-05	0.000112899	4.08786E-13

The predicted saturated hydraulic conductivity results are plotted together with the measured values obtained from flexible permeameter. Figures 2.26 and 2.27 illustrate the results, from which can be deduced that the experimental results are consistent with the predicted ones for SB samples whereas there is no good agreement in SBC

results. This can be attributed to the technical difficulties encountered during testing, where specimens were either deformed or flow could not be maintained through the sample, but along the outer surface.

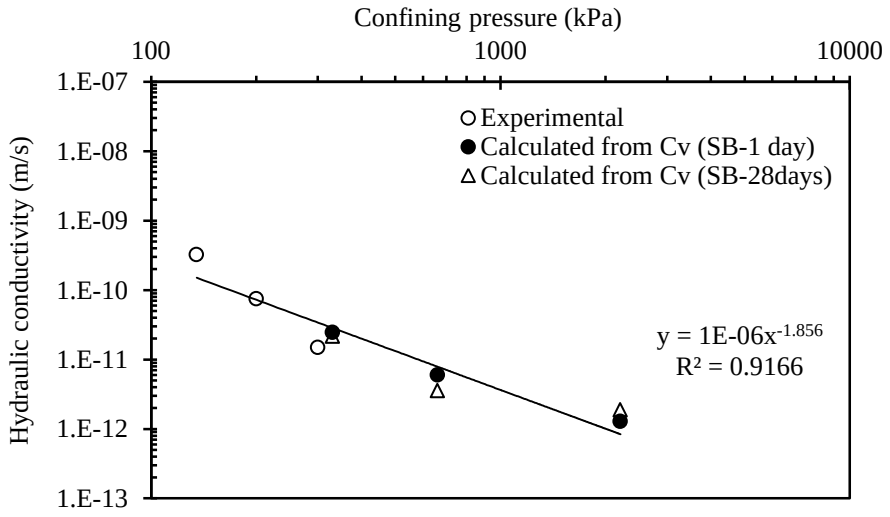

Figure 3.26. Experimental and predicted saturated hydraulic conductivity values versus effective confining pressure for SB sample.

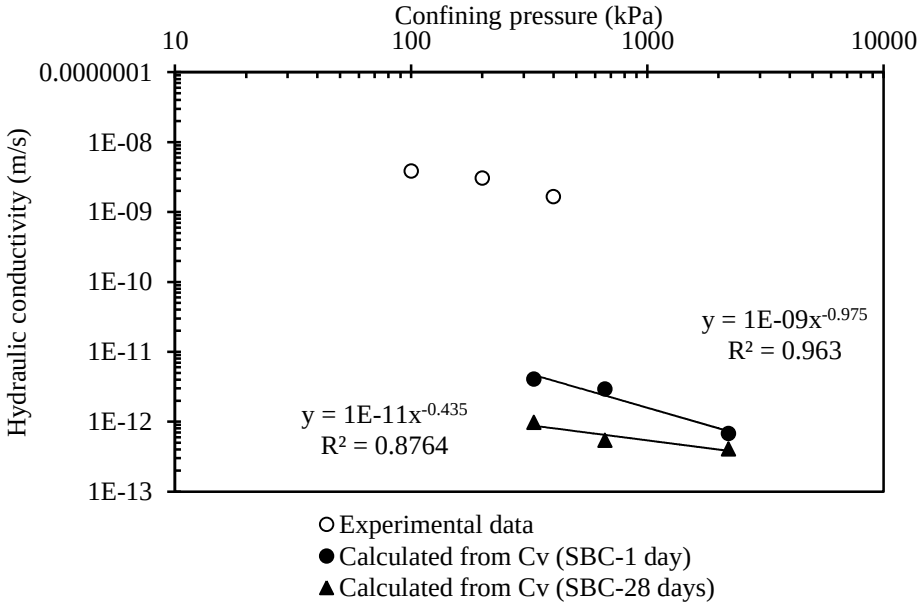

Figure 3.27. Experimental and predicted saturated hydraulic conductivity values versus effective confining pressure for SBC sample.

Tables 3.12 and 3.13 display the saturated hydraulic conductivities of SB and SBC samples calculated from consolidation tests on 1 mole NaCl permeated samples. Comparing with the results in distilled water, both SB and SBC samples possess appreciably higher hydraulic conductivity values. Clay minerals in contact with salt solution undergo large interlayer shrinkage, which causes the reduction in diffuse double layer (DDL), also leading to potential cracking due to increase in hydraulic conductivity. According to Gouy-Chapman theory by increasing the ion concentration, the thickness of DDL decreases, leading to flocculation, creating large pore channels for flow to occur. Nevertheless, the hydraulic conductivity of SBC samples remained below the maximum allowed value for effective pressures higher than 220 kPa.

Table 3.12. Saturated hydraulic conductivity of SB permeated with NaCl.

Pressure range		Void ratio		m_v (m^2/N)	c_v (m^2/min)	k (m/s)
6.9	220	0.62671	0.56767	0.00043	0.00036	2.54051E-08
220	441	0.56767	0.55515	0.00009	0.00048	6.86895E-09
441	882	0.55515	0.54090	0.00005	0.00036	2.91295E-09
882	3530	0.54090	0.50403	0.00002	0.00041	1.41291E-09

Table 3.13. Saturated hydraulic conductivity of SBC permeated with NaCl.

Pressure range		Void ratio		m_v (m^2/N)	c_v (m^2/min)	k (m/s)
6.9	220	0.570	0.535	0.000249	0.000059	2.40048E-09
220	441	0.535	0.526	0.000066	0.000059	6.34316E-10
441	882	0.526	0.515	0.000038	0.000066	4.08219E-10
882	3530	0.515	0.488	0.000015	0.000075	1.84158E-10

In Tables 3.14 and 3.15 hydraulic conductivity results of SB and SBC samples are measured under elevated temperature of 60°C In comparison to samples tested at room temperature, the hydraulic conductivity is slightly reduced in the lower

effective stress range of 6.9- 220 kPa in both SB and SBC, however above 220 kPa hydraulic conductivity of samples increases significantly.

Table 3.14. Saturated hydraulic conductivity of SB at 60°C.

Pressure range		Void ratio		m_v (m^2/N)	c_v (m^2/min)	k (m/s)
6.9	220	0.958	0.764	0.001602	0.000024	6.24703E-09
220	441	0.764	0.691	0.000560	0.000075	6.81994E-09
441	882	0.691	0.648	0.000159	0.000075	1.93991E-09
882	3530	0.648	0.579	0.000042	0.000059	4.00113E-10

Table 3.15. Saturated hydraulic conductivity of SBC at 60°C.

Pressure range		Void ratio		m_v (m^2/N)	c_v (m^2/min)	k (m/s)
6.9	220	0.596	0.554	0.000310	0.000075	3.7812E-09
220	441	0.554	0.533	0.000144	0.000075	1.76053E-09
441	882	0.533	0.521	0.000040	0.000059	3.84099E-10
882	3530	0.521	0.480	0.000023	0.000033	1.2496E-10

The overall evaluation of the saturated hydraulic conductivity values under different conditions along increasing effective confining pressures is summarized in Figure 3.28. It is clearly seen that the hydraulic conductivity values of cured SB samples under the effect of NaCl permeation and 60°C present the highest values, above the maximum limit. Salt permeation and temperature also had an adverse effect on the SBC samples. However, the hydraulic conductivity of SBC, while remained below the limit in salt permeation for all effective pressure ranges, the values for low confining pressures at 60°C are slightly above the limit.

3.8.6 Shrinkage Behavior

Sand-bentonite-cement mixtures are less susceptible to damage by desiccation due to the rigid matrix formed by cement and sand, and in case of presence of water,

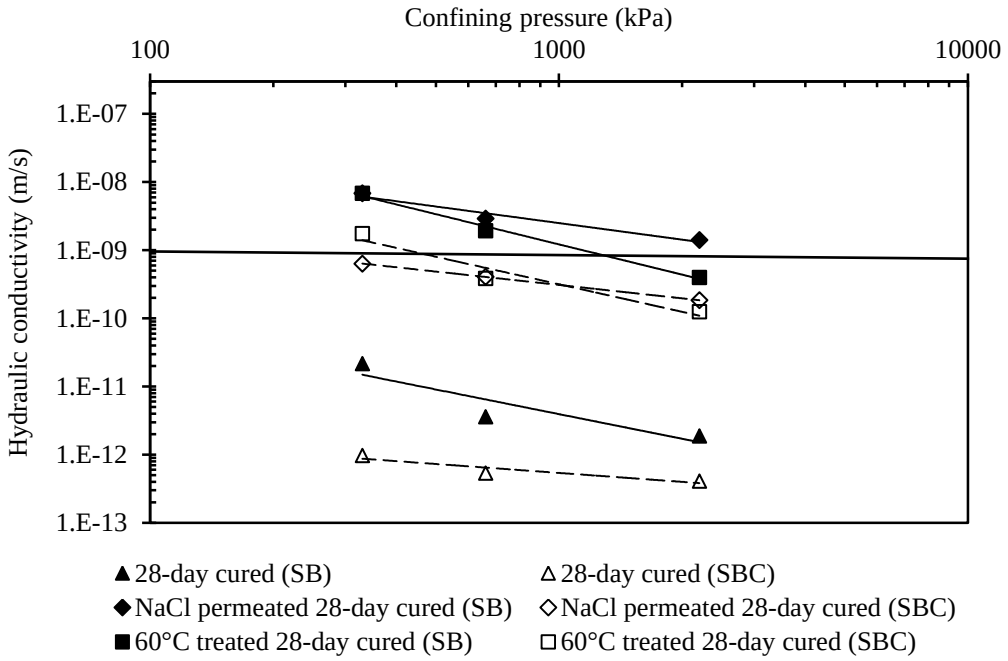

Figure 3.28. Hydraulic conductivity versus effective confining pressure relationships for all the cases studied.

swelling of bentonite closes the cracks formed. The bentonite reduces the hydraulic conductivity, while the sand reduces the bentonite cracking under shrinkage. Shrinkage phenomenon is the reduction of soil volume caused by loss of water. The shrinking process continues until the sample reaches a water content called shrinkage limit, at which further reduction of water content will not affect the volume of sample. In this condition the clay particles are at a very small distance from each other, and continued drying of the soil does not result in further decrease of the sample volume. The main aim of the shrinkage test is to attain the constitutive law that relates water content to the strain. The temperature and relative humidity during the shrinkage tests only affect the rate of drying (Briaud, 2003). In this study, the temperature of the testing room and oven were kept constant and the humidity was assumed not to vary much. Therefore, it is believed that the shrinkage testing was conducted at almost constant temperature and humidity conditions.

Figure 3.29 shows the relative change in axial strain ($\Delta H/H_0$) and relative change in volumetric strain ($\Delta V/V_0$) as a function of time. There were no cracks observed in fully dried samples.

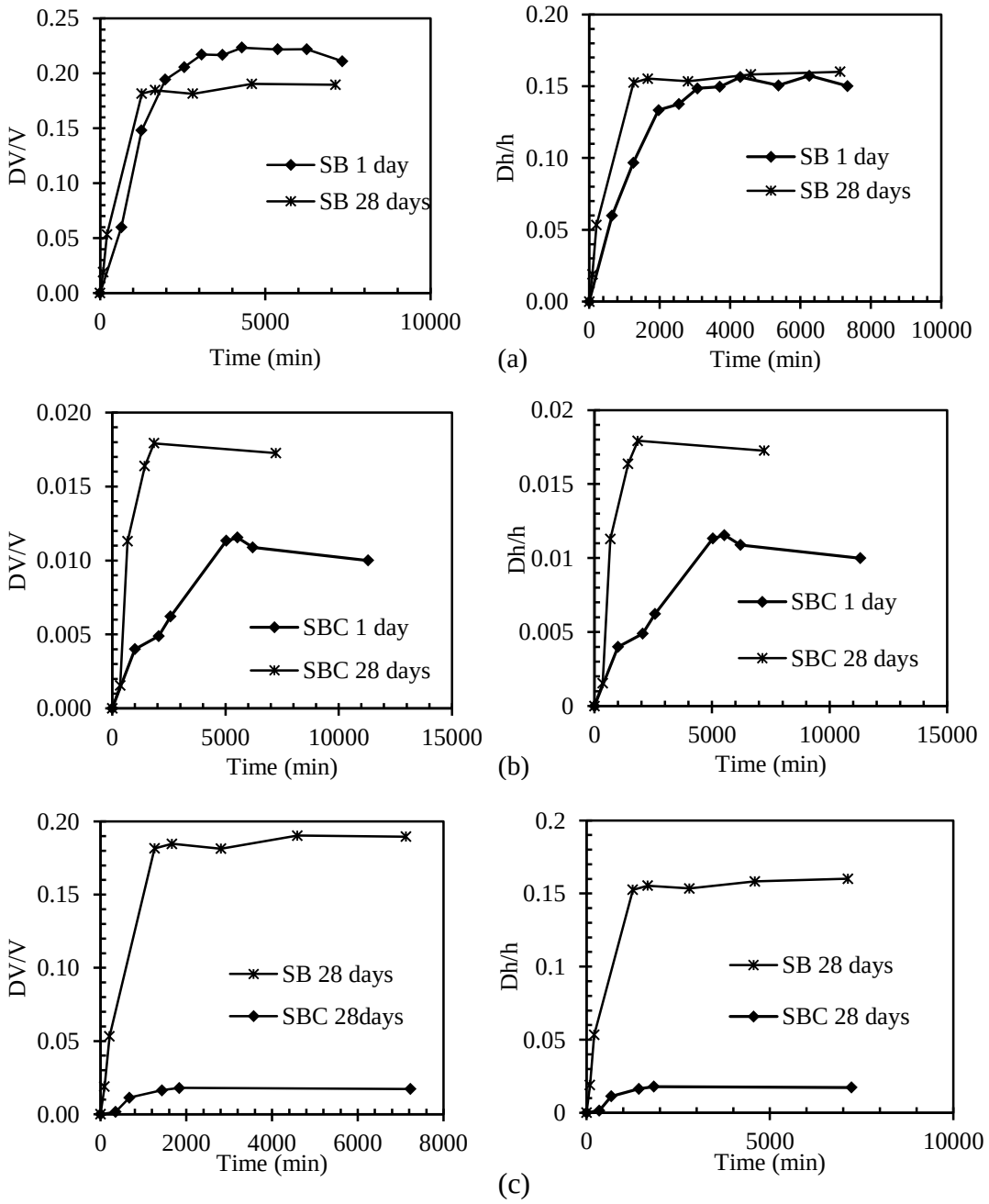

Figure 3.29. The relationship of change in height and change in volume with respect to time in (a) SB, (b) SBC samples and (c) comparison of SB and SBC samples.

Since the shrinkage strain versus time curves represent rectangular hyperbolas, the hyperbolic model can also be implemented to the shrinkage results to predict the ultimate values. The hyperbolic models of volumetric shrinkage curves are presented in Figure 3.30 and the results are displayed in Table 3.16. The measured and predicted values are almost the same. Therefore, maximum values can be predicted instead of laborious work involved in data recording during desiccation process.

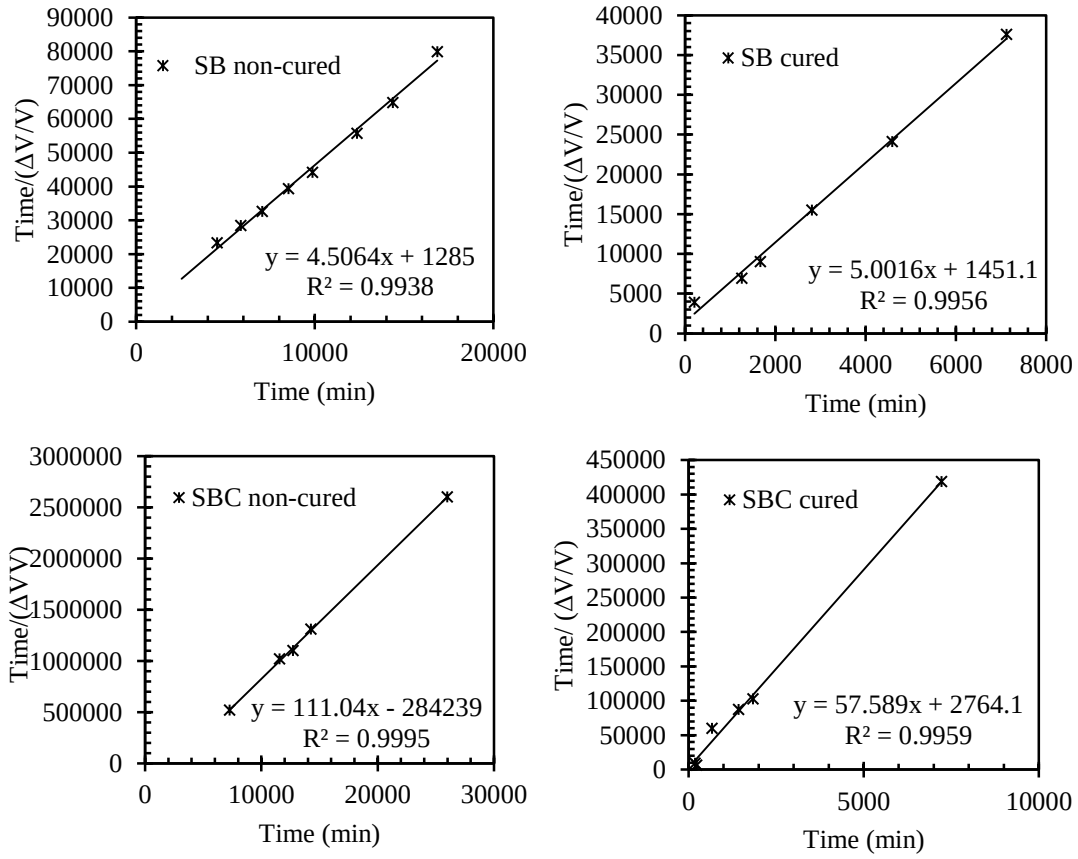

Figure 3.30. Time/(ΔV/V) versus time relationships of SB and SBC samples.

Table 3.16. Shrinkage properties and predicted shrinkage values.

Swell properties	SB		SBC	
	1-day cured	28-day cured	1-day cured	28-day cured
Measured max. shrinkage (%)	22	19	1.1	1.7
Hyperbolic constant, a	1285	1451.1	284239	2764.1
Hyperbolic constant, b	4.51	5.00	111.04	57.59
Predicted maximum shrinkage (%)	22.19	19.99	0.90	1.74

3.8.7 Shrinkage Curves

The void ratio versus water content relationships of sand bentonite and sand bentonite cement samples is illustrated in Figure 3.31.

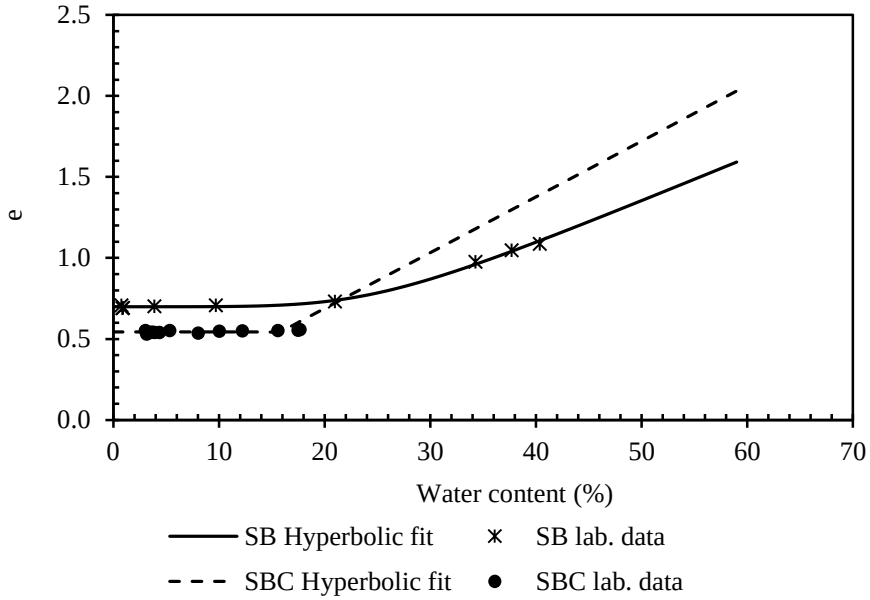

Figure 3.31. Shrinkage test results modeled with hyperbolic fit.

The shrinkage curve provides volumetric data for a soil as it dries and therefore allows calculations of volumetric properties for the SWCC. For modeling the shrinkage curves soil vision program has been used. The hyperbolic equation for determination of void ratio at any water content e(w) can be written as in Equation 3.8 (SoilVision, 2001).

$$e(w) = a_{sh}\left[\frac{w^{c_{sh}}}{b_{sh}^{\,c_{sh}}} + 1\right]^{\left(\frac{1}{c_{sh}}\right)} \tag{3.8}$$

In this equation the parameter a_{sh} represents the minimum void ratio the dried specimens attained, and the b_{sh} value is the minimum water content at which volume change ceased, which is the intersection of the minimum void ratio and the saturation

lines, and is referred to as shrinkage limit. The c_{sh} is curvature of the shrinkage curve, (Fredlund et al., 2002b).

The output data of shrinkage test can be used to obtain the constitutive law that links the water content to the strain. In Figure 3.32 shrinkage curve of sand bentonite sample is illustrated together with 100%, 80% and 60% saturation lines. As it can be seen from the graph the void ratio of sand bentonite sample decreases significantly from 1.1 at full saturation condition to 0.71 at the dried condition, which is a reduction of 35%. Compared to 30% swell percentage of this sample it shows a rational result since the swelling was started at optimum water content and not dry condition.

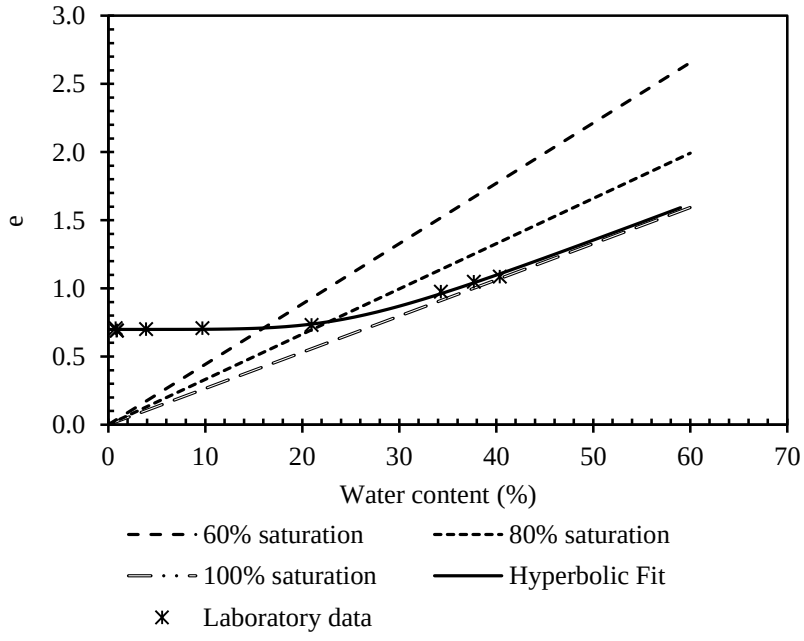

Figure 3.32. Shrinkage curve of 28 days cured SB.

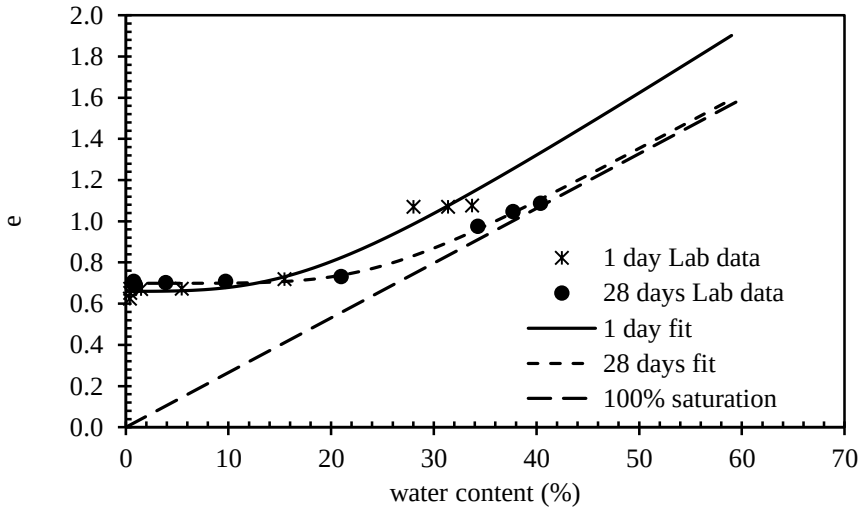

Figure 3.33. Shrinkage curves of SB samples with 1 and 28-day curing time.

Figure 3.33 illustrates the comparison of 1-day cured SB sample with the sample cured for 28 days. The 1-day cured sample shows a rather sharper curve than 28-day cured sample which means faster drying and higher volume change.

In Figures 3.34 and 3.35 the shrinkage curves of 28-day cured cement enhanced sand bentonite and comparison of it with 1-day cured sample are shown respectively. Both samples have almost zero shrinkage as the cement bonds are too strong to let the bentonite to expand. There were no cracks observed in fully air-dried samples with 5% cement addition. For a given desiccation rate the amount of cracking increases with the plasticity index of the sample. The amount of cracking is characteristically higher when the soil sample passes from saturated to unsaturated state which would be around the shrinkage limit (Briaud, 2003). In Table 3.17 the parameters of 1-day and 28-day cured SB and SBC samples are given. The maximum curvature of 1-day cured SB sample is almost two times more than 28-days cured SB sample, however, the minimum attained void ratio (a_{sh}) and minimum water content that volume change has happened (b_{sh}) are almost the same in both SB samples. The shrinkage fit

errors of cement enhanced samples are considerably high which represent the unreliability of fitting models for these types of specimens. As SBC samples act more like a rigid material, similar to concrete, rather than a compacted soil sample, the expectations of shrinkage parameters should also be different from an expansive soil.

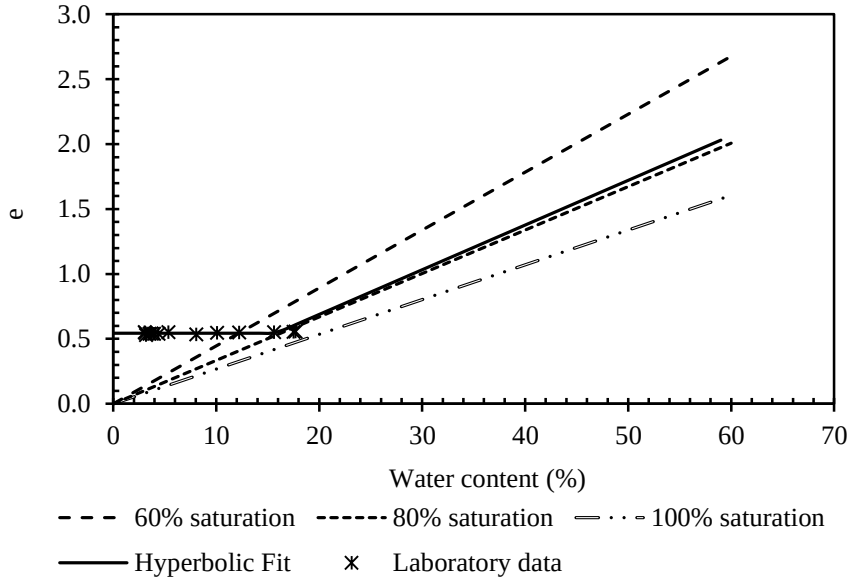

Figure 3.34. Shrinkage curve of 28 days cured SBC.

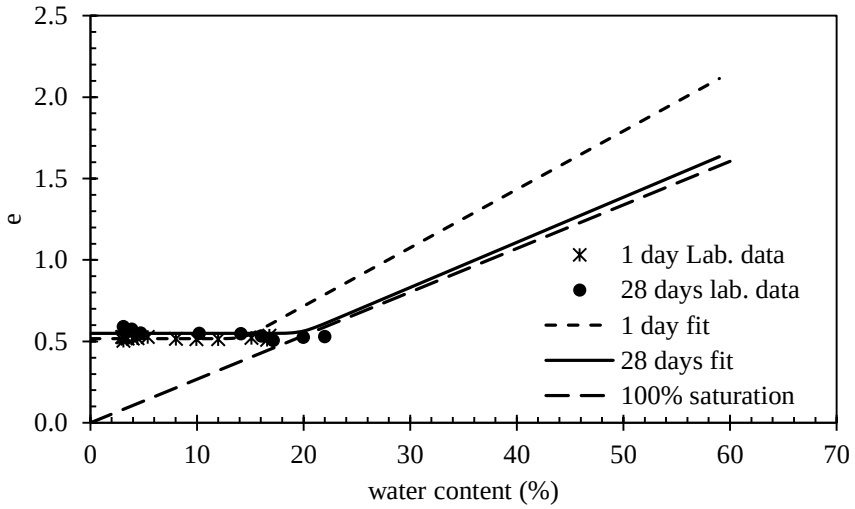

Figure 3.35. Shrinkage curves of SBC samples with 1 and 28-day curing time.

Table 3.17. Shrinkage parameters of SB and SBC samples.

Specimens	a_{sh}	b_{sh}	c_{sh}	Shrinkage Limit	Shrinkage Fit Error
SB 1 day	0.69	0.25	10.66	0.25	0.99
SB 28 day	0.70	0.26	5.21	0.26	1.00
SBC 1day	0.54	0.16	73.38	0.16	-6.00
SBC 28days	0.57	0.22	19.92	0.22	0.18

3.8.8 Cyclic Swell-Shrink

Cyclic swell shrink test was repeated for five cycles and the results are shown as percentage strain in accordance to initial compacted condition in Figure 3.36. The effect of wetting and drying is visibly significant in SB samples and after the fifth cycle swell percentage stabilizes at a value almost equal to the first cycle. In Figure 3.37 it can be seen that at the end of each cycle the distortion and damage happened in samples get more visible together with each cycle, at the end of fifth cycle the cracks forming after drying are large enough to almost separate the top part of sample. The pictures of SBC samples after first and last cycles are shown in Figure 3.38. It can be observed that the cycles of wetting and drying did not have much effect on SBC samples and the structure of sample stayed mainly intact with some minor cracks/broken parts at the sides of the sample in contact with ring at the end of the fifth cycle.

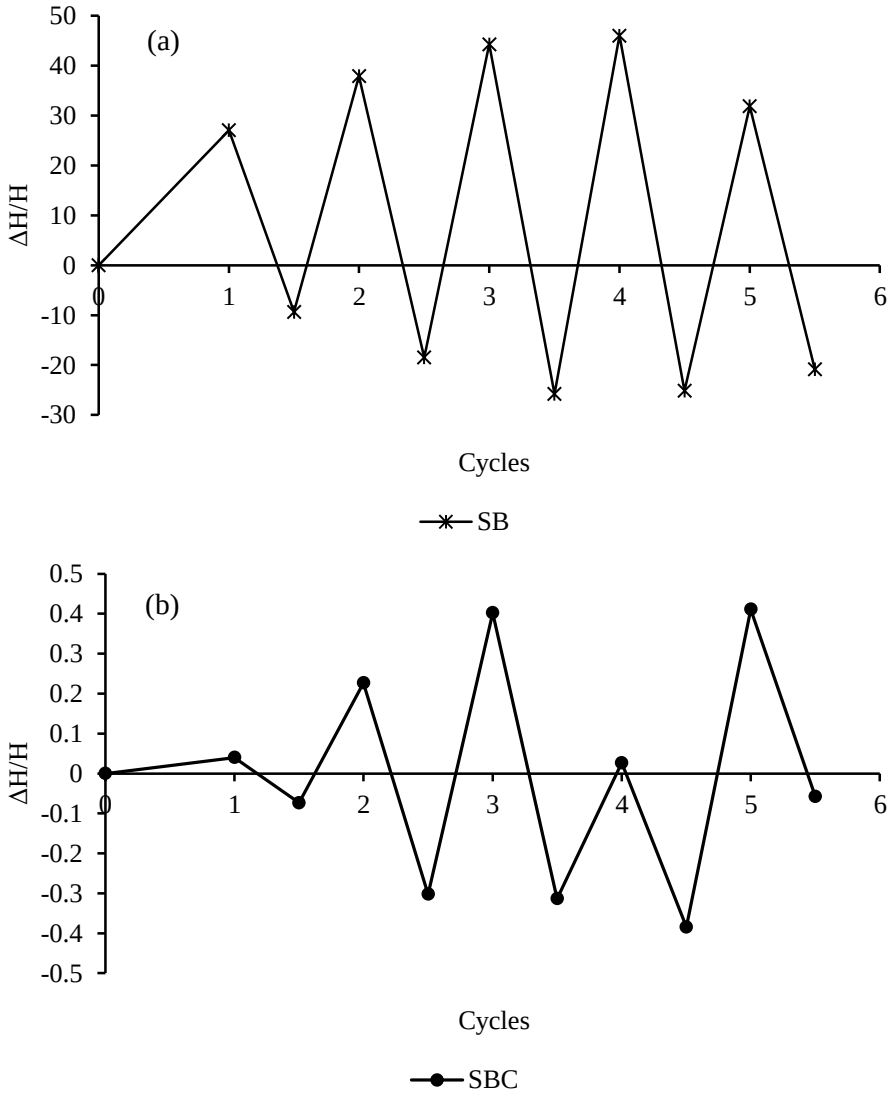

Figure 3.36. Strain variations of (a) SB and (b) SBC samples versus number of wetting and drying cycles.

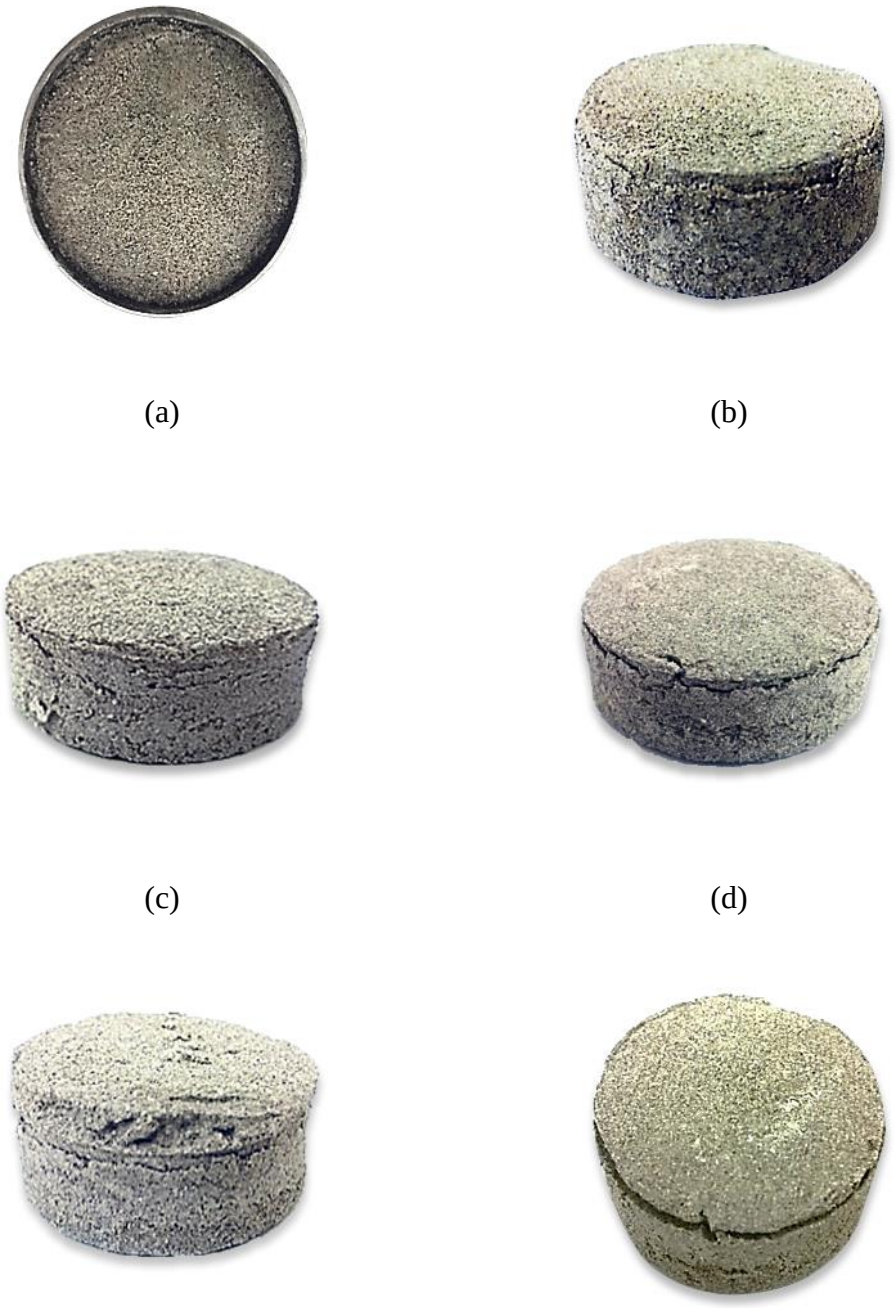

(a) (b)

(c) (d)

(e) (f)

Figure 3.37. Sand-bentonite sample at (a) beginning of the test, (b) after the first drying cycle, (c) after the 2nd drying cycle, (d) after the 3rd drying cycle, (e) after the 4th drying cycle, (f) after the 5th drying cycle.

(a) (b)

Figure 3.38. Sand bentonite cement sample after (a) first wetting –drying cycle, (b) fifth wetting–drying cycle.

3.9 Microstructural Comparison of Aged SB and SBC

Ye et al. (2013) observed that swelling and swell pressure of 90 days aged samples decreased with curing time with a more noticeable decrease in first days of aging, which can be attributed to bonding effects and hydration of smectite. Right after preparation of sample, the suction is not fully equilibrated within the various levels of microstructure. However, it was noted that swell properties of soil decreased with aging, which is explained as the arrangement of clay particles through time. Yet the swell properties that stay after aging of sample would be still sufficient to fulfill the engineered barriers requirements (Delage et al., 2006).

Ye et al. (2012) in an experimental study on densely compacted bentonite reported that for 40°C and 60°C the unsaturated hydraulic conductivity reduces slightly in the early stages of hydration, and it becomes constant as hydration progresses. At the final stage the conductivity increases rapidly as suction decreases and saturation is reached. In confined conditions, hydraulic conductivity increases together with

temperature. It was also detected that the effect of temperature on the hydraulic conductivity is relatively suction-dependent. At suctions higher than 60 MPa the temperature effect is mainly due to its influence on water viscosity; while in lower suctions temperature effect is related to the water viscosity and the macro-pores closing phenomenon both.

The microstructural changes within the SB and SBC samples after 1 year curing period were studied using scanning electron microscopy (SEM). Micro-structure in this context is defined as the arrangement of sand- bentonite particles and sand-bentonite-cement particles respectively. At low magnification (x 200) SEM image shows that larger particles of sand are separated by a matrix of bentonite and finer sand particles as can be depicted in Figure 3.39 (a). The particle coating is the primary mode by which bentonite fills the pores (Abichou et al., 2002). The flakey montmorillonitic appearance of the bentonite coating on the sand disappears in Figure 3.39 (b) with the cement treatment where distinct montmorillonite particles could no longer be observed. Instead large clay-cement clusters are observed due to grouping of clay and cement particles when mixed and interacted with water (Horpibulsuk et al., 2010). The fabric changes developing during the curing of SBC lead from a mixture of discrete soil particles and cement grains to a more homogeneous texture.

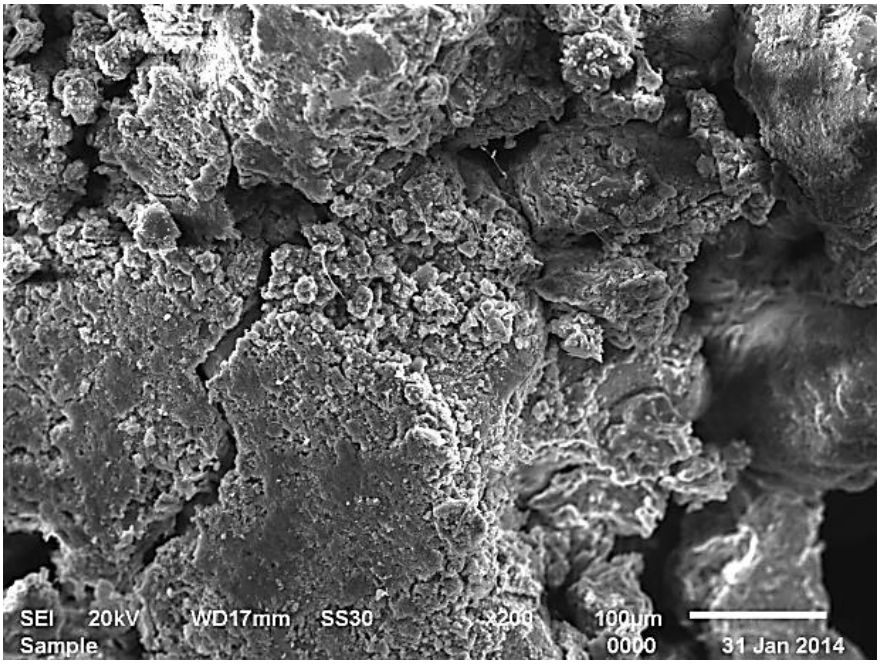

(a)

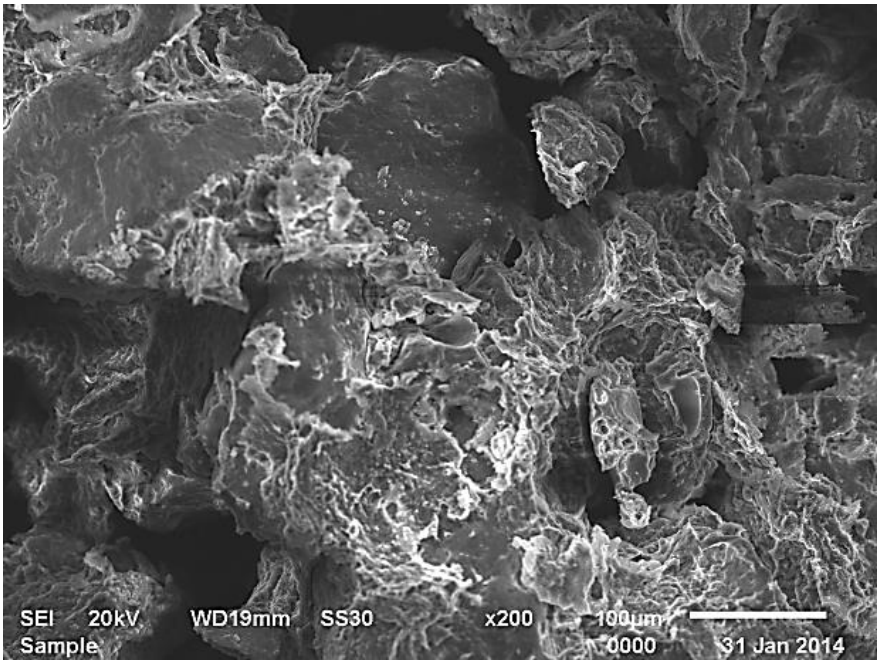

(b)

Figure 3.39. Scanning electron micrographs of (a) SB (x 200), (b) SBC (x 200), (c) SB (x 2000), (d) SBC (x 2000).

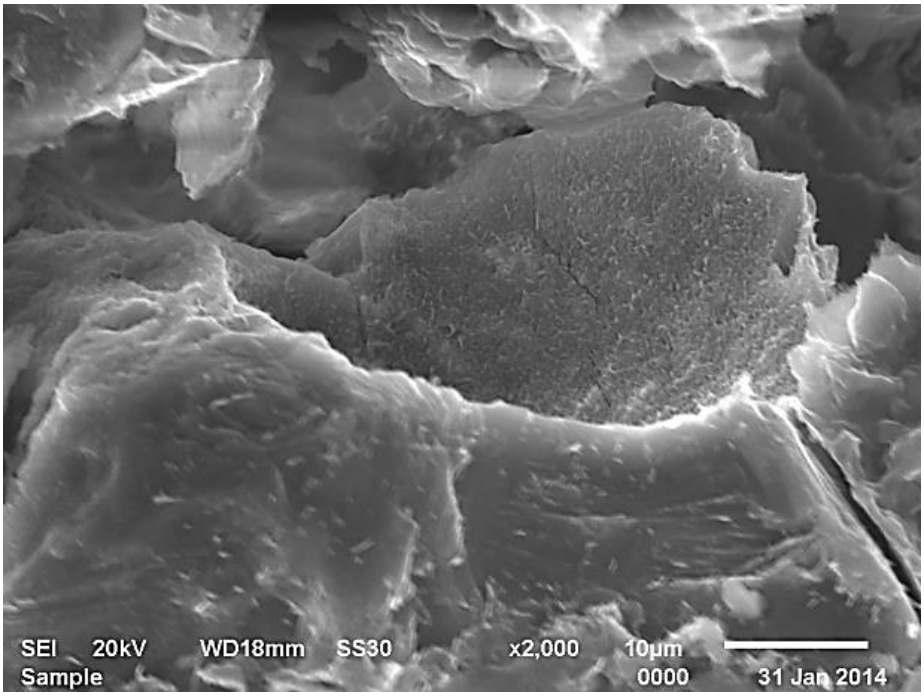

(c)

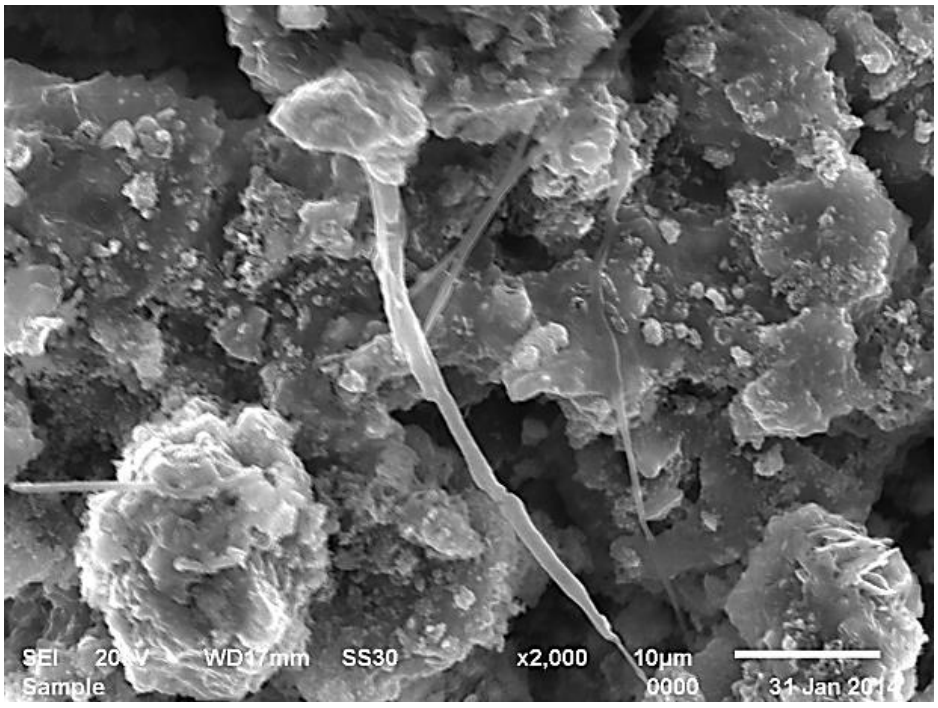

(d)

Figure 3.39. (continued)

Figure 3.39 (c) and (d) depict x 2000 magnification of SB and SBC specimens respectively.

The tobermorite-like gels (CSH) can be observed in Figure 3.39 (d) forming around the edges of soil particles binding soil particles together. Lime liberated during hydration of the Portland cement enters into almost immediate reaction with the clay particles resulting in rapid consumption of lime and breakdown of the clay phase. As time of curing increases, the abundance of cement hydrate increases. Some of the soil particles become poorly crystalline and may lose their identity completely. Formation and growth of these reaction products made the stabilized soil structures denser and stronger, resulting in an increase in strength (Nontananandh et al. 2005). As hydration of the cement begins, cement gel forms along the edges of groups of particles, probably diffusing away from the initially unhydrated cement grain. Simultaneously, lime liberated from the hydrating cement begins to break down the soil particles. Additional calcium silicate hydrates can form from breakdown of clay particle surfaces and calcium aluminum silicate hydrates may develop at particle edges. As these processes progress the structure becomes more and more interlaced with cement gel, particle surfaces become more irregular and the mixture appears more compact. Ultimately the breakdown of the soil particles and diffusion of the cement gel progresses to the point where the separate phases are virtually undistinguishable.

3.10 Unsaturated Behavior of SB and SBC

3.10.1 SWCC of SB and SBC

In order to predict the performance of sand-bentonite barriers, it is essential to determine the suction characteristics. In this study the suction measurements were done according to filter paper method. SoilVision (1998) software, a knowledge-based system database, was used to fit the models and calculate the fitting parameters of soil water characteristic curve (SWCC), and shrinkage curves. The models of van Genuchten (1980) and Fredlund and Xing (1994) are fit to the experimental data.

Van Genuchten equation (1980) presented an equation with flexibility of fitting a wide range of soils by using three parameters (Equation 3.9).

$$w_w = w_{rvg} + (w_s - w_{rvg})\left[\frac{1}{\left[1+\left(a_{vg}\psi\right)^{n_{vg}}\right]^{m_{vg}}}\right] \tag{3.9}$$

Where:

w_w is the gravimetric water content at any soil suction,

w_{rvg} is residual gravimetric water content,

w_s is saturated gravimetric water content,

a_{vg} is a soil parameter which is primarily a function of the air entry value in (kPa)

n_{vg} is a soil parameter which is primarily a function of the rate of water extraction from the soil once the air entry value has been exceeded

m_{vg} is fitting parameter

Fredlund and Xing (1994) presented an equation with three parameters which fit a wide range of soils and also is modified to be more accurate in high ranges of suction (Equation 3.10).

$$w_w = w_s\left[1-\frac{\ln\left(1+\frac{\psi}{h_r}\right)}{\ln\left(1+\frac{10^6}{h_r}\right)}\right]\left[\frac{1}{\left[\ln\left[\exp(1)+\left(\frac{\psi}{a_f}\right)^{n_f}\right]\right]^{m_f}}\right] \qquad (3.10)$$

Where:

w_w is the gravimetric water content at any soil suction,

w_s is saturated gravimetric water content,

a_f is a soil parameter which is primarily a function of the air entry value in (kPa)

n_f is a soil parameter which is primarily a function of the rate of water extraction from the soil once the air entry value has been exceeded

m_f is a soil parameter which is primarily a function of the residual water content

h_r is suction at which residual water content occurs (kPa).

As it can be seen in Figure 3.40, the SWCC curve of SB is steep and sharp showing high sensitivity of soil suction to reduction of water content, however in SBC samples the difference between saturation water content and water content at natural dried condition is not significant and also suction properties of cement included samples do not show high sensitivity during desorption. Therefore the SWCC curve of cement included samples is slowly decaying as suction is increased. In Figure 3.41 the same laboratory data is modeled with Fredlund and Xing (1994) equation in

Soilvision software. In both modeling systems the air entry value (AEV) of SBC samples are slightly lower than AEV in SB samples.

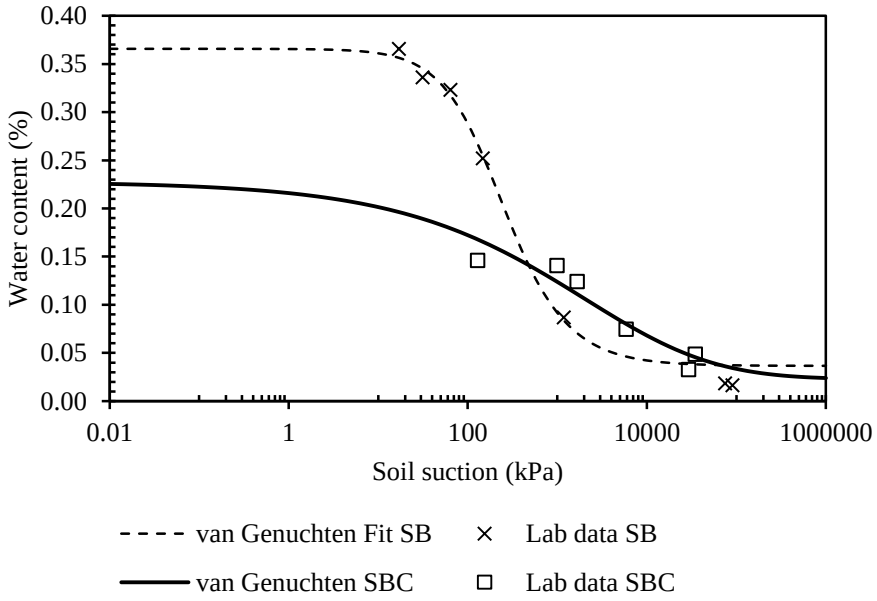

Figure 3.40. SWCC of SB and SBC fitted by van Genuchten (1980) model.

Table 3.18. van Genuchten (1980) SWCC model parameters.

Sample	a_{VG}	n_{VG}	m_{VG}	Residual WC, w_r (%)	AEV (kN/m^2)	R^2
SB	0.00535561	1.3547	0.753	10%	49.39	0.99
SBC	9.8072E-06	0.3712	4.280	10%	17.37	0.90

WC: water content.

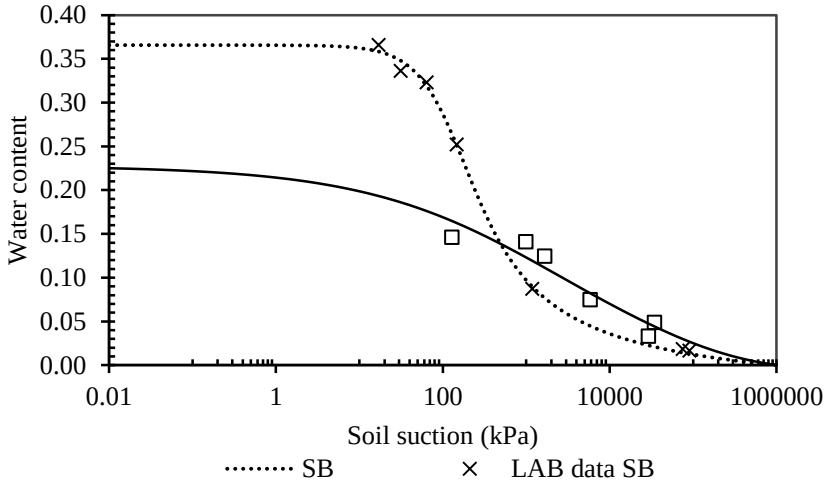

Figure 3.41. SB & SBC Fredlund and Xing (1994) Fit.

Table 3.19. Fredlund and Xing (1994) SWCC model parameters.

Sample	a_F	n_F	m_F	hr	Residual VWC (%)	AEV (kN/m^2)	R_2
SB	112.68	1.58	0.96	913.15	0.06	47.67	1.00
SBC	2499.96	0.37	2.91	84672.43	0.02	12.61	0.91

VWC: volumetric water content.

3.10.2 Unsaturated Hydraulic Conductivity Prediction

Compacted sand-bentonite mixtures have been favored as suitable barrier materials for the disposal of municipal waste. Initially unsaturated on placement, the barriers may become saturated upon availability of fluid, mainly from the waste material. The liner must prevent this leachate from draining into the ground water. Therefore, liners must be properly designed and installed to prevent these ill effects. Hence the materials to be used must be selected in right proportions and the mixtures must be evaluated and studied well. Therefore, in order to gain a thorough understanding of the behavior and for ensuring the reliability of the disposal system required for geoenvironmental protection, saturated as well as unsaturated hydraulic conductivity must be fully studied.

The hydraulic conductivity is not a constant in unsaturated soils but is a function of soil suction. Various research works have shown that there is a relationship between the soil-water characteristic curve of soils and their unsaturated properties. Using Fredlund et al. (1994) predictive model for the hydraulic conductivity the unsaturated hydraulic conductivity for different suction values can be obtained from Equation 3.11.

$$k_r(\psi) = \frac{\int_{\ln(\psi)}^{b} \frac{\theta(e^y) - \theta(\psi)}{e^y} \theta'(e^y) dy}{\int_{\ln(\psi_{aev})}^{b} \frac{\theta(e^y) - \theta_s}{e^y} \theta'(e^y) dy} \quad (3.11)$$

Where:

$\psi =$ soil suction, given a function of volumetric water content

$\theta =$ volumetric water content

$\theta_s =$ saturated volumetric water content

$\theta_r =$ residual volumetric water content

$b =$ ln(1,000,000)

$y =$ dummy variable of integration representing the logarithm of suction

$aev =$ air-entry value (Fredlund et al, 1994).

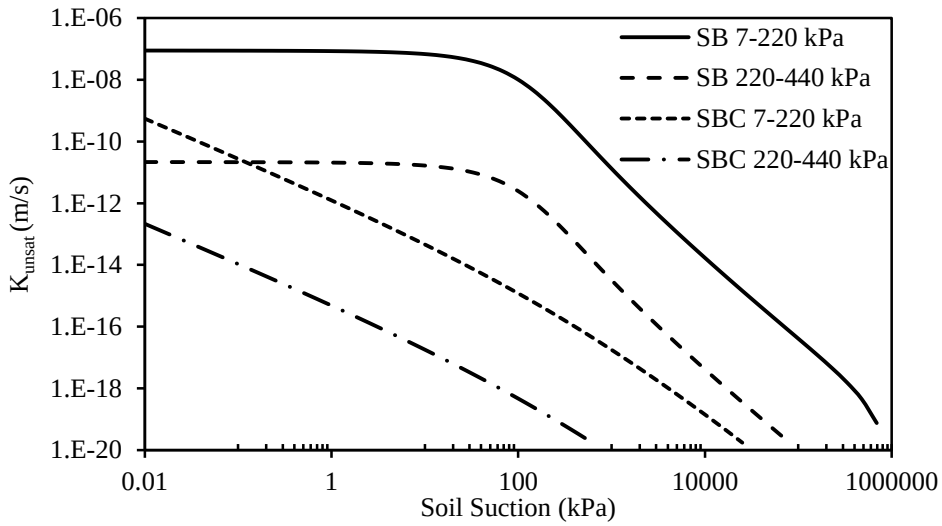

Figure 3.42. Unsaturated hydraulic conductivity versus suction relationships of non-cured SB and SBC samples under effective stresses of 7-220 kPa and 220-440 kPa.

The unsaturated hydraulic conductivity predictions for SB and SBC under two ranges of effective confining pressures are presented in Figure 3.42. The SB samples remain saturated until the air entry value which is higher than the air entry of SBC. The unsaturated hydraulic conductivity diminishes along the desorption phase faster than the SBC specimens, reaching to zero eventually.

3.10.3 Constitutive Surfaces

Figures 3.43 and 3.44 are the void ratio and water content constitutive surfaces of sand bentonite samples respectively and Figure 3.45 and 3.46 are presenting void ratio and water content constitutive surfaces of SBC. In Table 3.20 the volumetric deformation indices are shown. All volume change indices, the slope of void ratio with respect to suction, C_m, slope of void ratio curve with respect to pressure, C_t, soil water characteristic surface with respect to suction, D_m, and slope of water content with respect to pressure, Dt reduces by addition of cement.

Table 3.20. Volumetric deformation indices.

	C_m	C_t	D_m	D_t
SB	0.3930	0.1985	0.0993	0.0747
SBC	0.0039	0.0399	0.0735	0.0133

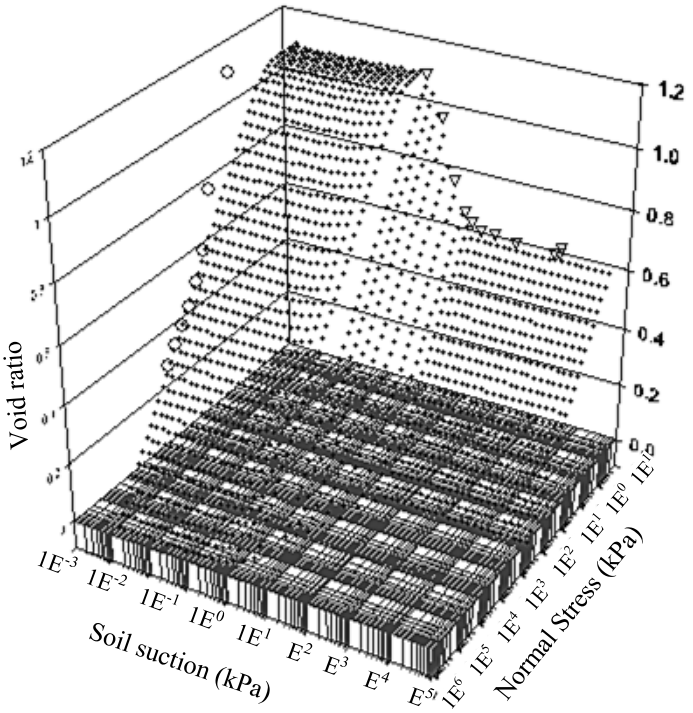

Figure 3.43. Constitutive surface of SB, demonstrating the relationship of void ratio, normal stress and soil suction.

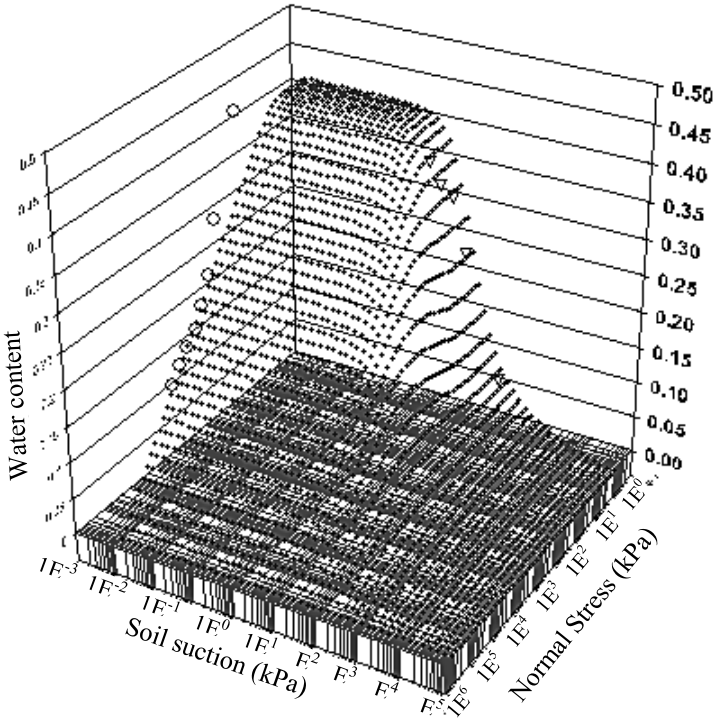

Figure 3.44. Constitutive surface of SB, demonstrating the relationship of water content, normal stress and soil suction.

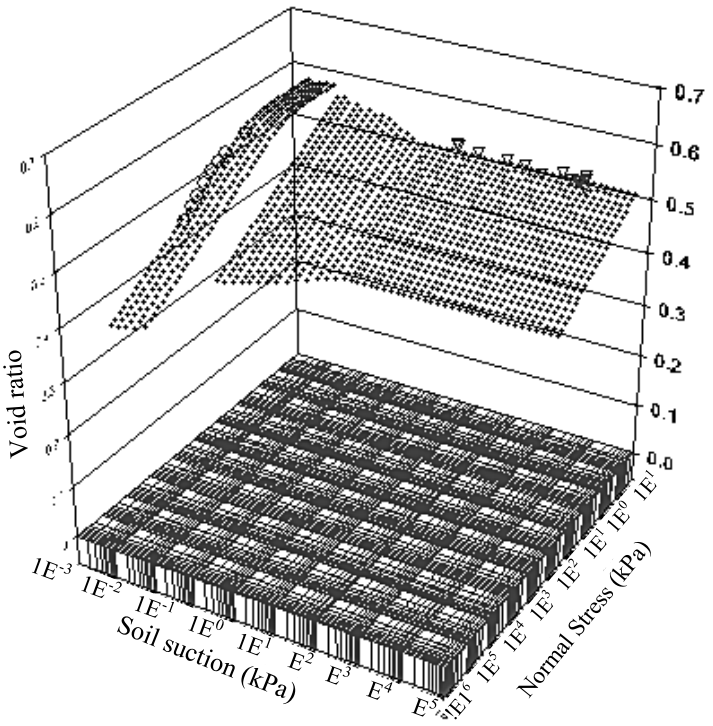

Figure 3.45. Constitutive surface of SBC, demonstrating the relationship of void ratio, normal stress and soil suction.

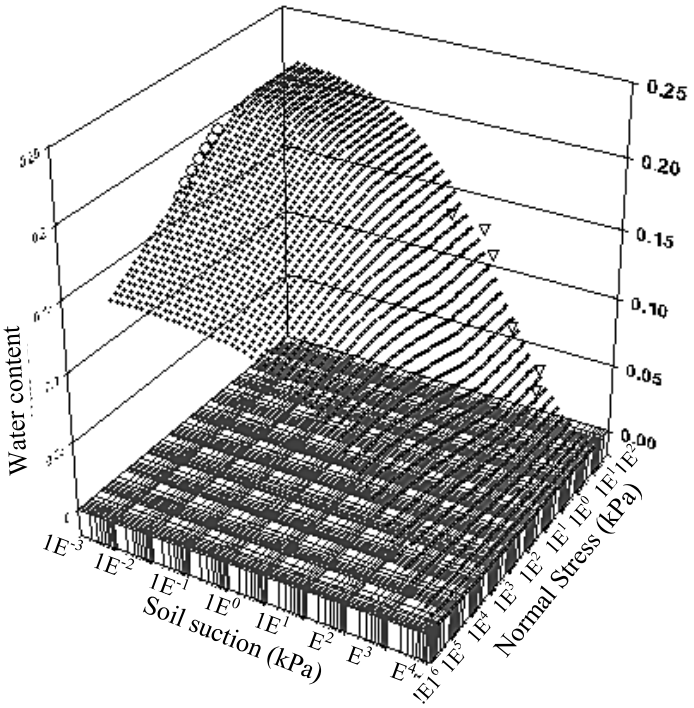

Figure 3.46. Constitutive surface of SBC, demonstrating the relationship of water content, normal stress and soil suction.

3.11 Conclusions

The proposed barrier material proportions selected in Chapter 2 has been experimentally studied investigating on the volume change, hydraulic conductivity and unsaturated behavior of SB and SBC. Volume change includes swell-shrinking and swell-compressibility, whereas unsaturated behavior studied consists of soil water retention capacity or soil-water characteristic curve, and predictions of unsaturated hydraulic conductivity and constitutive behavior under compression in unsaturated condition. The effect of curing up to 28 days is also examined in both macro and micro behavior, and further tested to assess the durability of the mixtures aged by studying the effects of cyclic wetting-drying, elevated temperature of maximum 60°C, and permeation of external water with high concentration of NaCl. The influence of all these changing conditions on hydraulic conductivity, which is the most important parameter, required for the sustainability of landfill barriers, is assessed and the summary of observations and conclusions are listed as follows:

1. One dimensional swell percentage reduced by 3% when SB specimens were aged for 28 days whereas swell percentage reduced almost 100% with the addition of 5% cement, which remained almost the same within 28 days of curing.
2. When the 28-days cured SB specimens were permeated with 1 mol. NaCl solution the swell percentage reduced from 27% to 0.45%, which is almost 100% reduction. In the SBC samples, however, a negligible magnitude of swelling was observed when subjected to saline water, which can be attributed to the intercalation effect.

3. The swell potential of SB samples has reduced by 19% when the swelling occurred under 60°C, whereas for SBC samples, a minor increment in swell potential was recorded which was very negligible.
4. The void ratio versus effective pressure relationships displayed bilinear characteristics in SB samples under compression, C_c reducing after a threshold effective pressure value.
5. The compression index is reduced by 40% in the aged SB samples until the threshold effective pressure, remaining almost the same thereafter.
6. The effect of NaCl permeation caused a reduction of 83% in compression index of aged SB, and eliminated the bilinearity of the compression curve.
7. When consolidating at 60°C, the bilinearity of the compression curve remained and the compression indices were only slightly affected by the temperature increase.
8. The rebound indices obtained indicate a 27% increment when SB specimens age in 28 days, 27% reduction as aged specimens are permeated with salt solution, and 64% increment when rebounded at 60°C. The latter is in good agreement with the observed increment in swell pressure at the elevated temperature.
9. The compression indices of 1-day and 28-day cured SBC specimens are approximately 88% and 84% less than the corresponding SB specimens below 400 kPa and 60% and 70% less above 400 kPa effective pressure.
10. The measured maximum swell values are in good agreement with the predicted ultimate values obtained from the hyperbolic model. This can

facilitate the swell potential determination which is a laborious and time consuming procedure.

11. The hydraulic conductivity values of SB specimens measured by flexible permeameter were found to be consistent with the predicted values from consolidation test data. For SBC specimens, however, the measured values are completely far from the trend of predicted ones.
12. The hydraulic conductivity determination depicts that it reduces with the effect of NaCl permeation and effect of temperature for 28-day aged SB specimens when under low effective confining pressures, below 220 kPa. However, under this pressure range all the values are nevertheless higher than 1×10^{-9} m/s. Under confining pressures higher than 220 kPa, the 28-day aged SB possesses a value much lower than the allowed limit, which increases and exceeds this limiting value by almost 100-fold when NaCl permeation and temperature elevation occur. Under confining pressures higher than 400 kPa, the hydraulic conductivities reduce significantly, however the detrimental effect of salinity and elevated temperatures remain.
13. The hydraulic conductivity determination of SBC specimens displays higher values than 1×10^{-9} m/s in the low confining pressure range, reducing slightly with the NaCl permeation while significantly increasing with the elevated temperature. At confining pressure range of 220-440 kPa, the hydraulic conductivity reaches to the desirable values except when temperature effect is included. All the values reduce below the allowed limit appreciably under pressures above 440 kPa.

14. It was also observed that while NaCl permeation adversely affects the hydraulic conductivity of SB specimens, it is the temperature elevation which influences the hydraulic conductivity most in SBC specimens.
15. It can be inferred from the volumetric and axial shrinkage strains obtained from shrinkage testing that the maximum strains reduced by 94% when cement was added. The hyperbolic model was suitable for shrinkage data also, since shrinkage curves represent rectangular hyperbolas. Hence the ultimate shrinkage strains can be predicted from the model for future work when prolonged shrinkage measurements are required.
16. Based on the relationships of void ratio versus water content during shrinkage process, the fitting parameters obtained from SoilVision are related to the minimum void ratio and the shrinkage limit of the desiccated samples. The minimum void ratio slightly increases in 28-day cured SB specimens whereas 5% increment was noted in cured SBC samples. It is also observed that the shrinkage limit increased insignificantly in SB while 38% increment was recorded for cured SBC samples.
17. Cyclic swell-shrink testing on SB displayed gradual increase both in swell and shrinkage at successive cycles, which shows a reduction of 30% in swell and 17% in shrinkage at the end of fifth cycle. The cyclic behavior of SBC samples, however does not follow a regular trend, and the magnitudes of swell and shrinkage are almost negligible.
18. The SEM studies on the specimens aged for 1 year clearly illustrate the tobermorite (CSH) formation in the cement treated specimens.
19. In the context of unsaturated behavioral study, the soil-water characteristic curves obtained for SB and SBC specimens during desorption were fitted by

van Genuchten (1980) and Fredlund and Xing (1994) models and the model parameters displayed a moderate increase in the air entry value whereas the rate of desorption significantly reduces when cement was added.

20. Unsaturated hydraulic conductivity function was predicted using Fredlund et al. (1994) pedo-transfer function which utilizes SWCC. The results present the reduction of unsaturated hydraulic conductivity with increasing suction. The saturated hydraulic conductivity for SB which is higher than the limiting value under low confining pressures reduces to the limiting value at 600 kPa suction, which corresponds to 5% water content. Therefore, under low confining pressures, the hydraulic conductivity may be safe, however the low water content is not very realistic in the practical application.
21. The unsaturated compressibility function can be predicted based on the consolidation and shrinkage test results as well as SWCC. The three-dimensional surfaces are presented in this thesis as a representation of the unsaturated behavior in compression.
22. The unsaturated behavior of specimens under the effect of aging, NaCl permeation and temperature elevation are not included in this study.

Chapter 4

STRENGTH PROPERTIES OF SAND-BENTONITE MIXTURES AND THE EFFECT OF CEMENT ENHANCEMENT

4.1 Introduction

In most countries the primary method of waste disposal is the use of landfills which are containment facilities preventing or minimizing pollutant migration to the underground water and the local environments. Compacted mixtures of sand-bentonite are commonly used as landfill barriers due to lower susceptibility to frost damage and lower potential for volumetric changes during wetting and drying processes (Montanez, 2002). Bentonite as a clay material with high amounts of montmorillonite appears to be a good option to be used together with sand due to its high water absorption capacity and very low hydraulic conductivity, while sand holds the main structure of the compacted mixture together. Montmorillonite is an alteration product of volcanic ash, a highly colloidal mineral composed of one gibbsite sheet squeezed in between two silica sheets. In between each layer of montmorillonite there are few amounts of exchangeable cations and large quantity of water molecules. The negative charge of outer layer of this mineral attracts water molecules which makes the basal spacing of it to range from 9.6 Å to complete separation in full hydration (Das, 2006; Mitchell, 1993). Upon desiccation due to climatic changes or elevated temperatures in the landfill containment caused by biochemical processes, shrinkage occurs, leading to crack formation in the compacted barriers. The crack formation creates preferential flow paths for

contaminant leakage, and reduces the resistance of the compacted containment material due to development of stress concentrations at the crack tips (Vesga, 2009). Using sufficient amounts of bentonite produces a combination that can absorb water and swell in saturated condition sealing the voids as well as developing resistance to desiccation cracks in dry season (Stewart et al., 2003). Therefore, while the granular particles of sand maintain the strength and stability of composite, the small particles of bentonite seal the voids between them and reduce hydraulic conductivity.

Determining the tensile strength of soil is useful in designing compacted layers which are intended to be used as hydraulic barriers, as they may be subjected to erosion due to tensile cracks imposed by climatic changes. The need for studying tensile strength arises mainly from the study of unsaturated soils, as the tensile strength is directly related to the suction potential of the unsaturated soils (Peters and Leavell, 1988). Tensile cracks represent Mode I failure as described in fracture mechanics. This phenomenon is not very well studied in geotechnical approaches, mainly due to lack of a standard laboratory testing technique devised for soils (Fang and Chen, 1972; Kim et al., 2012). The importance of studying tensile characteristics of compacted soils is emphasized by various researchers. Leonards and Narain (1963) investigated the cracking behavior of earth dams by testing the flexural strength (tensile-bending) of a clay-beam. Conlon (1966) performed unconfined tensile testing (direct tension) on soft silt by necking the mid portion of the specimens so as failure occurred in this zone. Suklje (1969) indicated that when cohesive layers at the base of open excavations are subjected to artesian water pressures, tensile fissures can appear, and the critical hydraulic gradients depend on the shearing strength as well as tensile resistance of soil. The effect of tensile

strength in cohesive slopes was studied by Spencer (1968) and Suklje (1969) who indicated that creep and critical state stresses with tensile principal stress develop in the upper parts of slopes. George (1970) and Sih and Fang (1972) applied fracture mechanics theory in assessing the tensile characteristics and cracking in various highway materials.

Cement may be used in small amounts as an additive to increase strength of compacted sand-bentonite, reduce hydraulic conductivity and possibility of crack formation (Maher and Ho, 1993; Kvennas et al., 2009; Consoli et al., 2010; Verastegui Flores et al., 2010; Consoli et al., 2013). A major factor in considering soil-cement liner for sanitary or hazardous waste landfill sites is its compatibility with stored wastes. After a week of curing, cement hydration process within the soil leads to formation of elongate tobermorite-like gels (CSH) around the soil particle edges and with further curing of up to 28 days, the CSH fibers increase and result in a homogenous structure that combine the particles of clay and cement together. The change in structure and fabric of soil developed by this process reflects in mechanical properties of soil in terms of increasing strength and durability. The hydration process proceeds over a long period yet at a continuously decreasing rate (Mitchell and El Jack, 1966). According to Grubbs (1965) the degree of stabilization achieved by cement addition in soils depends on type of soil, amount of cement added, amount of free water in soil during compaction and density achieved after compaction. The calcium ions released during the initial cement hydration reactions and the cation exchange leads to reduction in plasticity of the cement-stabilized soil. Bonding between the adjacent soil grains and cementation is the other effect of cement addition to cohesive soils. Azeredo et al. (2007) have done a study on different

factors that affect the results of strength tests of soil-cement mortars and concluded that these are confinement, height to diameter ratio and method of displacement measurement. Bahar et al. (2004) studied on the performance of cement-stabilized soil by various methods of compaction and included that compaction at optimum water content of mixture is important in order to achieve higher strength and durability. They also studied the effect of curing with water and observed that direct contact of stabilized soil blocks with water would result in a decrease in compressive strength of the soil after 48 hours.

In this study, strength properties of sand-bentonite (SB) and sand-bentonite-cement (SBC) mixtures are studied and compared by operating unconfined compression, split tensile (Brazilian), flexural strength, double punch (unconfined penetration) and cubic compressive strength tests. Unconfined compression test has been used to verify the effect of cement addition to strength of compacted soil and as a control test for comparing results derived from other strength tests substantiating the findings obtained in similar studies carried out earlier (Kvennas et al., 2009; Consoli et al., 2010; Verastegui Flores et al., 2010; Consoli et al., 2011; Consoli et al., 2013). Split tensile and flexural strength test methods were adopted to indirectly obtain tensile strength of compacted samples. Cubic compression test is implemented on the end pieces of the compacted flexure beam remaining at the end of flexural strength test with the aim of indirectly estimating the unconfined compressive strength. The aging effects on strength properties are also studied over curing periods of 1, 7 and 28 days in all tests, up to 90 days for unconfined compressive strength test and up to 365 days for flexural and cubic compressive strength tests. The aging effects are also

explained in terms of micro structural changes as observed in scanning electron micrographs.

4.2 Sample Preparation

The mixtures were prepared by pre-drying sand and bentonite in oven, the drying temperature not exceeding 60°C for bentonite. Sand was then passed through 2.00 mm sieve to eliminate impurities. The optimum water content and maximum dry density were calculated through standard Proctor compaction test according to ASTM D698-12. In order to attain homogenous moisture content within each sample, the batches were mixed thoroughly in mechanical mixer, sealed in double nylon bags and kept for 24 hours prior to compaction. For cement included samples the required percentage of cement by dry mass of sand-bentonite mixture was added right before compaction, ensuring that the mixing and compacting period would not exceed the setting time. In order to achieve identical samples, Proctor maximum dry density and optimum water content values were used to prepare statically compacted samples required for strength tests. The mold sizes for unconfined compression split tensile and flexural strength tests were 38x76 mm, 50x100 mm and 4x4x16 mm respectively.

Unconfined compression test series were carried out according to ASTM D2166-06. Samples were compacted statically at their maximum dry density and optimum water content, with modified CBR machine. The moist mixture was placed in mold and compacted in three layers, each layer being scratched at the surface for uniformity in a 38 x 76 mm diameter and height mold. The tests were then carried out in a triaxial test system, and the data was collected through data logger (Figure 4.1).

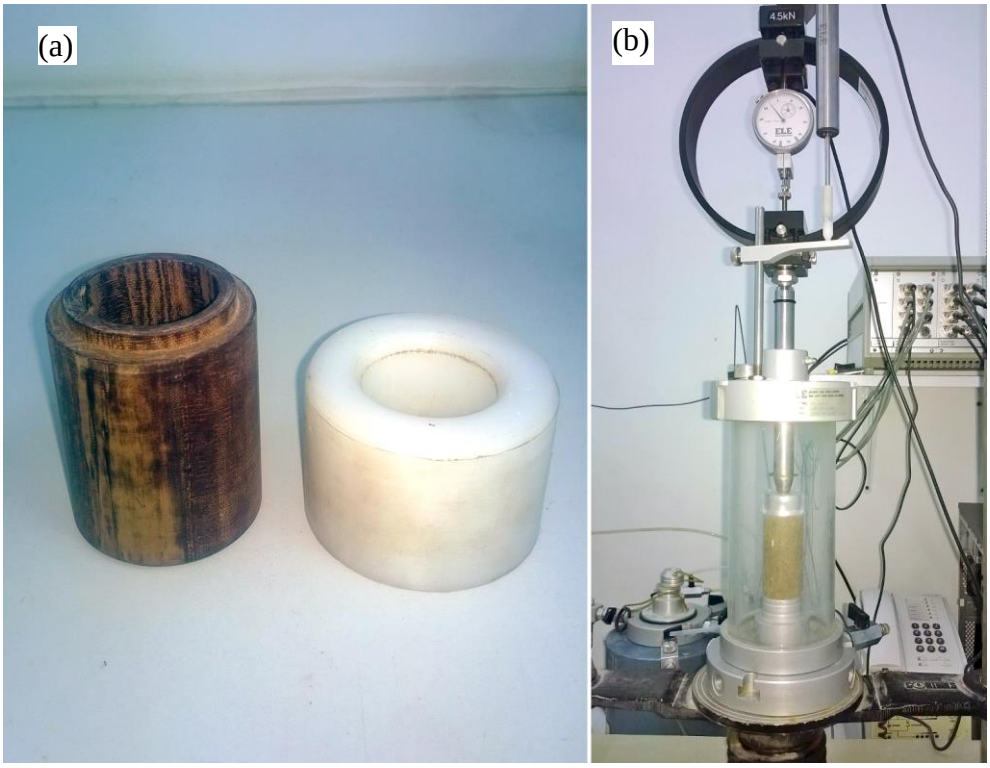

Figure 4.1. Unconfined compression test, (a) mold and collar, (b) test operation.

Split tensile (Brazilian) test was used as one of the methods for determination of tensile strength of specimens. This test involves loading a cylindrical sample perpendicular to its diametric plane and measuring the failure stress using (4.1).

$$\delta_t = \frac{2P}{\pi l d} \tag{4.1}$$

where δ_t is split tensile strength in kPa, P is applied maximum load, l is length and d is diameter of sample.

Since this equation is basically for brittle materials like concrete, Frydman (1964) suggested a reshaping factor g(x) to be multiplied with the result as a correction to plastic deformation and flattening that occurs on the surface along the length of the specimen before splitting, depending on the moisture content of soil sample as given in Equation 4.2.

$$g(x) = -\frac{D}{2a}\left\{2f - \sin 2f - \frac{2y_1}{D}\log\tan\left(\frac{\pi}{4} + \frac{f}{2}\right)\right\} \quad (4.2)$$

where $f = a/y$, and a is half width of flattened area, y is half distance between the portions at failure and D is the diameter of sample.

The wet mass needed to fill volume of mold in order to reach the target maximum dry density was weighed prior to each compaction. For split tensile and unconfined compression tests the compacting molds were made with extra collars to accommodate the initial bulk volume of moist mixture. Each sample was compacted in three layers and the surface of compacted layer was scratched before placing next layer, to secure uniformity of sample and prevent transitional plates within the specimen. The metal hammers for static compaction were prepared and got screwed to the CBR machine. A groove of 2 mm was carved in bottom of metal mold's holder to fit the CBR's lower plate. The samples were compacted at 1 mm/min rate with a 28 kN load ring (Figure 4.2).

Figure 4.2. Static compaction (a) using CBR machine, (b) split tensile sample preparation mold, collar, hammer and bottom plate and (c) bottom plate modified for CBR.

This test was done according to ASTM D3967-08, the deformation and load variations were monitored through computer with data logger system. The 5 x 10 cm samples were laid horizontally and the load was applied to sample through a thin bar (Figure 4.3).

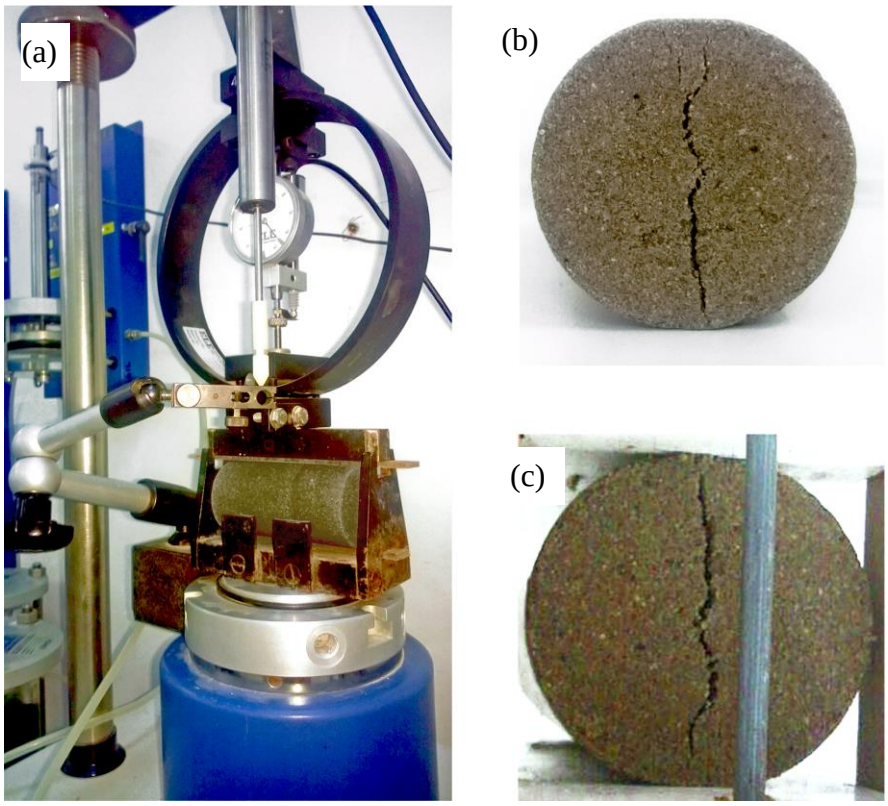

Figure 4.3. Split tensile test setup, (a) test process and (b) and (c) samples at failure.

For determination of flexural strength of samples, flexural test was modified from ASTM C348–08, standard test method for Flexural Strength of Hydraulic-Cement Mortars. Preparation of beams for flexural tests was done by help of a rectangular hammer to transmit the load from the machine and compact mixture uniformly over the whole surface area. The designed mold for flexural test beams contained two rectangular plates at ends fitting in grooves of two other side plates, being held together with two horizontal screws, the collar got fixed to the mold with vertical screws and the whole system was fit to the lower plate in a rectangular groove (Figure 4.4). It was important to have a mold that can be assembled and de-assembled for flexural test beams. Since the tensile strength of soils are generally very low, the attempt to extrude the rectangular sample from mold may result in applying extra friction force to sample and consequently lateral cracks.

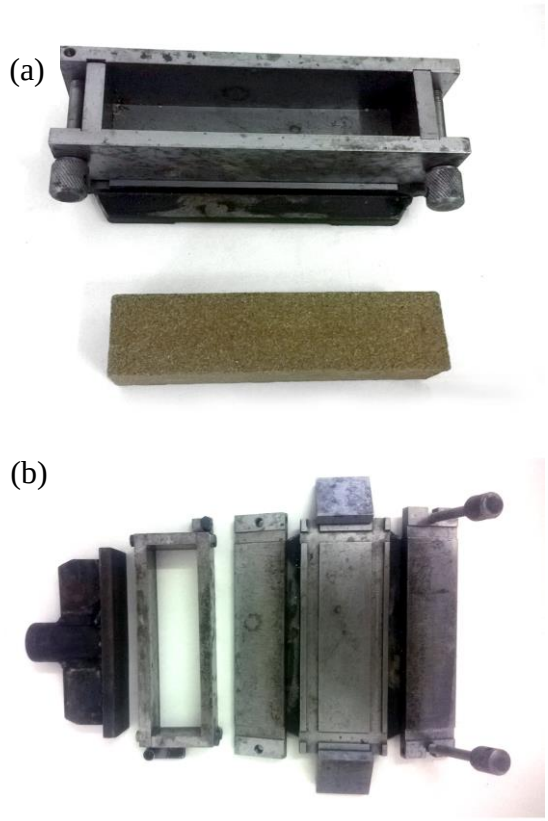

Figure 4.4. (a) Flexural beam mold with a prepared beam and (b) flexural mold parts, collar and hammer.

The samples prepared for flexural test had dimensions 16 × 4 × 4 cm with 10 cm distance between the supports according to ASTM C 348–08. The tensile strength of the samples was calculated using Equation 4.3.

$$f = 1.5\frac{Fl}{bd^2} \tag{4.3}$$

where, F is applied force, l is the span between two supports, b is the width of sample and d is the height of sample. Figure 4.5 shows the test setup and a failed soil beam under flexure.

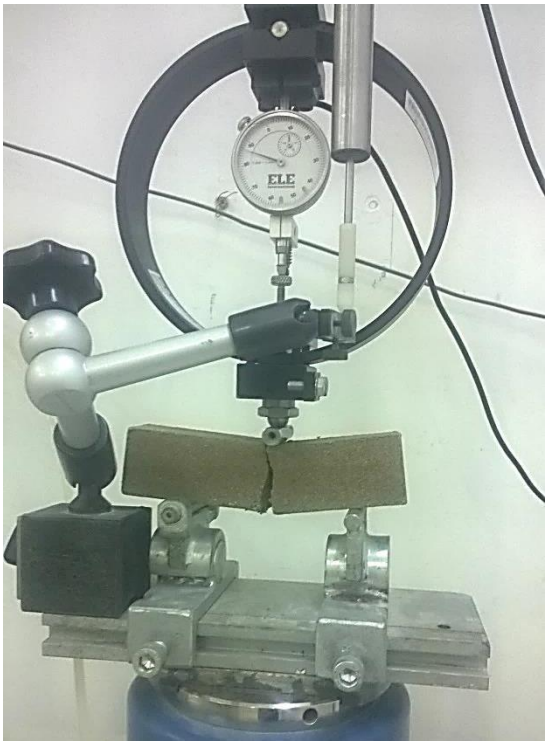

Figure 4.5. Failure of a SB sample in flexural test.

Double punch or unconfined penetration test can be briefly described as using two steel discs centered on both top and bottom surfaces of a cylindrical soil sample and applying load on the discs till the failure of specimen. In this process a cone with 38.1 mm diameter penetrates in the ratio of 1mm per minute to a compacted sample. In this study the samples were compacted in standard Proctor compaction molds with 101.6 x 116.8 mm diameter and height, to their maximum dry density and optimum water content. Then samples were cured in 1, 7 and 28 days and were tested. Steel spacer disc diameters were 38.1 mm as one of the disc sizes suggested by Kim et al. (2007). It is of great significance to apply the load on center of sample, therefore top and bottom metal discs should be applying load to the same vertical axis. In order to reduce the measurement errors a top and bottom cap were produced out of Teflon material -to keep them light weight- with holes in their centers in the same size of the metal discs. These caps were connected to each other during the test procedure with

tiny springs, so the external pressure on sample would be minimal (Figure 4.6). The double punch setup and sample after failure is shown in (Figure 4.7).

Figure 4.6. Top and bottom caps, metal discs and springs used for double punch test.

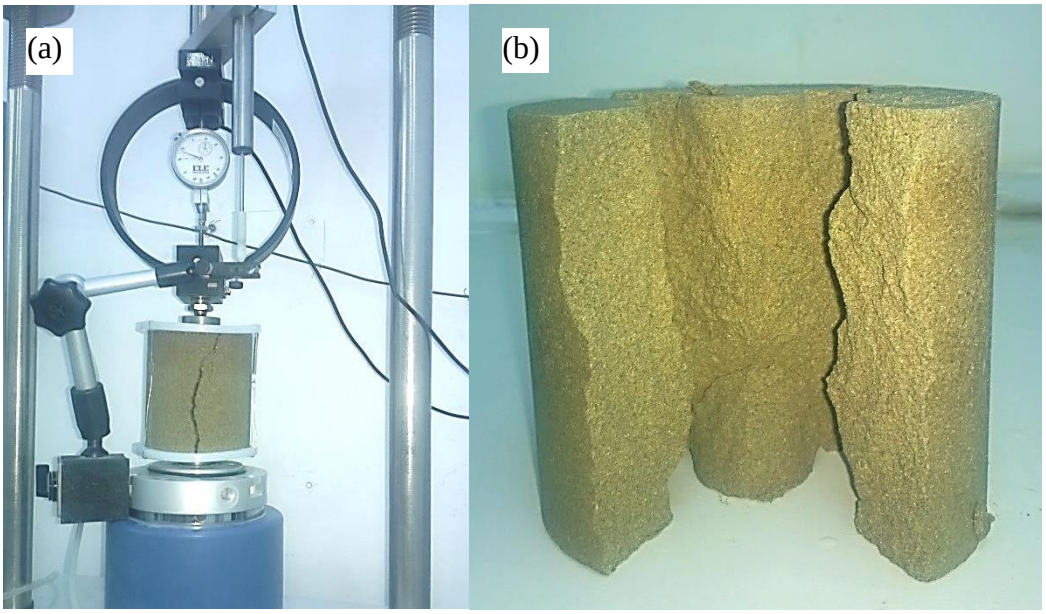

Figure 4.7. Double punch (a) test setup, (b) SBC sample after failure.

Figure 4.8 shows an ideal failure mechanism for a double-punch test on a cylindrical compacted specimen. It consists of many small tension cracks parallel to the radial direction and two cone-shaped rupture surfaces right beneath the punches. As the

force is applied cone shapes move toward each other as rigid body and dislocate the surrounding material sideways. The rupture cone and failed sample is shown in Figure 4.9. The relative velocity vector δ_w, at each point on the cone surface is inclined at an angle, φ to the surface (Figure 4.8). The compatible velocity relation is also presented in Figure 4.8 (b). The rate of dissipation of energy can be found by multiplying the area of each cutoff surface by σ_t times the separation velocity across the surface for a tensile crack or q(1- sin φ)/2 multiply the relative velocity across the cone-shaped rupture surface. Formulating the external rate of work to the total rate of inner dissipation produces the value of the upper bound on the applied load P, as given in Equation 4.4 (Kim et al., 2007; Fang, 1970).

$$\frac{P}{\pi a^2} = \frac{1 - sin\varphi}{\sin\alpha\cos(\alpha+\varphi)}\frac{q_u}{2} + \tan(\alpha+\varphi)(\frac{bH}{a^2} - \cot\alpha)\sigma_t \tag{4.4}$$

where, α is the angle of cone, a is radius of the disc, b is radius of specimen and H is height of specimen.

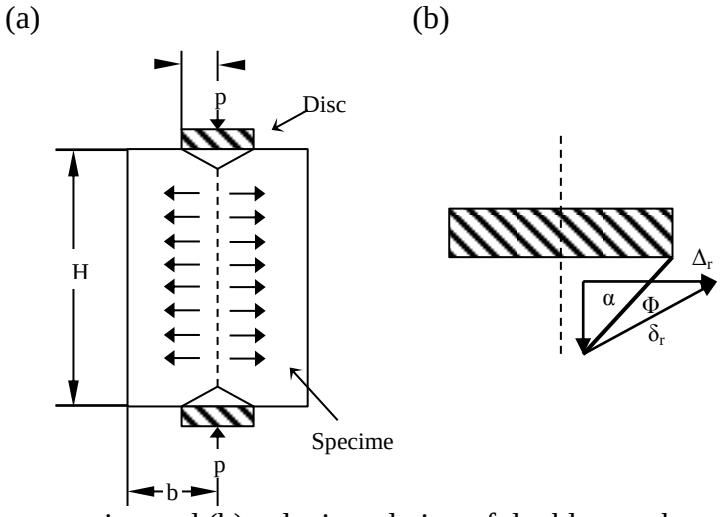

Figure 4.8. (a) Cross section and (b) velocity relation of double punch test.

(a)

(b)

Figure 4.9. (a) The rupture surface cone, and (b) sample with radial tension cracks.

In the condition of maximum pressure responsible for failure the equation can be reduced to Equation 4.5, and tensile strength can be computed.

$$\delta_t = \frac{p}{\pi(kbh - a^2)} \tag{4.5}$$

Where, p = applied load, a = steel disc diameter, b = specimen diameter, h= height of specimen and k is a constant equal to k= tan (2α+φ).

The value of k depends on the angle of friction, compression-tensile strength ratio and sample-punch dimension ratio. The variations of the k value are shown in Table 4.1. The sizes of specimen recommended by Fang and Chen (1972) are Proctor and CBR molds where the values of φ were assumed to be 0 and 20 degrees. These values of k were recommended for practical use by Kim et al. (2007), Fang (1970) and Fang and Chen (1971).

Table 4.1. Recommended values of k (Fang and Chen, 1972).

	Soil	Stabilized Materials
Proctor Mold	1	1.2
CBR Mold	0.8	1

The modified Mohr-Coulomb failure envelope, which is suggested by Chen and Drucker (1969) is achieved graphically in this study. The failure envelope is formed by three Mohr-Coulomb circles and the failure envelope. The diameter of the smallest Mohr circle, σ_t, is equal to the magnitude of the tensile strength which is determined by double punch test. The q_u circle has a diameter equal to the unconfined compressive strength. These two circles are outer tangent to each other. There will be a third circle inner tangent to tensile strength Mohr circle and intersecting unconfined compression Mohr circle. The failure envelope tangent to unconfined compression Mohr circle at one point and to the third circle at another point will intersect the τ-axis to define the cohesion (Figure 4.10).

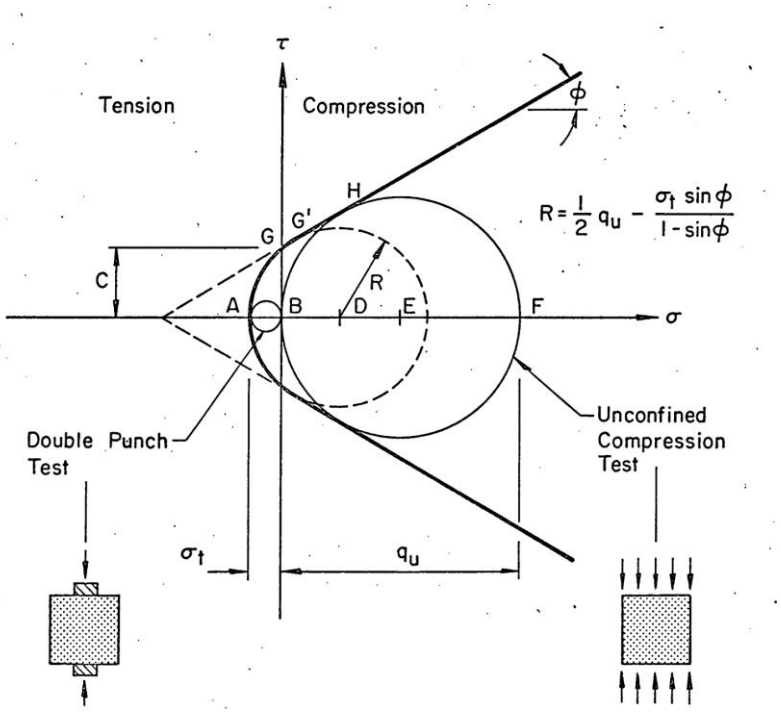

Figure 4.10. Modified Mohr-Coulomb failure criterion (Fang and Hirst, 1973).

The cohesion, c, is related to the tensile strength of the material, Equation 4.6.

$$c = \frac{\sigma_t}{\xi} \tag{4.6}$$

Where, ξ is a function of plasticity index suggested by Fang and Hirst (1973) as Equation 4.7.

$$\xi = 0.34 + 0.01 \text{ PI} \tag{4.7}$$

By measuring plasticity index, it is possible to find all the necessary parameters to draw Mohr circles. In the figure above, using properties of circle and tangent line, the internal friction angle φ can be determined geometrically. Connecting the center point of unconfined compression Mohr circle to the tangent point, a perpendicular triangle is constructed with one angle of φ. It is obvious from the figure above that connecting the center to the τ-axis, there will be two identical right-angled triangles

with one angle of $\frac{90-\varphi}{2}$. Therefore internal friction angle φ can be calculated using tangent of this angle using Equations 4.8-4.12.

$$\operatorname{cotan}\ 45-\frac{\varphi}{2}=\frac{\frac{q_u}{2}}{c} \tag{4.8}$$

$$\tan\left[90-\left(45-\frac{\varphi}{2}\right)\right]=\frac{\frac{q_u}{2}}{c} \tag{4.9}$$

$$\tan\left(\frac{\varphi}{2}+45\right)=\frac{\frac{q_u}{2}}{c} \tag{4.10}$$

$$\tan^{-1}\frac{q_u}{2c}=\frac{\varphi}{2}+45 \tag{4.11}$$

$$\varphi=2\left(\tan^{-1}\frac{q_u}{2c}-45\right) \tag{4.12}$$

where, c is cohesion, φ is internal friction angle and q_u is unconfined compressive strength.

In order to form the failure envelope, third Mohr circle's radius is calculated using trigonometric relations given in Equations 4.13-4.20.

$$\tan\varphi=\frac{c}{|OA|+\sigma_t} \tag{4.13}$$

$$|OA|\tan\varphi+\sigma_t\tan\varphi=c \tag{4.14}$$

$$|OA|=\frac{c-\sigma_t\tan\varphi}{\tan\varphi} \tag{4.15}$$

$$\sin\varphi=\frac{R}{|OA|+R} \tag{4.16}$$

$$|OA|\sin\varphi=R(1-\sin\varphi) \tag{4.17}$$

$$R=\frac{|OA|\sin\varphi}{1-\sin\varphi} \tag{4.18}$$

$$R = \frac{\frac{c - \sigma_t \tan\varphi}{\tan\varphi}\sin\varphi}{1 - \sin\varphi} \tag{4.19}$$

$$R = \frac{c\cos\varphi - \sigma_t \sin\varphi}{1 - \sin\varphi} \tag{4.20}$$

The flexure prisms, which are the end pieces of the flexure beam, were used to test the compressive strength of a 40 x 40 mm cubic sample similar to hydraulic cement mortar according to ASTM C349-08. The test setup is shown in Figure 4.11. This procedure is studied to correlate the cubic compressive strength to unconfined compressive strength which can be utilized to indirectly yield the unconfined compressive strength of cement stabilized soils. Therefore a compacted flexure beam could be used for both tensile and unconfined compressive strength determination. However, it should be ensured according to the aforementioned standard that the broken portions that are used for cubic compressive strength test should not be less than 65 mm in length and should not have visible defects or cracks.

Figure 4.11. Cubic compressive strength test.

Samples tested with this method generally fail with diagonal cracks toward the centre of sample in both SB and SBC samples (Figure 4.12).

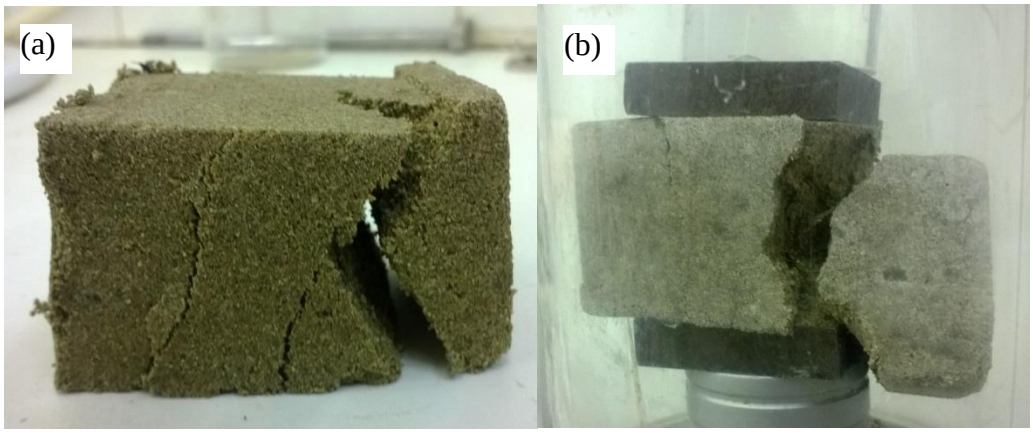

Figure 4.12. (a) SB prism after cubic compression test and (b) failing moment in SBC sample.

4.3 Experimental Results and Discussions

4.3.1 Compaction Test

It can be observed in Figure 4.13 that compaction curve of SB mixture is flatter than SBC, indicating that water content variations do not have a notable effect on dry density. In optimum water content condition, fine particles of bentonite work as lubricant by filling the voids between the sand grains. This homogenous matrix leads to a better compaction and hence higher dry density. However, addition of cement to the mixture increases the maximum dry density significantly due to the higher specific gravity of cement. SBC samples demonstrate high sensitivity to water content variations as well, small increments of moisture causing visible reductions in dry density. However, since sand is not capable of absorbing water, replacement of 5% sand with cement in SBC mixture does not have a noticeable effect on optimum water content compared to SB mixture. Maximum dry densities of SB and SBC are 1.624 gr/cm^3 and 1.663 gr/cm^3 respectively and optimum water content for both is

17%. The specific gravities of SB and SBC mixtures are obtained to be 2.656 and 2.676 respectively.

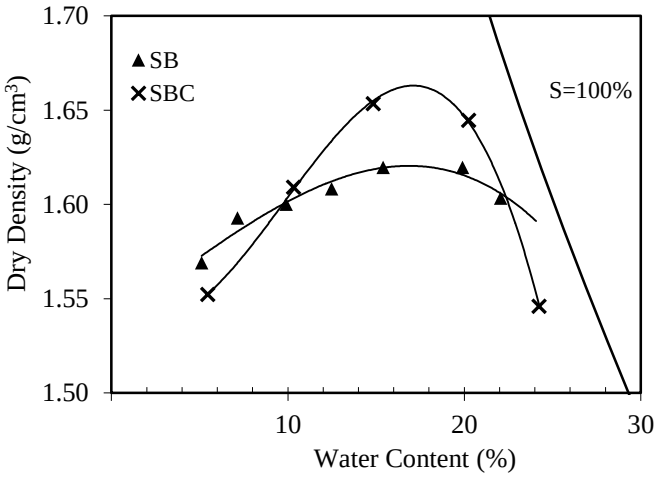

Figure 4.13. Compaction curves.

4.3.2 Unconfined Compression Test

The test results of unconfined compression test are presented as axial stress versus axial strain curves in Figure 4.14 for sand-bentonite and sand-bentonite-cement samples respectively. The curves for SB show a ductile behavior with a mild failure at yielding point followed by deformation of sample before complete fracturing. The failure form of samples can be observed in Figure 4.15, SB samples bulge and form a lot of small cracks prior to failure in lower curing time, but with increase of curing time they behave more brittle and bulge less. On the other hand SBC samples act brittle and show diagonal cracks at failure in all curing times (Figure 4.16).

Curing of samples increased the maximum strength reached with time, which can be explained by the partial or full strength regain. Lower failure strains in cured samples can be inferred as the usage of moisture in samples for completion of bentonite swelling resulting in more homogenous and drier specimens.

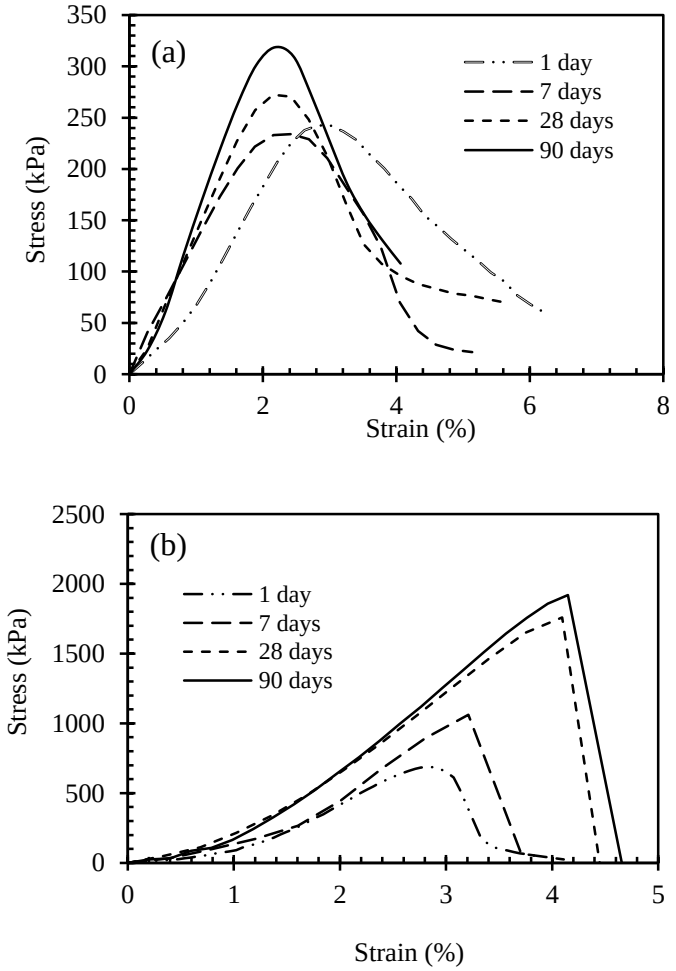

Figure 4.14. Unconfined compression test results at 1,7,28, 90 days of curing of (a) sand-bentonite-cement, and (b) sand-bentonite samples.

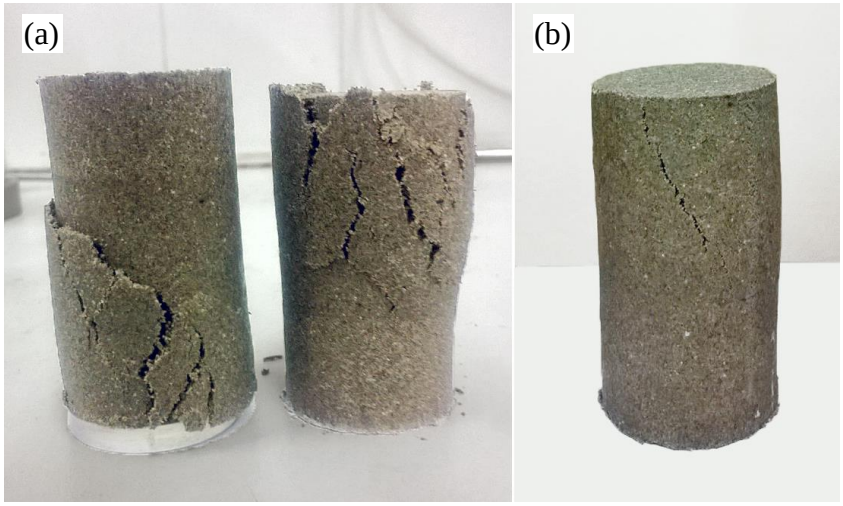

Figure 4.15. Failure form of SB samples at (a) 7 days curing, (b) 90 days curing.

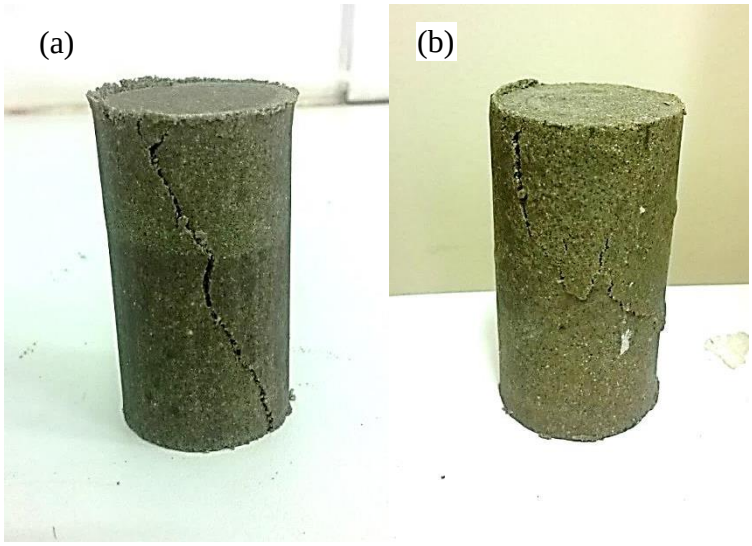

Figure 4.16. Failure form of SBC samples at (a) 7 days curing, (b) 90 days curing.

The strength gain in sand-bentonite samples can be explained with the concept of "thixotropy", which is strength regain or age-hardening, described by Mitchell (1993) as isothermal, reversible, time dependent process which occurs under constant composition and volume and involves the hardening of soils at rest, and softening when disturbed (Blazejczak et al., 1995). Compaction is a rapid process which cannot maintain water equilibrium at different microstructure levels, inter-aggregate and intra-aggregate pores, inside the sample. Water redistribution occurs in a compacted specimen due to suction equilibration at constant water content after compaction, which is a very slow process due to low permeability and strong clay-water bonds (Delage et al., 2006). According to Rao and Tripathy (2003) particle rearrangement occurs with time causing formation of bonds during the aging process hence increasing shear strength of compacted soils. Therefore, both water redistribution and bonding within the bentonite cause increase in shear strength and decrease in swelling (Ye et al., 2013). Strength gain versus time is depicted in Figure 4.17.

In cement added samples, a more significant increase is observed in strength with curing time compared to SB samples. Adding 5% cement to sand-bentonite mixtures increased strength of samples by 3- fold after 1 day curing, reaching to 6- fold after 90 days curing. The strength gain resumes as hydration of cement continues within the samples, however, the rate reduces after 28 days as free water within samples reduces. Thus the maximum strength achieved in 90 days is only slightly more than 28 day strength. These observations are in good agreement with findings of Verastegui Flores et al. (2010), and Cokca and Yilmaz (2004). The condition of curing is very important in strength gain of cement containing material as lack of moisture would stop hydration process and therefore the strength gain (Neville, 1995). In this study the samples were wrapped in cellophane wrap and kept in desiccators to minimize the moisture loss. The failure of samples after 1 day curing is rather ductile but after a week it starts to have brittle concrete-like failure as samples get harder and drier.

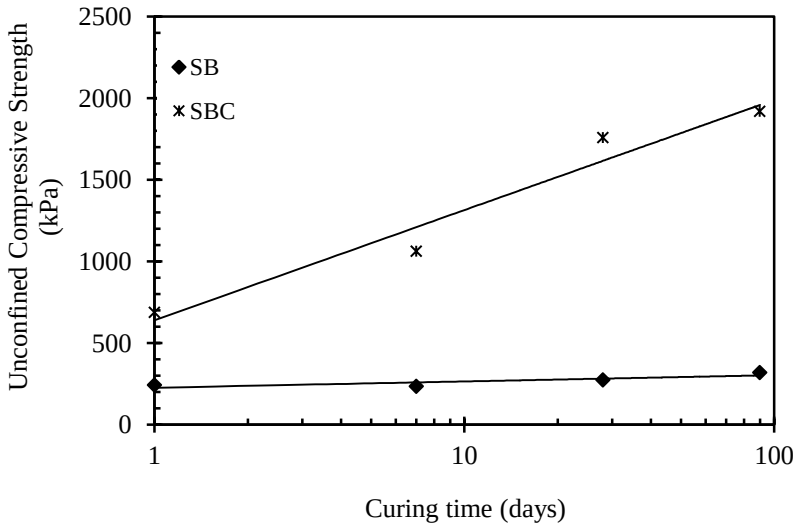

Figure 4.17. Unconfined compressive strength of SB and SBC versus curing time.

4.3.3 Tensile Strength

Covers and liners of a waste repository are subjected to tensile stresses and strains mainly due to climatic effects. The direct tension test is generally believed to provide a more accurate measure of tensile strength. However, it is not preferred in this study due to its failure to produce reproducible results mainly because of the means of holding the specimen creating secondary stresses influencing the test results (Hudson and Kennedy, 1968; Arellano and Thompson, 1998). Raad (1976) demonstrated that the tensile strengths from split tensile and the direct tension tests are about equal. Therefore, split tensile test is adopted in this work, the results of which are correlated to other strength values.

4.3.3.1 Split Tensile Test

Split tensile (Brazilian) test is used in many tensile strength related research as a relatively simple, indirect test method (Błażejczak et al., 1995; Cokca and Yilmaz, 2004; Consoli et al., 2013; Hannawi et al., 2013; Sobhan and Mashnad, 2002).

The results are depicted in Figure 4.18 as split tensile strength versus curing time for SB and SBC samples. The test results indicate a 1.5-fold increase in the split tensile strength of SB and 3-fold increase in SBC specimens at the end of 28 days curing period.

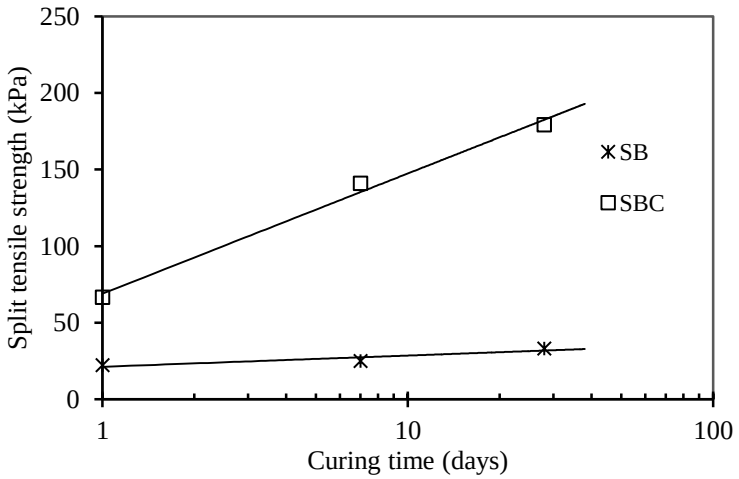

Figure 4.18. Split tensile strength versus curing time.

4.3.3.2 Flexural Strength Test

The test results are presented in Figure 4.19 for SB and SBC samples as plots of stress versus strain at curing times of 1, 7, 28, 365 days. The results indicate increase in peak and residual strengths in the SB samples which displayed a smoother and more ductile behavior at failure, whereas the SBC samples had a linear increase of stress-strain behavior until the peak value followed by a sharp and brittle failure. Figure 4.20 depicts the flexural strength increase with curing time, from which it can be deduced that the strength increases linearly in SB specimens, while it increases linearly up to 28 days of curing for SBC specimens after which it displays almost a constant value until 365 days. In both cases the maximum flexural strength gained with aging is almost three times more of the initial values at 1 day curing. The strain softening behavior that can be seen at post-yield state, attribute to the break up of the cementation bond (Horpibulsuk, 2005).

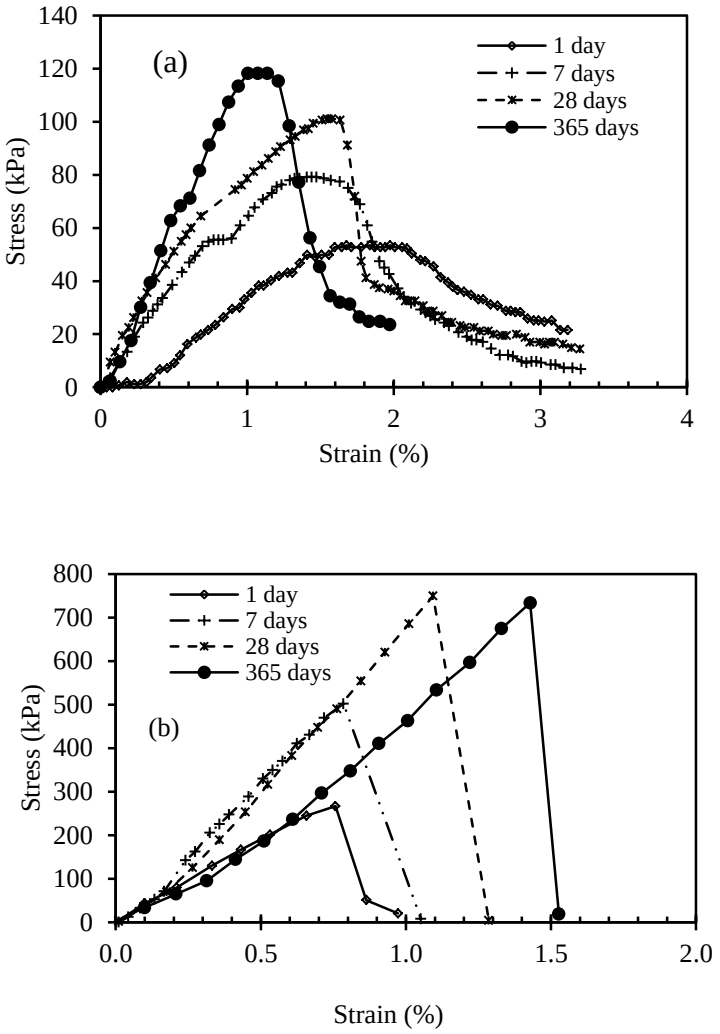

Figure 4.19. Flexural strength test results (a) SB and (b) SBC in different curing times.

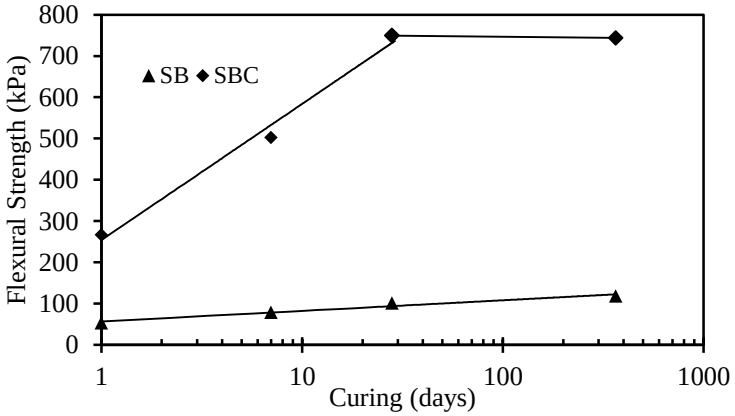

Figure 4.20. Flexural strength of SB and SBC samples at different curing times.

Toughness determined in terms of area under the load-deflection curve is an indication of the energy absorption capability of a certain test specimen and, therefore, its magnitude depends directly on the geometrical characteristics of the test specimen and the loading system (ASTM C1018). Fracture toughness is a significant mechanical parameter of the material to show its ability to resist fracture failure under mode I load conditions in fracture mechanics (Wang et al., 2007).

The flexural performance of material can display either deflection-softening or deflection-hardening behavior. The point at which the linearity of the load-deflection curve ends (P_1), the initial peak, also known as the limit of proportionality (LOP) as described in ASTM C1609-10 is determined and compared with the peak flexural load (P_f).

A sample of load-deflection behavior is presented in Figure 4.21. If the initial and failure loads are almost equal, the flexural behavior is deflection-softening, conversely if $\frac{\mathbf{P_f}}{\mathbf{P_1}}$ is greater than one then the deflection-hardening occurs. Deflection-hardening behavior indicates a high toughness material. Toughness is the ability of a material to absorb energy during fracture (Jamsawang et al., 2015).

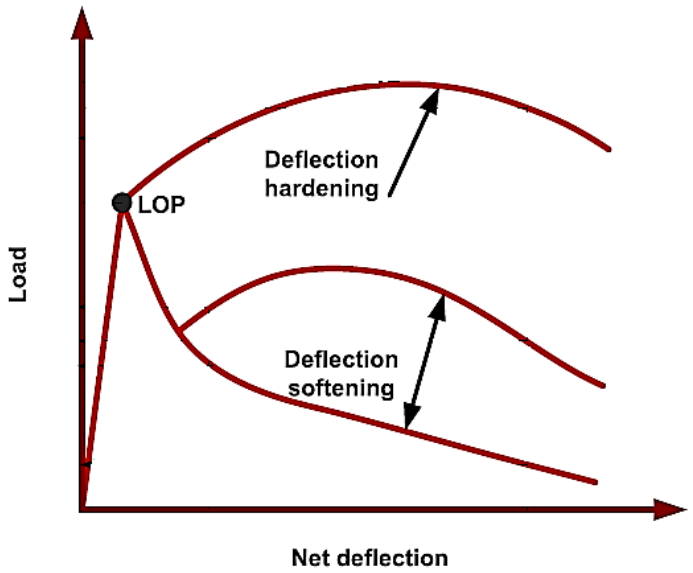

Figure 4.21. Load-deflection curve behavior (Jamsawang et al., 2015).

The toughness of SB and SBC samples are calculated till the residual stress of samples, and compared to toughness at peak load. However, the residual load, P_r, value is generally lower in cement containing samples because of brittle behavior of cement. Sand bentonite samples present a $\frac{P_f}{P_1}$ ratio higher than 100% which indicate its deflection hardening behavior; conversely all SBC samples present deflection softening behavior. The results shown in Tables 4.2 and 4.3 also indicate an increase in flexural toughness, T_p, and residual toughness, T_r, in both SB and SBC samples along with increase of curing time. Nevertheless, this increase is smaller for sand bentonite samples and shows a decrease from 28 days to 365 days.

Table 4.2. Flexural performance data of SB samples.

	Curing time	P_1(N)	P_f (N)	P_f/P_1	P_r(N)	T_r (kPa/m)	T_p (kPa/m)
SB	1 day	68	118	1.7353	9.6	18.45	11.76
	7 days	64	101	1.5781	3.7	22.78	12.66
	28 days	54	79	1.463	7.2	24.65	18.18
	365 days	38	53	1.3947	10.47	21.68	13.58

Table 4.3. Flexural performance data of SBC samples.

	Curing time	P_1(N)	P_f (N)	P_f/P_1	P_r(N)	T_r (kPa/m)	T_p (kPa/m)
SBC	1 day	116	116	1.00	3.5	23.96	18.96
	7 days	214	214	1.00	2.7	44.76	32.82
	28 days	327	327	1.00	1.9	78.63	65.78
	365 days	325	325	1.00	5.3	88.96	81.96

Wang et al. (2007) studied fracture toughness of a clayey soil used in an earth-rock fill dam, by three point bending beam. The fracture toughness values found were varying from 7.10 to 31.43 kPa/m, depending on the water contents or dry densities of the soil beams. These data are in the same range with results attained from SB samples in this study.

4.3.3.3 Double Punch Test

Figure 4.22 and Figure 4.23 show the results of double punch test. The yielding point of each curve shows the maximum tensile strength of sample. These results can be compared together with tensile strength results obtained from other tensile strength test methods.

As it can be seen from Figure 4.24 the tensile strength of sand-bentonite samples is not much affected by duration of curing time and they only show a slight increase in tensile strength as curing time is extended, however the deformation of samples before failure is in samples with 28 days cure which is in agreement with previous other test results. As it is expected the failure of sand bentonite samples are generally ductile due to presence of swelled bentonite.

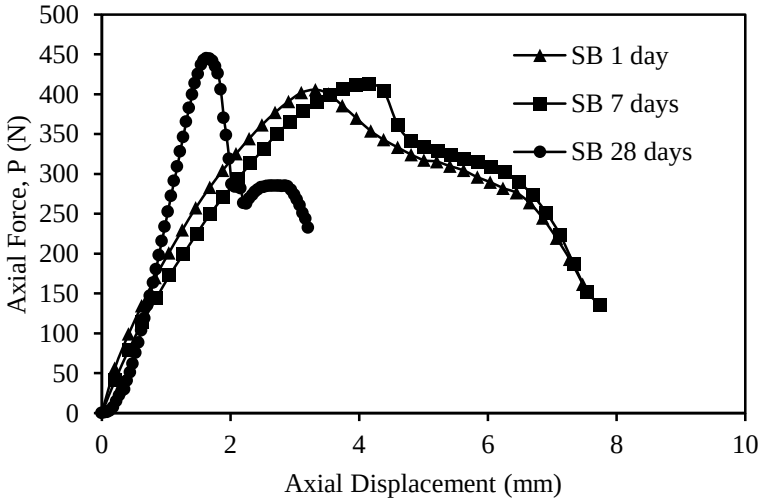

Figure 4.22. SB double punch test results.

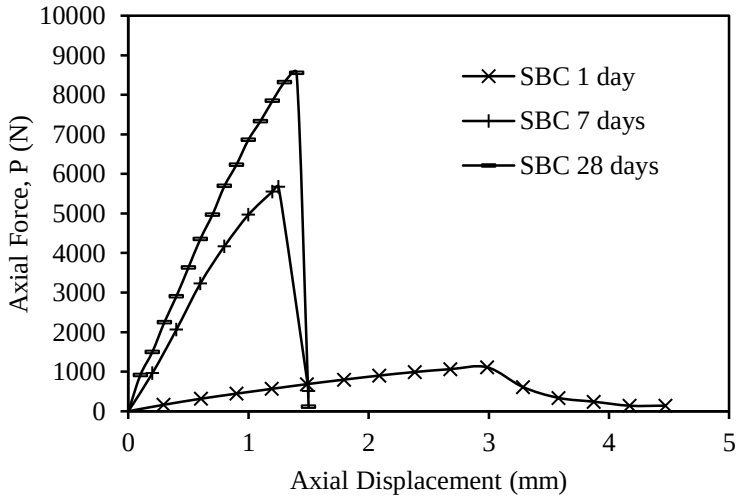

Figure 4.23. SBC double punch test results.

In Figure 4.23 the results of double punch test on cured SBC samples is shown. As compared to SB sample the tensile strength of 28 days cured SBC sample is increased about 19 folds. Although 1 day cured sample shows relatively ductile failure and low tensile strength, as the cement inside mixture get hydrated the bonding between the grains get more and therefore strength of samples raises up to five times in seven days and eight times in 28 days of cure.

The results are depicted in Figure 4.24 as tensile strength versus curing time for SB and SBC samples. The test results indicate a 1.2-fold increase in the double punch tensile strength of SB and 7-fold increase in SBC specimens at the end of 28 days curing period. The tensile strength results obtained from split tensile and double punch test of SB and SBC samples are in good correlation, however in SBC samples double punch test present higher results in 7 and 28 days curing periods (Figure 4.25).

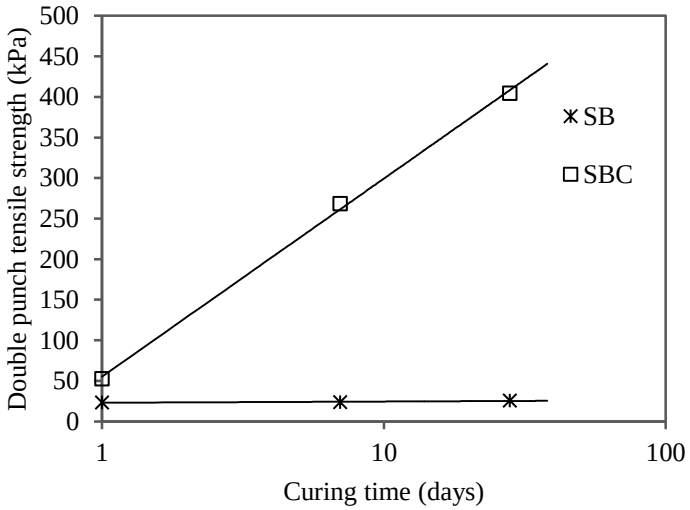

Figure 4.24. Tensile strength determined with double punch test versus curing time.

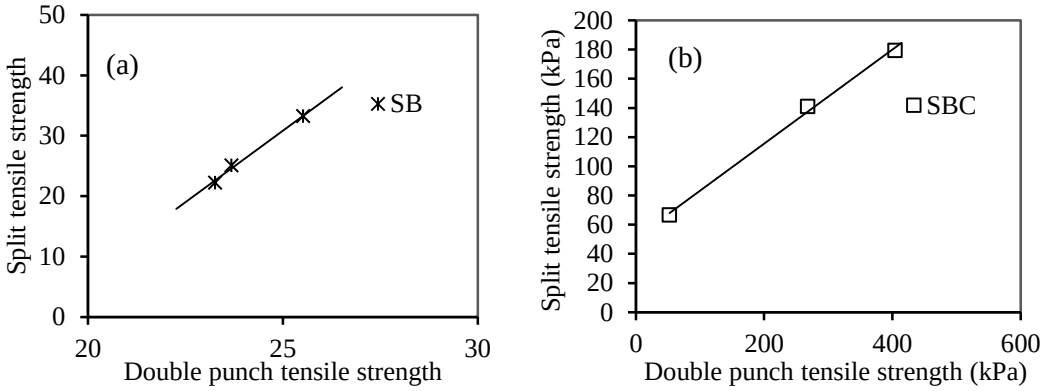

Figure 4.25. Correlation of tensile strength results obtained from Split tensile and double punch test of, (a) SB samples, (b) SBC samples.

As suggested by Fang and Hirst (1973) strength parameters of a soil and stabilized materials, cohesion c, and internal friction angle φ can be determined by knowing the tensile strength and unconfined compressive strength through graphical method. Cohesion is correlated with plasticity index of soil, using Equation 4.6 and 4.7 cohesion of samples can be predicted (Table 4.4).

Table 4.4. Atterberg limits of mixtures and predicted cohesion values in kPa.

	SB	SBC
PL (%)	30	33
LL (%)	51	64
c (1 day)	42	81
c (7 days)	43	413
c (28 days)	46	622

Knowing strength parameters of soils cohesion, c, and internal friction angle φ, unconfined compressive strength q_u and tensile strength, σ_t is essential in conventional analyses of the stability of soil systems. The test methods that are commonly used for establishing c and φ include direct and triaxial shear tests. These test methods are generally expensive and time-consuming and are particularly not suited to test the stabilized material because of the large particle sizes and high strengths involved. This often demands the use of large test samples and higher load cells/rings (Fang and Hirst, 1973).

Using double punch tensile strength and unconfined compression test would be a simple method to determine undrained cohesion and internal friction angle of soil and stabilized materials. Undrained internal friction angle of SB and SBC samples in 1 day, 7 day and 28 days are shown in Table 4.5. These values were calculated

graphically through Mohr-Coulomb circles shown in Figure 4.26 and 4.27. As it can be seen cohesion and internal friction angle of sand bentonite samples slightly increase with increase of curing time. The increase of cohesion in SBC samples is significant which was expected as the hydration of cement continues to bond the grains. However the φ values of SBC decreased with curing time, which may be contributed to soil getting hardened and act concrete-like. Horpibulsuk (2005) indicates that role of the cement in induced cemented clay is mostly to increase the cohesion intercept with insignificant change in internal friction angle.

Table 4.5. Internal friction angles calculated from graphical method.

	SB		SBC	
	φ (radians)	φ (degrees)	φ (radians)	φ (degrees)
1-day	0.86	49.45	1.08	62.09
7-day	0.87	49.73	0.25	14.27
28-day	0.92	52.66	0.34	19.39

A considerable amount of the cohesion in soil is due to water phase tension and surface tension associated with air-water interface. Cohesion of soils as correlated by aggregate stabilities and moduli of rupture - flexural strength- increases with time. Some cohesive forces can associated with water layer holding the soil particles together in moist soils. Though, cohesion of soils when oven dried, indicate formation of solid phase bonds at particle-to-particle contacts. Increase of cohesion with time of storage or "curing" under air-dry conditions, specify that migration of bonding components continue to strengthen the bonds even when there is as little as one molecular layer of water on the mineral surfaces. Moreover, as long as the pressure in the air exceeds the pressure of water phase, water causes some cohesion

in the soil. However, when the water pressure becomes equal to or more than the air pressure and the soil becomes saturated, the water does not help soil particles to cohere anymore. Therefore curing the soil before saturating it helps remolded soil to regain solid phase cohesion and disintegrate less (Kemper and Rosenau, 1984).

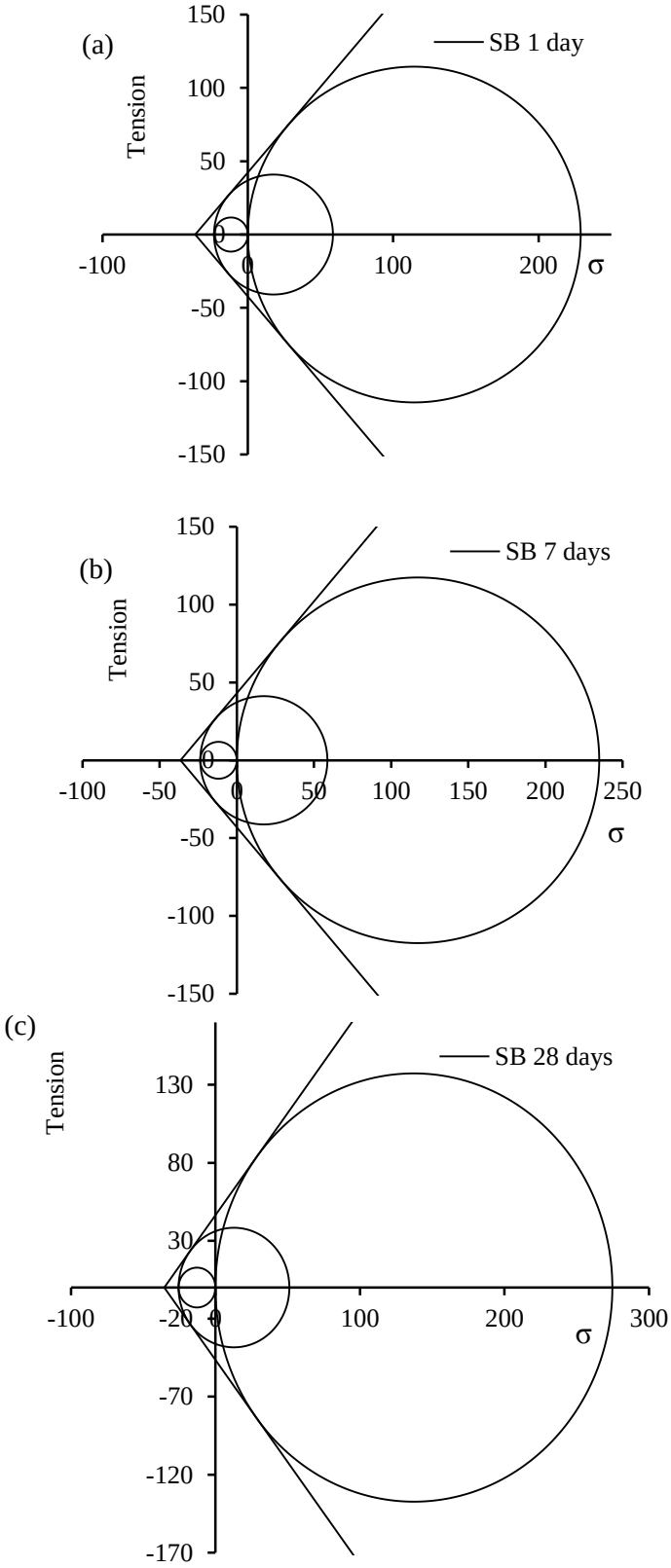

Figure 4.26. Modified Mohr-Coulomb failure criterion for SB, (a) 1 day, (b) 7 days, and (c) 28 days.

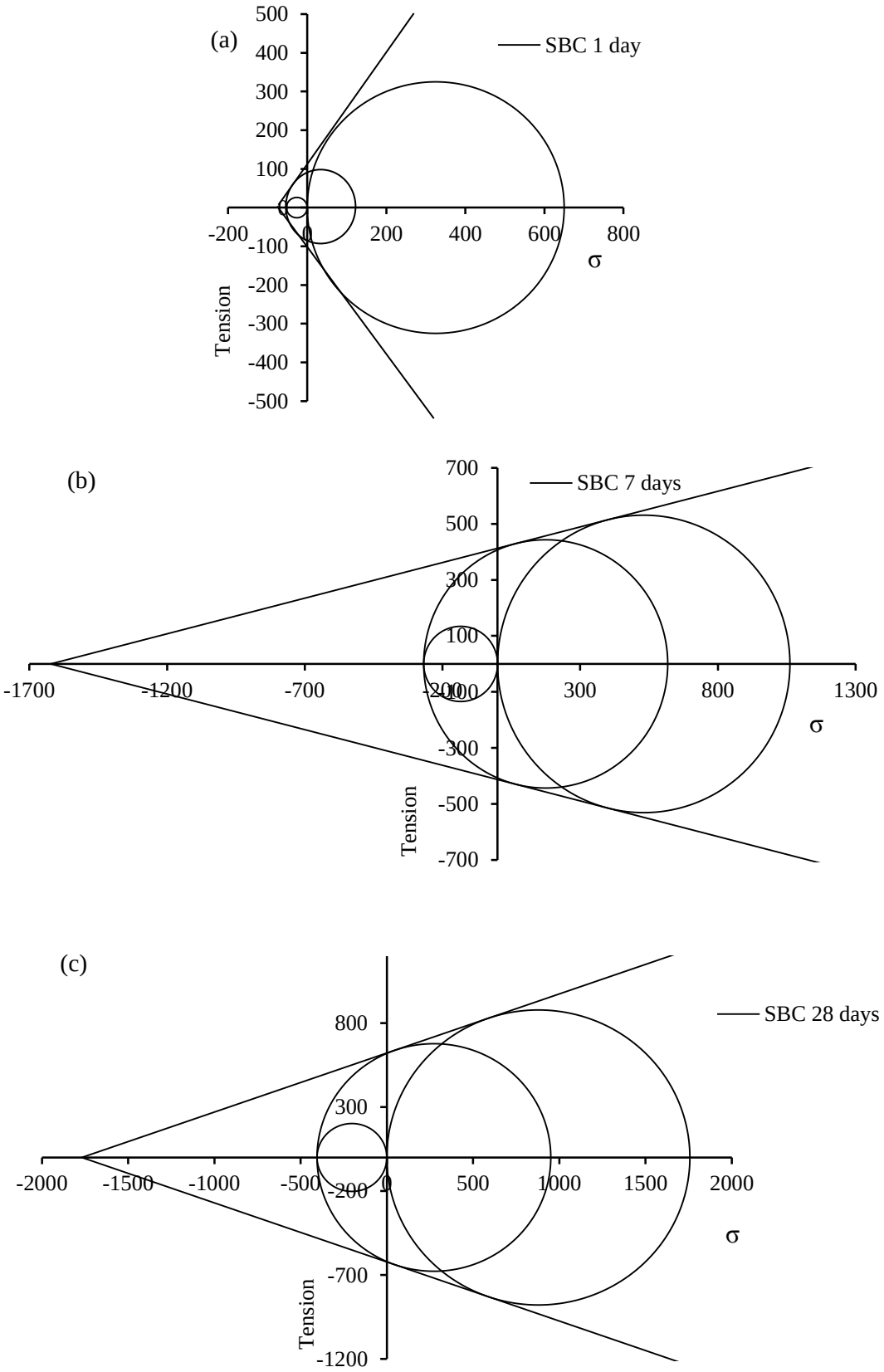

Figure 4.27. Modified Mohr-Coulomb failure criterion for SBC, (a) 1 day, (b) 7 days, and (c) 28 days.

4.3.4 Cubic Compressive Strength

The cubes subjected to compression yielded the results given in Figure 4.28, showing a more ductile behavior in SB than SBC specimens, with an appreciable amount of residual strength remaining after the peak value. The residual strength after 365 days is almost the same as the peak value at 1 day curing. The SBC specimens fail in a more brittle behavior with no residual strength except the 1- day cured sample. The strain at failure however is markedly increasing in SBC samples, while it remains almost the same after 28 days curing in SB samples. Figure 4.29 shows a progressive increase in the cubic strength with aging in both samples within 365 days of curing, the rate of increment being higher in the cement included samples.

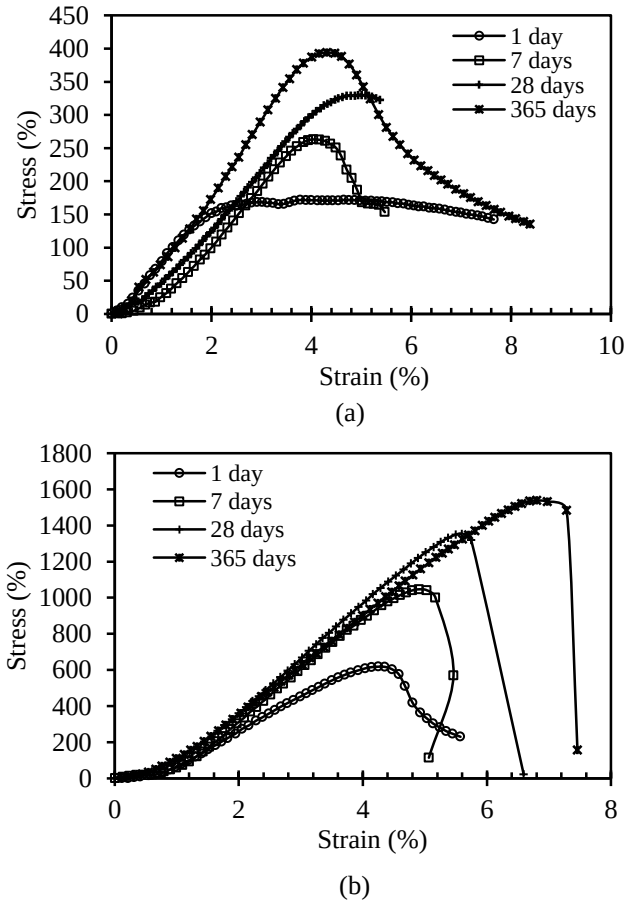

Figure 4.28. Cubic compressive strength of (a) SB and (b) SBC samples at different curing times.

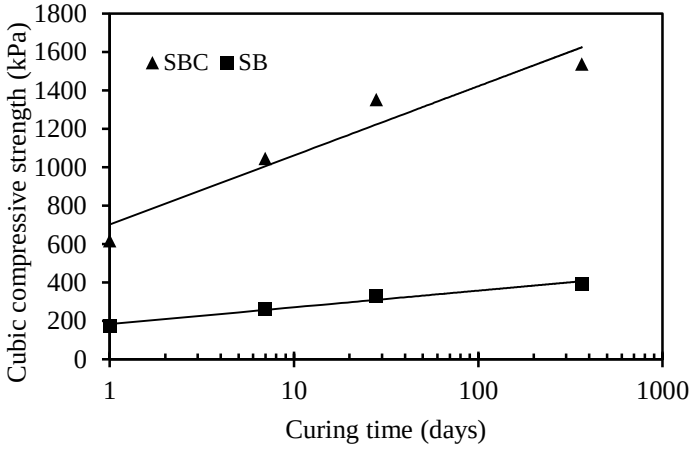

Figure 4.29. Cubic compressive strength of SB and SBC samples at different curing times.

4.3.5 Relationship Between Different Strength Values and Moduli

Figure 4.30 shows the correlation between split and flexural tensile strengths, which indicates split tensile strength to be in the range of 24-29% of the flexural strength in the SB where 21-27% of the flexural strength in the SBC samples. Therefore, it can be concluded that for both SB and SBC specimens on the average the split tensile strength is almost a quarter of the flexural strength.

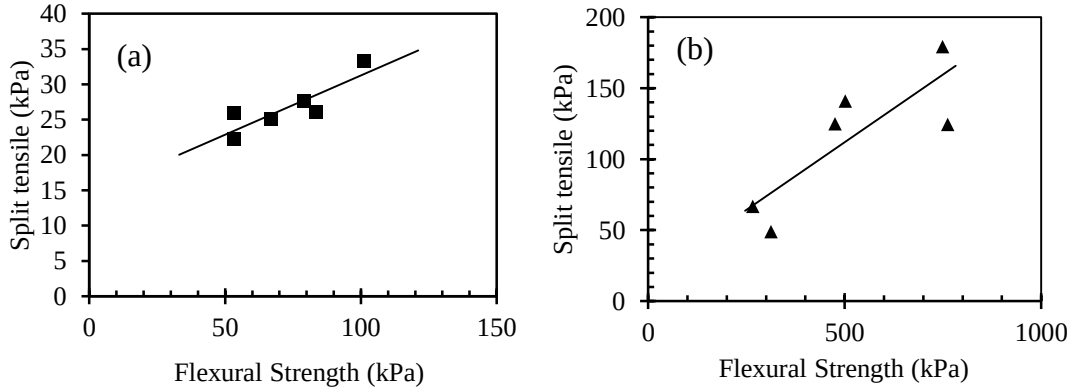

Figure 4.30. Split tensile strength of (a) SB and (b) SBC samples versus flexural strength.

The correlation between tensile strength and unconfined compressive strength as depicted in Figure 4.31 reveals that in both cases the unconfined compressive

strength is higher than the tensile strength. Overall the flexural strength is 30% and split tensile strength is 10% of the unconfined compressive strength for both SB and SBC specimens. Based on literature the range of flexural strength is generally 20-25% of the unconfined compressive strength and the split tensile strength is about 10-15% of the compressive strength of cement treated soil (Arellano and Thompson 1998; Kolias et al., 2004). Therefore the findings of this study are quite compatible with the earlier work except in flexural strength which is 5% higher than the maximum range.

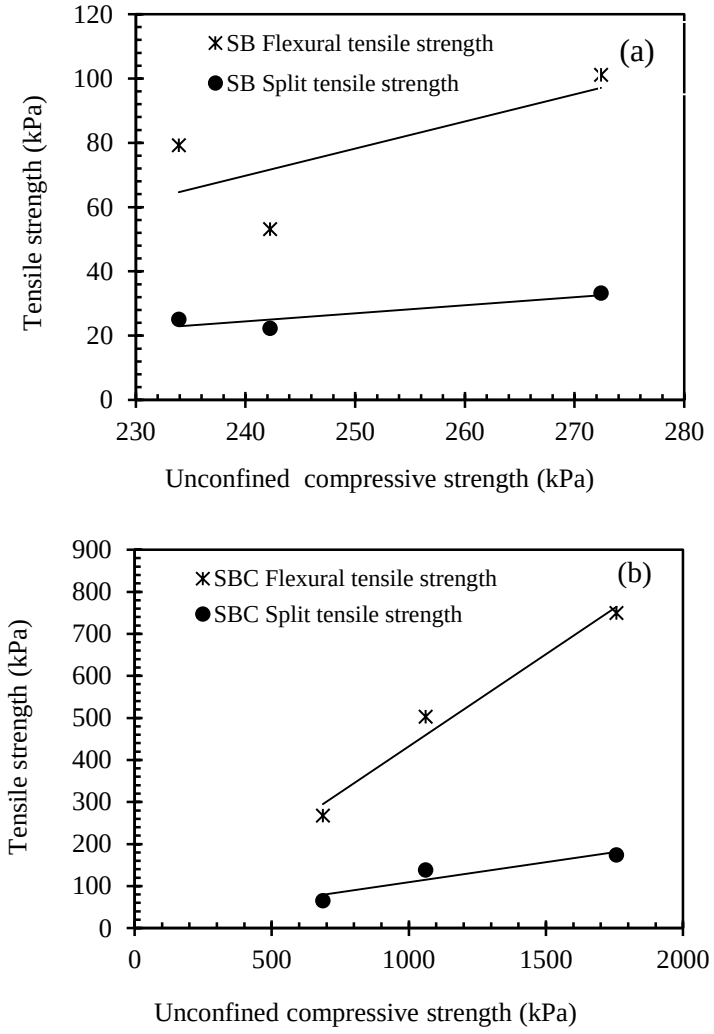

Figure 4.31. Relationship between tensile strength and unconfined compressive strength of (a) SB and (b) SBC samples.

The relationship between cubic and unconfined compressive strengths are presented in Figure 4.32. In SB specimens within the stress ranges studied the cubic compressive strength on the average is almost equal to the unconfined compressive strength. In SBC specimens within a range of 500-900 kPa of unconfined compressive strength, the cubic strength is almost equal to the unconfined compressive strength, whereas for a range of 1000-2000 kPa the cubic strength is 75% of the unconfined compressive strength.

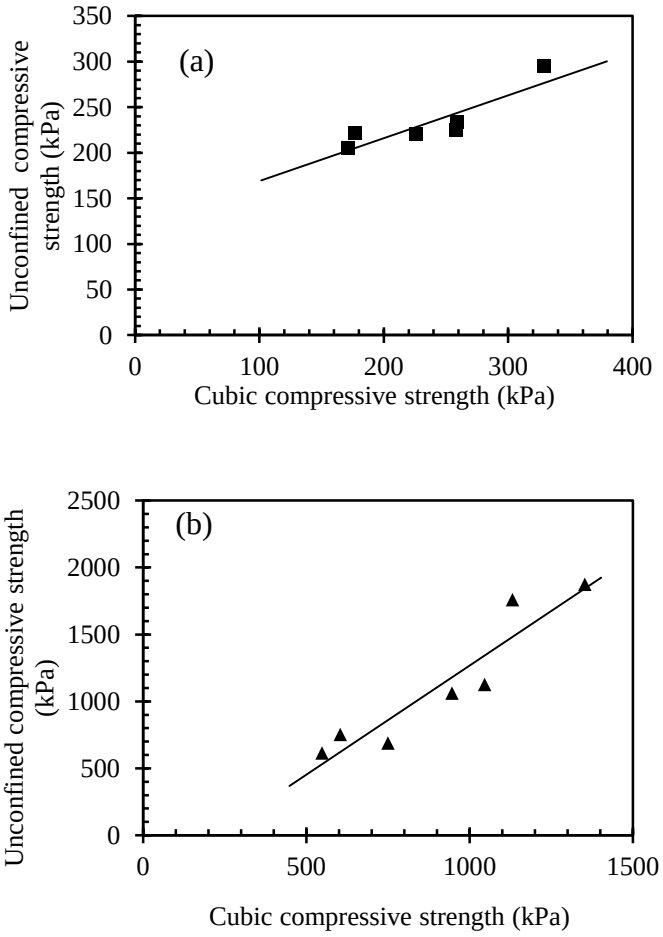

Figure 4.32. Cubic compressive strength of (a) SB and (b) SBC samples versus unconfined compressive strength.

Raad (1976) demonstrated that the various strength test procedures provide significant strength differences because the modulus of elasticity of cement- treated materials is not the same in compression and tension. Figure 4.33 presents the initial,

flexural and cubic moduli variations with curing time. Flexural modulus increases with curing time in both SB and SBC specimens and is almost ten times higher in SBC specimens than the SB specimens at each curing time. The initial modulus displays an increasing trend with curing time in both specimens which is notably higher at 7 days with a reduced rate of increment until 28 days for both specimens. The cement included specimens attained an initial modulus approximately four times larger than the SB specimens. Cubic modulus, which is measured as the slope of the elastic portion of the stress-strain curve under cubic compression, however was observed to have no significance in SB specimens, whereas in SBC specimens it indicated an increment of 1.5 fold after 7 days curing. The cubic compression modulus of SB specimens is observed to be on the average 54% of the initial modulus attained in 28 days, while in SBC specimens it displayed a value of 62% of initial modulus. Therefore, cubic portions of the compacted flexure beam specimens can be used to obtain information on both unconfined compressive strength and initial modulus without implementing the unconfined compression test. The correlation, however are more reliable for cement treated soil which will be hard enough to maintain the flexure prisms in good condition to test in cubic compression.

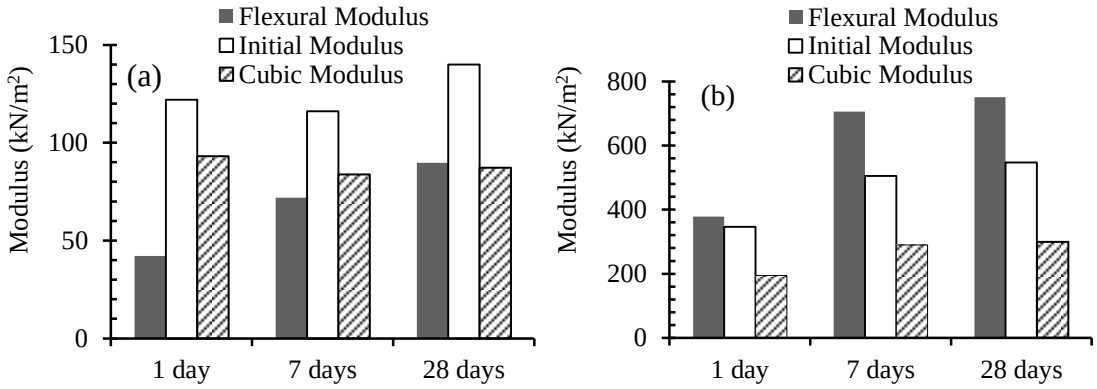

Figure 4.33. Comparing moduli for (a) SB and (b) SBC samples.

4.4 Conclusions

Unconfined compressive, tensile and cubic compressive strengths of sand-bentonite with and without cement inclusion are studied. Correlations between different strength and moduli are evaluated considering the aging effect as well. The following conclusions are drawn from this study:

1. Unconfined compressive strength reaches to its maximum value in 90 days in both sand-bentonite and sand-bentonite-cement mixtures, of which 90% is gained in 28 days of curing. The maximum strength gained is 30% more in SB samples, and almost three times more than the initial strength in SBC samples. Conversely, the failure strain reduces with curing and remains almost the same after 28 days, hence displaying a more brittle behavior with aging in SB specimens. With cement addition, however the failure strain increases with curing and reaches a value almost 50% more than the initial strain. Therefore, while the cured SB samples exhibit a brittle behavior, the SBC samples show a progressively increasing ductile behavior with time.

2. Tensile strength findings demonstrated similar results to unconfined compressive strength. Maximum split tensile strength gained in 28 days curing period is 1.5 and 3 times the initial value in SB and SBC samples respectively. Similarly, the flexural strength displayed 2-fold and 3-fold increments in SB and SBC specimens respectively, gaining 85% of the maximum strength in SB, and almost 100% in SBC within the first 28 days. The failure strain also showed a similar behavior as obtained in unconfined compression test. Aging caused the SB samples to become more brittle, with

a 47% reduction in failure strain, whereas the SBC specimens become more ductile with a two-fold increment in failure strain.

3. The utilization of the end pieces of the flexure beam in cubic compression provided a promising technique for future applications as a practical means of correlating both tensile and compressive strengths of cement treated soils using the same specimen. The results indicated that curing increases the cubic strength to a value 2.5-fold in the SBC specimens, and a 65% increment is observed in failure strain. Even though the cubic strength behavior is studied for SB samples as well as SBC, it is believed that this procedure is more reliable in cement treated soils which are stiffer and easier to obtain end pieces in a non-deformed condition.

4. Correlations between different strength values revealed that split tensile strength is almost 25% of the flexural strength for both samples without and with cement inclusion. Likewise, the split tensile strength is 10% and flexural strength is 30% of the unconfined compressive strength.

5. Studying the initial, flexural and cubic moduli, determined as the slope of the elastic portion of the unconfined compression, flexural and cubic compression results plotted as stress-strain, it is observed that the increment is 4-fold, 10-fold and 1.5-fold respectively.

6. The effect of cement enhancement is also studied by examining the structural changes at micro level as observed by scanning electron microscopy images.

The specimens studied were aged for more than 365 days which indicated clearly the cementation product of tobermorite-like gel (CSH) binding the particles.

7. Double punch test is a simple method for determining the tensile strength of samples. In cement stabilized samples with extended curing time it shows up to two times higher tensile strength values than the values found from split tensile test.

8. Using double punch tensile strength and unconfined compression test would be a simple method to determine undrained cohesion and internal friction angle of soil and stabilized materials through Mohr-Coulomb circle method.

The overall conclusion derived from this study is the efficacy of using cement as an additive to enhance the strength properties of sand-bentonite to be used as a buffer material, the effect of which is studied through five different strength tests and micro-structural investigations during aging period. Furthermore, the use of cubic compression test modified from cement mortar testing procedure is concluded to be a practical means of indirect determination of the unconfined compressive strength of cement added soils.

Chapter 5

CONCLUSIONS AND RECOMMENDATIONS FOR FURTHER RESEARCH

5.1 Conclusions

A study on the hydro-mechanical behavior of bentonite-sand to be utilized as landfill barrier material in a semi arid climate, with and without cement amendment has been presented. Firstly the material proportions were selected based on preliminary tests including compaction, swell-compressibility with hydraulic conductivity determinations. The selected materials were then tested in different aspects of engineering behavior determination to ascertain the possibility of proposing a sustainable solution. An experimental study was undertaken to achive the primary aim of this study, which was the assessment of the engineering behavior of selected material combinations. The secondary aim was to establish a comprehensive understanding of the correlations between different tensile strength test outcomes as well as unconfined compressive strength, thoroughly investigated in Chapter 4. The emphasis on tensile strength was mainly to understand the effect of tensile stresses developing due to desiccation of barriers with environmental influences as well as heat generated in the landfills due to exothermic aerobic and anaerobic reactions of the waste. The study herein attempted to apply some predictive approaches and empirical correlations to facilitate the material property determinations in a more practical way, which otherwise would have taken weeks or sometimes months to evaluate parameters like swell-shrinkage potential and hydraulic conductivity.

The selected materials are the 15%bentonite-85%sand and 15%bentonite-5%cement-80%sand. In the as compacted state and after aging for 28 days, both combinations proved to possess hydraulic conductivities less than 1 x 10^{-9} m/s under any effective pressure confinement. However, when a high concentration NaCl solution was permeated or when swell-consolidation was processed under 60°C, the hydraulic conductivity values were influenced considerably. When sand-bentonite (SB) was tested under these influences, the salt solution completely diminished the swelling capacity of SB, hence the hydraulic conductivity under any range of confinement increased above the allowed limit. Elevated temperature almost displayed the same effect except when effective confining pressures are higher than 1000 kPa. The SBC sample under the effect of NaCl permeation experienced increase in hydraulic conductivity, however for all confining pressure ranges this value remained below the maximum limit. Elevated temperature testing caused an adverse effect on SBC only for confining pressures less than 400 kPa. The volume change capacity was reduced appreciably with the cement inclusion. The micro-structural studies also proved the efficacy of cement usage after curing for one year. Therefore 5% cement has been very efficient as far as volume change studies are concerned within 28 days of curing period. The only disadvantage noted was the increased hydraulic conductivity when subjected to 60°C under low confining pressures.

As far as strength behavior of both mixtures are concerned, the cement amended mixtures proved to be more durable with increased tensile strength and compressive strength as well as failure strain. Therefore, even with 5% cement inclusion strength properties were significantly improved.

5.2 Recommendations for Further Research

Sand-bentonite-cement mixture was assessed and concluded that it can be safely used in a semi-arid climate where compacted layers are subjected to climatic influences. Cement seemed to have reduced the volume change potential and increased the strength. However, based on the observations and experiences gained in this study, following improvements are recommended as a further research:

1. A slightly higher cement content can be considered in a future study with longer curing periods to ascertain lower hydraulic conductivities under lower confinement conditions as well.
2. A different sand gradation can be assessed as the base material of the mixture instead of the poorly graded beach sand.
3. A high concentration NaCl solution was used as a permeant based on the past research claiming that the leachate consists of dominantly sodium and chlorine ions. In case of an increased salinity, which is the main problem in coastal regions, again NaCl is the main component of sea water. However, different chemicals, preferably collected representative leachate from the locality can be tested instead which would be more realistic.
4. An experimental method for hydraulic conductivity testing should be modified for the available conditions and included in a research study solely concerned with this parameter. If in good agreement with the predictions from consolidation test results, then the predictions could have higher reliablility.

5. Longer aging/curing periods can be adopted in a future testing program to thoroughly study the durability of the material combination selected under chemical permeation and temperature elevation effects.
6. Soil water retention capacity, shrinkage behavior, and strength characteristics should also be studied under the effect of chemical permeation and temperature elevation.

Finally it is recomended to apply the selected materials in a full scale model to study the in situ behavior, which will yield more realistic results on the function of the proposed liner/cover system to contain municipal solid waste.

REFERENCES

Abichou, T., Benson, C. H. & Edil, T. B. (2002). Micro-structure and Hydraulic Conductivity of Simulated Sand-Bentonite Mixtures. *Clays and Clay Minerals*, 50(5), 537–545.

Adaska S.W. (1985). Soil–cement Liners in Hydraulic Barriers in Soil and Rock, *ASTM*. Special Technical Publication No. 874, 299–313.

Akcanca, F, & Aytekin, M. (2012). Effect of Wetting-drying Cycles on Swelling Behavior of Lime Stabilized Sand-bentonite Mixtures, *Environmental Earth Sciences*, 66(1), 67-74.

Ameta, N.K., and Wayal, A.S. (2008). Effect of Bentonite on Permeability of Dune Sand, *Electronic Journal of Geotechnical Engineering*, 13, Bund. A.

API 13 A, *Specification for Drilling Fluids* – Specifications and Testing, Guidelines Handbook, American Petroleum Institute, 18th Edition

Arellano, D. & Thompson, M. R. (1998). *Stabilized Base Properties (Strength, Modulus, Fatigue) for Mechanistic-based Airport Pavement Design*. Final Rep., COE Rep. No. 4, Center of Excellence for Airport Pavement Research, Univ. of Illinois, Urbana, IL.

Arifin, Y. F. & Schanz, T. (2007). Modified Isochoric Cell for Temperature Controlled Swelling Pressure Tests, Experimental Unsaturated Soil Mechanics, *Springer Proceedings in Physics*, 112, 229-241.

ASTM C1018 (1997). *Standard Test Method for Flexural Toughness and First-Crack Strength of Fiber-Reinforced Concrete (Using Beam With Third-Point Loading)*, Developed by Subcommittee: C09.42, American Society for Testing Materials.

ASTM C1609 (2010). *Standard Test Method for Flexural Performance of Fiber-Reinforced Concrete (Using Beam With Third-Point Loading)*. Vol. 04.02, American Society for Testing Materials.

ASTM C348 (2008). *Standard Test Method for Flexural Strength of Hydraulic-Cement Mortars*, Vol. 04.01, American Society for Testing Materials.

ASTM C349 (2008). *Standard Test Method for Compressive Strength of Hydraulic-Cement Mortars (Using Portions of Prisms Broken in Flexure*), Vol. 04.01, American Society for Testing Materials.

ASTM D 2435 (1999). *Standard Test Method for One-Dimensional Consolidation Properties of Soils,* Vol. 04.08, American Society for Testing Materials.

ASTM D2166 / D2166M (2013). *Standard Test Method for Unconfined Compressive Strength of Cohesive Soil,* Vol. 04.08, American Society for Testing Materials.

ASTM D3967 (2008). *Standard Test Method for Splitting Tensile Strength of Intact Rock Core Specimens*, American Society for Testing and Materials, West Conshohocken, PA.

ASTM D5084 (2010). *Standard Test Methods for Measurement of Hydraulic Conductivity of Saturated Porous Materials Using a Flexible Wall Permeameter*, Vol. 04.08, American Society for Testing Materials

ASTM D698 (2012). *Standard Test Methods for Laboratory Compaction Characteristics of Soil Using Standard Effort*, American Society for Testing and Materials, West Conshohocken, PA.

ASTM, C188 (2009). *Standard Test Method for Density of Hydraulic Cement*, Vol. 04.01, American Society for Testing Materials.

Azeredo, G., Morel, J.C. & Perazzo Barbossa, N. (2007). Compressive Strength Testing of Earth Mortars, *Journal of Urban and Environmental Engineering*, 1(1), 26–35.

Bahar, R., Benazzoug, M. & Kenai, S. (2004). Performance of Compacted Cement-stabilized Soil. *Cement and Concrete Composites*, 26(7), 811-820.

Bashitialshaaer, R.A.I., Persson, K. M., & Larson, M. (2009). Estimated Future Production of Desalinated Seawater in the MENA Countries and Consequences

for the Recipients, *IDA World Congress* – Atlantis, The Palm – Dubai, UAE, REF: IDAWC/DB09-149.

Bellezza I. & Fratalocchi E. (2006). Effectiveness of Cement on Hydraulic Conductivity of Compacted Soil–cement Mixtures, *Ground Improvement 10*, No. 2, 77–90.

Bielinski, A., Class, H., Jakobs, H. & Helmig, R. (2001). Numerical Simulation of Desiccation Processes in a Mineral Liner of a Waste-Disposal Site, *Proceedings of 3. Workshop*, Weimar, Germany, Heft 06, 113-128.

Bilsel, H. (2002). *Climatic Effects on the Engineering and the Physico-Chemical Properties of Calcareous Swelling Clays of Cyprus*, PhD thesis submitted to the Eastern Mediterranean University.

Błażejczak, D., Horn, R. & Pytka, J. (1995*). Soil Tensile Strength as Affected by Time, Water Content and Bulk Density*, International Agrophysics, Institute of Agrophysics Polish Academy of Sciences Lublin, Poland, 9(3).

Blight, G.E. & Fourie, A.B. 2005. Experimental Landfill Caps for Semi-Arid and Arid Climates, *J. Waste Management and Research*, 23, 113-125.

Bouma, J. (1989). Using Soil Survey Data for Quantitative Land Evaluation, *Advances in Soil Science*, 9, 177-213.

Briaud, J.L. (2003). Shrink Test-water Content Method for Shrink and Swell Predictions, *Journal of Geotechnical and Geoenvironmental Engineering*, 129(7), 590-560.

Chalermyanont, T. & Arrykul, S. (2005). Compacted Sand-bentonite Mixtures for Hydraulic Containment Liners, *Songklanakarin Journal of Science and Technology*, 27(2), 313-323.

Chapius, R.P. (1990). Sand-bentonite Liners: Predicting Permeability from Laboratory Tests, *Canadian Geotechnical Journal*, 27, 47-57.

Chen, W. F. & Drucker, D. C. (1969). Bearing Capacity of Concrete Blocks or Rock, *Journal of the Engineering Mechanics Division, Proc. ASCE*, 95, No. EM4, 955-978.

Cokca, E. & Yilmaz, Z. (2004). Use of Rubber and Bentonite Added Fly Ash as a Liner Material. *Journal of Waste Management*, 24(2), 153-64.

Conlon, R.T. (1966). Landslide on the Roulnustone River, Quebec. *Canadian Geotechnical Journal*, 3(3), 113-144.

Consoli, N. C., Arcari Bassani, M. A. & Festugato, L. (2010). Effect of Fiber-Reinforcement on the Strength of Cemented Soils, *Geotextiles and Geomembranes*, 28(4), 344-351.

Consoli, N. C., Rosa, D. A., Cruz, R. C. & Rosa, A. D. (2011). Water Content, Porosity and Cement Content as Parameters Controlling Strength Of Artificially Cemented Silty Soil, *Engineering Geology*, 122(3–4), 328-333.

Consoli, N., de Moraes, R. & Festugato, L. (2013). Parameters Controlling Tensile and Compressive Strength of Fiber-Reinforced Cemented Soil. *Journal of Materials in Civil Engineering.*, 25(10), 1568–1573.

Dafalla, M.A. & Al-Shamrani, M.A. (2011). Swell and Aging Effect on a Bentonite Sand Mixture, *Unsaturated Soils: Theory and Practice*, Kasetsart University, Thailand.

Dakshanamurthy, V. (1978). A New Method to Predict Swelling Using a Hyperbolic Equation, *Geotechnical Engineering, 9*, 79 –87.

Das, B. M. (2006). *Principles of Geotechnical Engineering*, Boston, PWS-Kent.

Delage, P., Marcial, D., Cui, Y. J. & Ruiz, X., (2006). Ageing Effects in a Compacted Bentonite: a Microstructure Approach, *Géotechnique* , 56(5), 291-304.

Díaz-Rodríguez, J.A. & Santamarina, J.C. (1999). Thixotropy: The Case of Mexico City Soils., *XI Panamerican Conference on Soil Mechanics and Geotechnical Engineering*, Iguazu Falls, Brazil, 1, 441-448.

DoE, (1995). *A Review of the Composition of Leachates for Domestic Wastes in Landfill Sites*. Department of Environment Report CWM 072/95.

Dramé, H., Beaudoin, J. J. & Raki, L. (2007). A comparative study of the volume stability of C–S–H (I) and Portland cement paste in aqueous salt solutions, *Journal of Materials Science*, 42(16), 6837-6846.

ELE (1998). Tri-flex 2, Permeability test system, Owner's manual, Rev.5:11/98.

EPA (2000). *Landfill Manuals of the Environmental Protection Agency*, Landfill Manuals: Landfill Site Design.

Fang, H. Y. & Chen, W. F. (1971). *New Method for Determination of Tensile Strength of Soils*, Highway Research Record, No. 345, 62-68.

Fang, H. Y. & Chen, W. F., (1972), *Further Study of Double-Punch Test for Tensile Strength of Soils*, Fritz Laboratory Reports, Paper 1969.

Fang, H. Y. (1970). *Method of Test for Tensile Strength of Soil, Rock and Stabilized Materials by Double Punch Test*, Fritz Laboratory Reports. Paper 1967

Fang, H.Y. & Hirst, T.J. (1973). A Method for Determining the Strength Parameters of Soils, *52nd Annual Meeting, Highway Research Board*, Washington, D.C.

Farajollahi, A., & Wareham, D.G. (1998) Numerical modelling of the effects of acidic contamination on pollutant migration through bentonite-sand liners. *Environmental Technology*, 19, 381-390.

Fell, R., MacGregor, P., Stapledon, D., & Bell, G., (2005). *Geotechnical Engineering of Dams*, CRC Press, 239-240.

Fredlund, D.G., & Rahardjo, H. (1993). *Soil Mechanics for Unsaturated Soils*, New York: John Wiley and Sons, Inc.

Fredlund, D.G. & Xing, A. (1994). Equations for the Soil-water Characteristic Curve, *Canadian Geotechnical Journal*, 31(3), 521-532.

Fredlund, D.G., Xing, A. & Huang, S. (1994). Predicting the permeability function for unsaturated soil using the soil-water characteristic curve, *Canadian Geotechnical Journal*, 31(3), 533-546.

Fredlund, M.D., Wilson, G.W. & Fredlund, D.G. (2002a). Use of the grain-size distribution for estimation of the soil-water characteristic curve, *Canadian Geotechnical Journal*, 39, 1103-1117.

Fredlund, M.D., Wilson, G.W. & Fredlund, D.G. (2002b). Representation and estimation of the shrinkage curve, *Proceedings of the Third International Conference on Unsaturated Soils*, UNSAT 2002, Recife, Brazil, 145-149.

Frydman, S. (1964). The Applicability of the Brazilian (Indirect Tension) Test to Soils. *Australian journal of applied science*, 15, 335-343.

Galvão, T. C., Kaya, A.,Mahler, C., Ören A. H. & Yükselen, Y. (2008). Innovative Technology for Liners, *Soil & Sediment Contamination*, 17(4), 411-424.

Gens, A. & Alonso, E.E. (1992). A Framework for the Behaviour of Unsaturated Expansive Clays, *Canadian Geotechnical Journal*, 29(1992), 1013–1032.

George, K. P. (1970). Theory of Brittle Fracture Applied to Soil Cement. *Journal of Soil Mechanics and Foundation Division*, 96(3), 991-1010.

Arkansas State Highway Department Division of Planning and Research in cooperation with U. S.

Guney, Y., Sari, D., Cetin, M. & Tuncan, M. (2007). Impact of Cyclic Wetting–drying on Swelling Behavior of Lime-stabilized Soil, *Building and Environment*, 42(2), 681-688.

Hannawi, K., Prince, W. & Bernard, S. (2013). Strain Capacity and Cracking Resistance Improvement in Mortars by Adding Plastic Particles. *Journal of Materials in Civil Engineering*, 25(11), 1602–1610.

Head, K.H. (1982). *Permeability, Shear Strength and Compressibility Tests*, London: Pentech Press, Manual of soil Laboratory testing, 2, 449-458.

Horpibulsuk, S. (2005). Mechanism Controlling Undrained Shear Characteristics of Induced Cemented Clays, *Lowland Technology International*, 7 *(*2), 9-18.

Horpibulsuk, S., Rachan, R., Chinkulkijniwat, A., Raksachon, Y. & Suddeepong, A. (2010). Analysis of Strength Development in Cement-Stabilized Silty Clay based on Microstructural considerations. *Construction and Building Materials*, 24(10), 2011-2021.

Hudson, W. R. & Kennedy, T. W. (1968). *An Indirect Tensile Test for Stabilized Materials*. Research Report 98-1, Center for Highway Research, University of Texas at Austin.

Jamsawang, P., Voottipruex, P. & Horpibulsuk, S., (2015). Flexural Strength Characteristics of Compacted Cement-polypropylene Fiber Sand. *Journal of Materials in Civil Engineering.* 27(9), 04014243.

Kazimoglu, Y.K., McDougall, J.R., & Pyrah, I.C. (2003). Moisture Retention Curve in Landfilled waste, *Proceedings of the International Conference "From Experimental Evidence towards Numerical Modeling of Unsaturated Soils"*, Weimar, Germany, 1, 59-67.

Kemper, W. D. & Rosenau, R.C. (1984). Soil Cohesion as Affected by Time and Water Content, *Soil Science Society of America Journal*, 48(6), 1001-1006.

Kenney, T.C., van Veen, W.A., Swallow, M.A. & Sungaila, M.A. (1992). Hydraulic Conductivity of Compacted Bentonite-sand Mixtures. *Canadian Geotechnical Journal* 29(3), 364 – 374.

Kim, T. H., Kim, T. H, Kang, G.C. & Ge, L. (2012). Factors Influencing Crack-Induced Tensile Strength of Compacted Soil. *Journal of Materials in Civil Engineering*, 24(3), 315–320.

Kim, T.H., Kim, C.K., Jung, S.J. & Lee, J.H. (2007). Tensile Strength Characteristics of Contaminated and Compacted Sand-Bentonite Mixtures, *Environmental Geology*, 52(4), 653-661.

Kolias, S., Kasselouri-Rigopoulou, V. & Karahalios, A. (2005). Stabilisation of Clayey Soils with high calcium fly Ash and Cement. *Cement and Concrete Composites*, 27, 301-313.

Komine, H. & Ogata,N. (1994). Experimental Study on Swelling Characteristics of Compacted Bentonite. *Canadian Geotechnical Journal*, 31(4), 478-490.

Komine, H. & Ogata,N. (1999). Experimental Study on Swelling Characteristics of Sand-Bentonite Mixture for Nuclear Waste Disposal, *Soils and Foundations*, 39(2), 83-97.

Kondner, R. L. (1963). Hyperbolic Stress-Strain Response: Cohesive Soils, *Journal of Soil Mechanics and Foundations Division, ASCE,* 89, No. SM1. Proc. Paper 3429, 115-143.

Kowalski S.J. (2003). *Thermomechanics of Drying Processes*, Berlin: Springer-Verlag, Heidelberg, New York, 365.

Krahn, J. & Fredlund, D.G. (1972). On total, Matric and Osmotic Suction. *Soil Science,* 115(5), 339- 348.

Kraus J.F., Benson C.H., Erickson A.E. & Chamberlain E.J. (1997). Freeze-thaw Cycling and Hydraulic Conductivity of Bentonitic Barriers. *ASCE Journal of Geotechnial Engineering,* 123, 229-238.

Kumar, S. & Stewart, J. (2003). Utilization of Illinois PCC Dry Bottom Ash for Compacted Landfill Barriers, *Soil and Sediment Contamina*tion, 12(3), 401-415.

Kumar, S., & Yong, W.L. (2002). Effect of Bentonite on Compacted Clay Landfill Barriers, *Journal of Soil and Sediment Contamination,* 11(1), 71-89.

Kvennas, M., Sparrevik, M. & Grim, R. S. (2009). Effects of Amendment Materials on Cement-Solidified Contaminated Marine Sediments, Mechanical Stability and Leaching of Heavy Metals, *Journal of ASTM International,* 6(4).

Laguros, J. G. (1962). *Effect of Chemicals on Soil-cement Stabilization*. Retrospective Theses and Dissertations, Iowa state university, Paper 2061.

Lambe, T.W. (1969). *Soil Mechanics, SI Version (series in soil Engineering),* John Wiley and Sons, Inc., New York, 71-92.

Leonards, G. A., & Narain, J. (1963). Flexibility of Clay and Cracking of Earth Dams: American Society of Civil Engineersm Proceedings, *Soil Mechanics and Foundations Division Journal*, 89, no. SM2, 47-98.

Lingnau, B.E., Graham, J., Yarechewski, D., Tanaka, N. & Gray, M.N. (1996). Effects of Temperature on Strength and Compressibility of Sand-bentonite Buffer, *Engineering Geology*, 41(1–4), 103–115.

Lloret, A. & Villar, M.V. (2007). Advances on the Knowledge of the Thermo-hydro-mechanical Behaviour of Heavily Compacted "FEBEX" Bentonite, *Physics and Chemistry of the Earth, Parts A/B/C*, 32(8–14), 701-715.

Maher, M. H. & Ho, Y. C. (1993). Behavior of Fiber-reinforced Cemented Sand Under Static and Cyclic Loads. *Geotechnical Testing Journal*, 16, 330–338.

Mainguy M., Coussy O. & Baroghel-Bouny, V. (2001). Role of Air Pressure in Drying of Weakly Permeable Materials, *Journal of Engineering Mechanics. ASCE*, 127(6), 582-592.

Marcial, D., Delage, P., Ruiz, X. & Cui, Y. J. (2006). Ageing Effects in a Compacted Bentonite: a Microstructure Approach, *Journal of Geotechnique* , 56(5), 291-304.

Minasny, B., McBratney, A.B. & Bristow K.L. (1999). Comparison of Different Approaches to the Development of Pedotransfer Functions for Water-retention Curves, *Geoderma Journal*, 93, 225-253.

Mitchell, J. K. & El Jack, S. A. (1966). The Fabric of Soil-Cement and Its Formation, *Clays and Clay Minerals*, 14, 297-305.

Mitchell, J. K. (1993). *Fundamentals of Soil Behavior, Second ed*. New York, John Willey and Sons, 30-39.

Mollins, L.H., Stewart, D.I., & Cousens, T.W. (1996). Predicting the Properties of Bentonite-Sand Mixtures, *Clay Minerals*, 31, 243-252.

Montanez, J.E.C., (2002). *Suction and Volume Changes of Compacted Sand-Bentonite Mixtures.* PhD thesis, University of London, Imperial College of Science, London, England.

Muntohar, A. S. & Hashim, R. (2003). Swelling Behaviour of Engineered Clay Soils, *22nd International Conference on Advances in Soft Soil Engineering and Technology*, 2-4 July, Putra Jaya, Malaysia.

Muntohar, A. S. (2003). Swelling and Compressibility Characteristics of Soil-Bentonite Mixtures, *Dimensi Teknik Sipil*, 5(2), 93–98.

Nagaraj, H., Munnas, M. & Sridharan, A. (2010). Swelling Behavior of Expansive Soils. *International Journal of Geotechnical Engineering*, 4(1), 99-110.

Najm, M. A., Jesiek, J., Mohtar, R. H., Lura, P. & Sant, G. (2012). Assessing the Role of the Pore Solution Concentration on Horizontal Deformations in an Unsaturated Soil Specimen During Drying, *Geoderma, Volumes 187–188*, 31-40.

Neville, A. M. (1995). *Properties of Concrete, fourth ed*. Pearson Education, Harlow, 322-324.

Neville, A.M. (1981). *Properties of Concrete, Pitman Publication*, URL https://igitgeotech.files.wordpress.com, retrieved at August 2015.

Nontananandh, S., Yoobanpot, T. & Boonyong, S., (2005). Scanning Electron Microscopic Investigations of Cement Stabilized Soil, *Proceedings of 10th National Conference on Civil Engineering*, Chonburi-Thailand, 23-26.

Peron, H., Laloui, L., Hueckel, T. & Hu, L.B. (2009). Desiccation Cracking of Soils, *European Journal of Civil and Environmental Engineering.* 13(7-8), 869-888.

Peters, J. F. & Leavell, D. A. (1988). Relationship between Tensile and Compressive Strengths of Compacted Soils. Advanced triaxial testing of soil and rock, *ASTM STP 977*, ASTM International, Philadelphia, 169–188.

Raad, L., (1976). *Design Criteria for Soil-cement Bases.* PhD dissertation, Dept. of Civil Engineering, Univ. of California, Berkeley, CA.

Rahardjo, H. & Leong, E.C. (1997). *Soil-water Characteristic Curves and Flux Boundary Models*, Unsaturated Soil Engineering practice: Geotechnical Special Publication No. 68, Geo Institute, ASCE, Utah.

Rao, K.S. & Tripathy, S. (2003). Effect of Aging on Swelling and Swell-Shrink Behavior of a Compacted Expansive soil. *ASTM Geotechnical Testing Journal*, 26(1), 36-46.

Rao, S.M., Reddy, B.V.V. & Muttharam, M. (2001). The Impact of Cyclic Wetting and Drying on the Swelling Behaviour of Stabilized Expansive Soils, *Engineering Geology*, 60(1–4), 223-233.

Rowe, R. K. (2005). Long-Term Performance of Contaminant Barrier Systems, 45th Rankine Lecture, *Géotechnique*, 55(9), 631–678.

Rowe, R.K. (2001). *Geotechnical and Geoenvironmental Engineering Handbook*, Kluwer Academic publishers, America, 825-838.

Sällfors, G. & Öberg-Högsta, A-L. (2002). Determination of Hydraulic Conductivity of Sand-bentonite Mixtures for Engineering Purposes, *Geotechnical & Geological Engineering,* 20*(*1), 65-80.

Sethi, R. & Molfetta, A.D. (2007). Heat Transport Modeling in an Aquifer Downgradient a Municipal Solid Waste Landfill in Italy, *American Journal of Environmental Sciences,* 3(3), 106-110.

Siddiqua, S., Blatz, J. & Siemens, G. (2011). Evaluation of the Impact of Pore Fluid Chemistry on the Hydromechanical Behaviour of Clay-based Sealing Materials, *Canadian Geotechnical Journal,* 48(2), 199-213, 10.1139/T10-064.

Sih, G. & Fang, H. Y. (1972). *Fracture Toughness Values of Highway Pavement Materials*, Institute of Fracture and Solid Mechanics, Lehigh University.

Sillers, W. S., Fredlund, D.G. & Zakerzaheh, N. (2001). Mathematical Attributes of Some Soil–water Characteristic Curve Models, *Geotechnical and Geological Engineering,* 19(3-4), 243-283.

Sobhan, K. & Mashnad, M. (2002). Tensile Strength and Toughness of Soil–Cement–Fly-Ash Composite Reinforced with Recycled High-Density Polyethylene Strips. *Journal of Materials in Civil Engineering,* 14(2), 177–184.

SoilVision Systems Ltd. (2001). *SoilVision Theory Guide*, Version 3.34, 2nd edition, Saskatoon, Saskatchewan, Canada.

Spencer, E. (1968). Effect of Tension of Stability of Embankment. *Journal of Soil Mechanics and Foundation Division, 94*(5), pp. 1159-1173.

Sridharan, A. (2003). Volume Change Behaviour of Fine Grained Soils, *Proceedings of the International Conference "From Experimental Evidence towards Numerical Modeling of Unsaturated Soils"*, Weimar, Germany, September 2003, 1, 209-226.

Stavridakis E. I. & Hatzigogos T. N. (1999). Influence of Liquid Limit and Slaking on Cement Stabilized Clayey Admixtures, *Geotechnical and Geological Engineering*, 17, 145-154.

Stewart, D.I., Studds, P.G. & Cousens, T. W. (2003). The Factors Controlling the Engineering Properties of Bentonite-Enhanced Sand, *Applied Clay Science,* 23(1–4), 97–110.

Studds P.G., Stewart D.I. & Cousens T.W. (1996). The Effect of Ion Valence on the Swelling Behaviour of Sodium Montmorillonite. *Proc. 4th lnt. Conference on Reuse of Contaminated Land and Landfills*, 139-142. Edinburgh. Engineering Technics Press.

Suklje, L. (1969). *Rheological Aspects of Soil Mechanics*, London, Wiley-Interscience, 456-473.

Sun, D., Sun, W., Yan, W. & Li, J. (2010). Hydro-mechanical behaviours of highly compacted sand-bentonite mixture, *Journal of Rock Mechanics and Geotechnical Engineering,* 2 (1), 79–85.

Tchakalova B. & Todorov K, (2008). Plastic soil-cement mixtures for isolation barriers, *Geologica Balcanica,* 37(1-2), 91-96.

Tietje, O. & Tapkenhinrichs, M. (1993). Evaluation of Pedo-Transfer Functions, *Journal of Soil Science Society of America,* 57, 1088-1095.

Tripathy, S., Leong, E.C., Rahardjo, H. (2003). Suction of Compacted Residual Soils, *Proceedings of the International Conference "From Experimental Evidence towards Numerical Modeling of Unsaturated Soils",* Weimar, Germany, September 2003, 1, 111-122.

Tripathy, S. & Subba Rao, K.S. (2009). Cyclic Swell–Shrink Behaviour of a Compacted Expansive Soil, *Geotechnical and Geological Engineering,* 27(1), 89-103.

TS EN 13500, *Petroleum and Natural Gas Industries-drilling Fluid Materials-specifications and Test*, Turkish Standard Institution.

Tsuchida, T., Kobayashi, M. & Mizukami J. (1991). Effect of ageing of marine clay and its duplication by high temperature consolidation, *Soils and Foundations,* 31 (4), 133-147.

Tsutsumi, A. & Tanaka, H. (2012), Combined Effects of Strain Rate and Temperature on Consolidation Behavior of Clayey Soils, *Soils and Foundations*, 52(2), 207–215.

van Genuchten, M. Th. (1980). A Closed-form Equation for Predicting the Hydraulic Conductivity of Unsaturated Soils. *Journal of Soil Science Society of America*. 44, 892–898.

Van Olphen,H. (1971). *An Introduction to Clay Colloid Chemistry*. Wiley-Interscience, New York, N. Y., 301.

Verastegui Flores, R.D., Di Emidio, G. & Van Impe, W. F. (2010). Small-Strain Shear Modulus and Strength Increase of Cement-Treated Clay, *Geotechnical Testing Journal*, 33(1), 62.

Vesga, L. F. (2009). Direct Tensile-Shear Test (DTS) in Unsaturated Kaolinite Clay. *Geotechnical Testing Journal, ASTM*, 32*(*5).

Villar, M.V. & Lloret, A. (2004). Influence of Temperature on the Hydro-mechanical behaviour of a Compacted Bentonite, *Applied Clay Science*, 26(1–4), 337-350.

Wang, J.J., Zhu, J.G., Chiu, C.F., Zhang, H. (2007), Experimental Study on Fracture Toughness and Tensile Strength of a Clay, *Engineering Geology* ,94(1–2), 65-75.

Ye, W.M., Lai, X.L., Liu, Y., Chen, Y.G. & Cui, Y.J. (2013). Ageing Effects on Swelling Behaviour of Compacted GMZ01 Bentonite, *Nuclear Engineering and Design*, 265, 262-268.

Ye,W.M., Wan, M., Chen, B., Chen, Y.G. & Cui,Y.J. (2012). Temperature Effects on the Unsaturated Permeability of the Densely Compacted GMZ01 Bentonite under Confined Conditions. *Engineering Geology*, 126, 1-7.

Yesiller, N., Hanson, J. L., Oettle, N. K. & Liu, W-L. (2008). Thermal Analysis of Cover Systems in Municipal Solid Waste Landfills. *Journal of Geotechnical and Geoenvironmental Engineering*, 134 (11), 1655-1664.

Zornberg, J., Jernigan, B., Sanglerat, T., & Cooley, B. (1999). Retention of Free Liquids in Landfills Undergoing Vertical Expansion, *Journal of Geotechnical Geoenvirontal Engineering*, 125(7), 583–594.